12

Research and Development Technical Report

ECOM-76-0881-F

WIRE OBJECT DETECTION STUDY

R. KLEEHAMMER
FAIRCHILD CAMERA & INSTRUMENT CORPORATION
SYOSSET, NEW YORK 11791

April 1978

Final Report for Period 30 April 1976–28 February 1977

Prepared for:

ECOM

US ARMY ELECTRONICS COMMAND FORT MONMOUTH, NEW JERSEY 07703

NOTICES

Disclaimers

The findings in this report are not to be construed as an official Department of the Army position, unless so designated by other authorized documents.

The citation of trade names and names of manufacturers in this report is not to be construed as official Government indorsement or approval of commercial products or services referenced herein.

Disposition

Destroy this report when it is no longer needed. Do not return it to the originator.

(14) ED-AX-86-A

UNCLASSIFIED (U)
SECURITY CLASSIFICATION OF THIS PAGE (When Data Entered)

REPORT DOCUMENTATION PAGE

READ INSTRUCTIONS BEFORE COMPLETING FORM

1. REPORT NUMBER: ECOM-76-0881-F	2. GOVT ACCESSION NO.
3. RECIPIENT'S CATALOG NUMBER	
4. TITLE (and Subtitle): (6) WIRE OBJECT DETECTION STUDY.	(9) 5. TYPE OF REPORT & PERIOD COVERED: FINAL rept. 30 Apr 76 to 28 Feb 77
	6. PERFORMING ORG. REPORT NUMBER: ED-AX-86-A
7. AUTHOR(s): (10) R. Kleehammer	8. CONTRACT OR GRANT NUMBER(s): (15) DAAB07-76-C-0881
9. PERFORMING ORGANIZATION NAME AND ADDRESS: FAIRCHILD CAMERA & INSTRUMENT CORP. SYOSSET, LI, NEW YORK	10. PROGRAM ELEMENT, PROJECT, TASK AREA & WORK UNIT NUMBERS: 6.2202A 1P2 62202 AH 85 12 34
11. CONTROLLING OFFICE NAME AND ADDRESS: US Army Avionics Research & Development Activity AVRADCOM ATTN: DAVAA-E, Ft. Monmouth, NJ	12. REPORT DATE: (11) Apr 78
	13. NUMBER OF PAGES: 166 (12) 157
14. MONITORING AGENCY NAME & ADDRESS (If different from Controlling Office): (16) 1F262202AH85 (11) 12	15. SECURITY CLASS. (of this report): UNCLASSIFIED
	15a. DECLASSIFICATION/DOWNGRADING SCHEDULE

16. DISTRIBUTION STATEMENT (of this Report)

APPROVED FOR PUBLIC RELEASE

(17) DCSM

DISTRIBUTION STATEMENT A
Approved for public release;
Distribution Unlimited

17. DISTRIBUTION STATEMENT (of the abstract entered in Block 20, if different from Report): (17) 14-1201-F

18. SUPPLEMENTARY NOTES

19. KEY WORDS (Continue on reverse side if necessary and identify by block number)

CHARGE COUPLED DEVICES	OPTICAL SCANNING
WIRE DETECTION	OPTICAL RADAR
PATTERN RECOGNITION	GATED LASER
SINGLE SITE ACTIVATION	GATING TECHNIQUES

20. ABSTRACT (Continue on reverse side if necessary and identify by block number)

AN ANALYTIC STUDY AND AN EXPERIMENTAL FEASIBILITY DEMONSTRATION OF THE DETECTION OF WIRE OBJECTS HAS BEEN COMPLETED. THE TECHNIQUES EMPLOYED WERE BASED UPON THE GEOMETRIC COMPATABILITY OF THE OBJECT TO BE DETECTED AND THE SENSOR USED, WHICH IN THIS INSTANCE WAS A 1 X 1728 CHARGED COUPLED DEVICE (CCD) ARRAY.

THE CONCEPT OF SINGLE SITE ACTIVATION WAS EXPERIMENTALLY ESTABLISHED AND ITS IMPORTANCE TO A PATTERN RECOGNITION MODE OF OPERATION WAS CLEARLY DELINEATED.

DD FORM 1 JAN 73 1473 EDITION OF 1 NOV 65 IS OBSOLETE

UNCLASSIFIED (U)
SECURITY CLASSIFICATION OF THIS PAGE (When Data Entered)

133 51

JE

20.

CCD GEOMETRIC FORMATS WERE CONSIDERED FROM A SYSTEMS INTEGRATION VIEWPOINT AS RELATED TO A VARIETY OF OPTICAL SCANNING TECHNIQUES.

FOREWORD

This Final Report was prepared by Fairchild Imaging Systems, a Division of Fairchild Camera and Instrument Corporation at Syosset, New York under Contract No. DAAB07-76-C-0881. The work was performed under the direction of the Avionics Research and Development Activity, Ft. Monmouth, New Jersey. Mr. A. Kleider was the project manager for the Army.

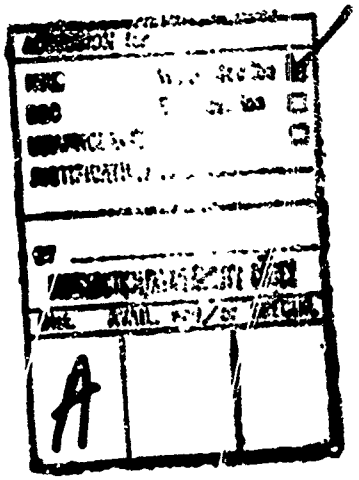

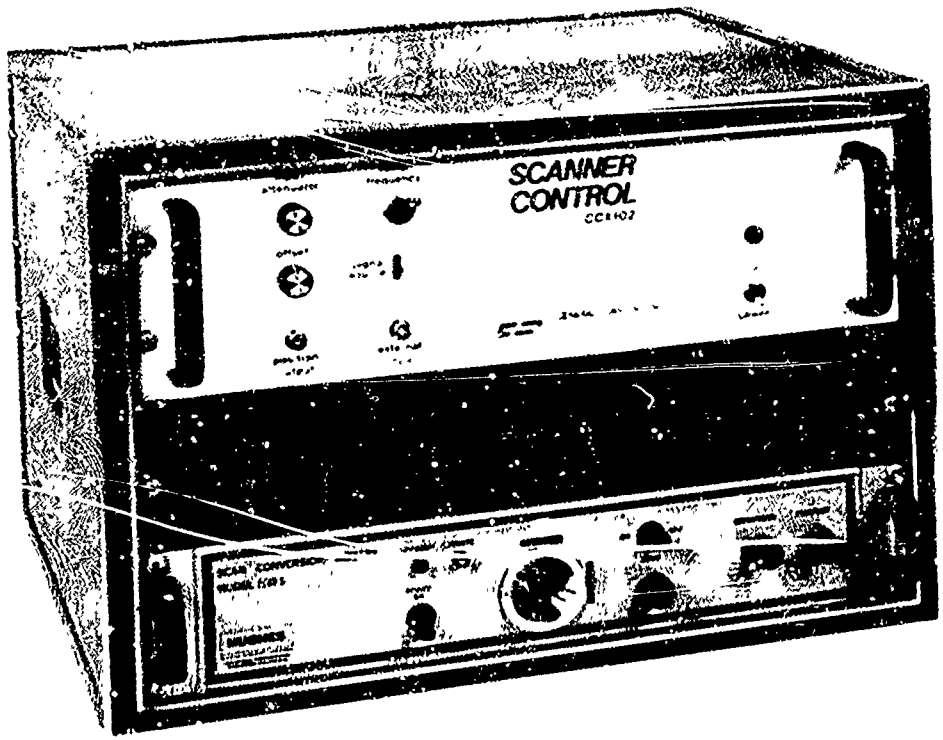

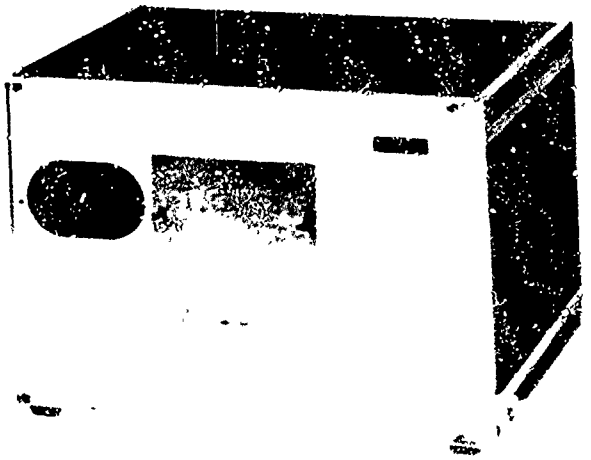

WIRE OBJECT DETECTION SIMULATOR (WODS)

TABLE OF CONTENTS

SECTION	TITLE	PAGE NO.
1.0	INTRODUCTION	1-1
2.0	TECHNICAL DISCUSSION	2-1
2.1	REVIEW OF WIRE OBJECT DETECTION	2-2
2.2	DETECTION REQUIREMENTS	2-5
2.2.1	Input to the Processing Algorithm	2-5
2.2.2	Review of Poisson Detection Statistics	2-6
2.2.3	Wire Detection - Definition	2-7
2.2.4	Estimate Of Spurious Detections	2-8
2.2.5	Effect of False Alarms	2-10
2.2.6.1	Generalized Requirements For WODS	2-11
2.2.6.2	Extension To Practical Cases	2-12
2.2.7	Background Noise Effects	2-13
2.2.7.1	Signal-To-Noise-Ratio	2-14
2.2.7.2	Fluctuations	2-17
2.3	SCANNING REQUIREMENTS	2-21
2.3.1	Review Of Scanning Methods	2-24
2.3.1.1	Laser Illumination Pattern	2-24
2.3.1.2	Flying Spot Scanner	2-25
2.3.1.3	Polygon Scanner	2-26
2.3.1.4	Mirror Behind Lens	2-27
2.3.1.5	Bandwidth Considerations	2-29
2.3.2	Charge Coupled Imaging Devices (CCD)	2-29
2.3.2.1	Application Of Area CCD Arrays	2-31
2.3.2.2	Application Of Linear CCD Arrays	2-33
2.3.2.3	Linear Array	2-34
2.3.2.4	Horizontal Array (Vertical Scan)	2-35

TABLE OF CONTENTS (Continued)

SECTION	TITLE	PAGE NO.
2.4	GATING TECHNIQUES	2-35
2.4.1	Electro-Optic Gating	2-35
2.4.2	Gated Image Tubes	2-37
2.4 3	"On-Chip" CCD Gating	2-37
2.5	TRADE-OFF ANALYSIS	2-38
2.5.1	Background Calculation	2-39
2.5.2	Range Equation	2-40
2.5.3	Linear Versus Area CCD	2-41
2.5.4	CCD Versus II	2-41
2.5.5	Extension To Other Wavelengths	2-43
2.5.6	Summary	2-45
3.0	CAMERA DESIGN	3-1
3.1	GENERAL DISCUSSION	3-1
3.2	CCD ARRAY DESCRIPTION	3-1
3.2.1	Technical Description	3-2
3.2.2	Shift Register Design	3-3
3.2.3	Photocell Design	3-3
3.2.4	On-Chip Amplifier	3-3
3.2.5	CCD Gating	3-6
3.2.6	Image Display	3-8
3.3	DESCRIPTION OF THE WODS CAMERA	3-8
3.3.1	Video Processor	3-9
3.3.2	Logic	3-11
3.3.3	Clock Drivers	3-12
3.3.4	X-Y Sweep Generation	3-12
3.3.5	Exposure Control Logic Systems	3-13

TABLE OF CONTENTS (Continued)

SECTION	TITLE	PAGE NO.
3.4	OPERATING PROCEDURE	3-14
3.4.1	Components	3-14
3.4.1.1	WODS Scanner	3-14
3.4.1.2	Scan Converter	3-14
3.4.1.3	Scan Controller	3-14
3.4.2	Wods Scanner Test	3-15
3.4.2.1	Scanner Setup	3-15
3.4.2.2	Turn-On	3-15
3.4.2.3.1	Operational Test	3-16
3.4.2.3 2	Zoom	3-17
3.4.3	Replacement of CCD Array	3-17
3.4.4	Verification of Gating and Synchronizing Signals	3-18
3.4.4.1	Verification of Gating Pulse	3-18
3.4.4.2	Verification of Illumination Source Position	3-19
4.0	FEASIBILITY EXPERIMENT DESCRIPTION AND GOALS	4-1
4.1	CCD ARRAY SELECTION	4-1
4.1.1	Test Equipment	4-1
4.1.2	Measurement Conditions	4-2
4.1.3	Test Description	4-2
4.1.4	Electro-Optical Performance	4-3
4.1.4.1	General Electrical Factors	4-3
4.1.4.2	Signal Output Versus Exposure Time (Normal Mode)	4-4
4.1.4.3	Signal Output Versus Exposure Time (Gating Mode)	4-4
4.1.4.4	Propagation Characteristics	4-4
4.1.4.5	Verification of Gating Capability	4-5
4.1.5	Summary of Gating Results	4-7

TABLE OF CONTENTS (Continued)

SECTION	TITLE	PAGE NO.
4.2	SCANNER PERFORMANCE	4-8
4.2.1	General Image Quality	4-8
4.2.2	Wire Object Detection	4-9
4.2.3	Single Site Activation	4-10
4.3	SUMMARY OF WODS PERFORMANCE	4-11
5.0	CONCLUSIONS AND RECOMMENDATIONS	5-1

LIST OF APPENDICES

A	WIRE DETECTION SYSTEM ANALYSIS	A-1
B	EXPERIMENT TEST PLAN	B-1

LIST OF FIGURES

FIGURE	DESCRIPTION	FOLLOWING PAGE NO.
2-1	NUMBER OF SCANS REQUIRED VERSUS FALSE ALARM	2-10
2-2	SIGNAL-TO-NOISE REQUIREMENTS FOR WIRE DETECTION	2-12
2-3	DETECTION CHARACTERISTICS FOR EXACTLY KNOWN SIGNALS	2-12
2-4	BACKGROUND ESTIMATION-SIMPLIFIED BLOCK DIAGRAM	2-19
2-5	AREA ARRAY TRADE-OFF	2-42
2-6	CCD VS II/CCD (λ =.85 μM)	2-42
2-7	RESPONSIVITY COMPARISON OF CCD AND II	2-43
2-8	SYSTEM MTF - IMAGE INTENSIFIER	2-44
2-9	CROSSTALK CHARACTERIZATION OF 1728 ELEMENT CCD	2-44
2-10	WAVELENGTH TRADE-OFF	2-44
3-1	CCD ILID - 1728 SCHEMATIC ODD FIELD READOUT	3-2
3-2	CCD ILID - 1728 SCHEMATIC EVEN FIELD READOUT	3-2
3-3	ILID 1728 AMPLIFIER SCHEMATIC	3-3
3-4	FLOATING GATE AMPLIFIER CROSS SECTION	3-4
3-5	FLOATING GATE AMPLIFIER CONFIGURATION	3-5
3-6	EXPOSURE CONTROL OPERATION - DRAIN	3-6
3-7	EXPOSURE CONTROL OPERATION - INTEGRATION	3-6
3-8	EXPOSURE CONTROL OPERATION - READOUT	3-6
3-9	WAVEFORMS	3-6
3-10	METHOD OF OUTPUT DISPLAY	3-8
3-11	SIMPLIFIED ARRAY TIMING DIAGRAM	3-9
3-12	VIDEO PROCESSOR	3-9
3-13	WIRE OBJECT DETECTION SIMULATOR (WODS) TOP VIEW	3-13
3-14	WIRE OBJECT DETECTION SIMULATOR (WODS) REAR PANEL	3-14

LIST OF FIGURES (Continued)

FIGURE	DESCRIPTION	FOLLOWING PAGE NO.
4-1	SIGNAL OUTPUT VERSUS EXPOSURE CONTROL VOLTAGE (NORMAL MODE)	4-4
4-2	SIGNAL OUTPUT VERSUS EXPOSURE TIME (GATING MODE)	4-4
4-3	PROPAGATION CHARACTERISTICS	4-5
4-4	TEMPORAL PHASING	4-5
4-5	GATING WITH INFRARED DIODE (500 NSEC)	4-6
4-6	GATING WITH XENON FLASH LAMP	4-6
4-7	WODS IMAGE QUALITY - PICTORIAL	4-8
4-8	WODS IMAGE QUALITY - TV TEST TARGET	4-9
4-9	WODS WIRE DETECTION	4-10
4-10	SINGLE SITE ACTIVATION: ILID 1728 ARRAY	4-10

LIST OF TABLES

TABLES	DESCRIPTION	FOLLOWING PAGE NO.
2-1	WIRE OBJECT DETECTION SYSTEM REQUIREMENTS	2-2
2-2	MINIMUM REQUIREMENTS FOR OBJECT DETECTION	2-11
2-3	EFFECT OF SHARP TRANSITION UPON BACKGROUND ESTIMATE	2-20
2-4	SYSTEM PARAMETERS	2-42
2-5	SILICON ARRAY VERSUS IMAGE INTENSIFIER CCD CHARACTERISTICS	2-42
2-6	SILICON ARRAY VERSUS IMAGE INTENSIFIER CCD TRADEOFF	2-42
2-7	WAVELENGTH TRADEOFF PARAMETERS	2-43
3-1	CCD 1728 PINOUT DESCRIPTION	3-7
3-2	EXPOSURE CONTROL SETTINGS	3-13
3-3	SWITCHES - LAYOUT	3-13
4-1	SIGNAL OUTPUT - NORMAL MODE	4-3
4-2	SIGNAL OUTPUT - GATING MODE	4-3
4-3	SIGNAL SITE ACTIVATION DEMONSTRATION	4-9

1.0 INTRODUCTION

Fairchild Imaging Systems has completed Contract DAAB07-76-C-0881 for the U.S. Army Electronics Command, Avionics Laboratory. This effort has addressed leading technology areas required for wire obstacle detection as based upon the use of a charge coupled device (CCD). The present effort has emphasized two separate aspects of wire detection: analytic studies of wire detection, and, secondly, an experimental feasibility demonstration of wire object detection using a charge coupled device. The technical discussion of Section 2.0 is organized to explore the utility of a CCD device for wire object detection. Several possible approaches to CCD wire detection are outlined in terms of optical radar principles, scanning requirements, detection statistics, and gating capability. Based upon available and projected components, a trade-off study has been performed to identify the optimum detector choice for use at different laser wavelengths.

In Section 3.0 the specific camera used for the feasibility demonstration is described in detail. It is shown how one particular CCD array, the Fairchild ILID 1728, provided the basis for both the single site activation, and gating experiments required for a full feasibility demonstration. The architecture of this array is explained and is shown to be compatible with the goals of this contract. Lastly, all camera controls and operating procedures are reviewed.

Section 4.0 contains the experimental data for both the gating and single site activation tests. Photographic records of oscilliscope and TV images are displayed. System performance is fully characterized.

Section 5.0 reports the conclusions derived from the previous studies and feasibility experiment: recommendations for further development of a CCD wire obstacle detection system are outlined.

2.0 TECHNICAL DISCUSSION

There is a need for a reliable, low cost, sensor system to provide detection and recognition of wire objects in the flight path of helicopters flying in nap-of-the-earth missions. Typically, missions of interest may take place in night conditions. Wire objects in the flight path represent serious hazards which must be detected and recognized in a timely way so that the pilot may execute evasive maneuvers. Wires as small as 1/8" in diameter cannot normally be detected in real time by the pilot at night by direct vision or aided vision due to the basic resolution limitations.

In general a dedicated sensor is required to perform the wire detection task which will provide an instrumental decision defining the presence of a wire object in the field-of-view. Such a sensor would be expected to serve as an automatic warning device when a pattern characteristic of a wire is within the FOV. The sensor is then a multi-function instrument which performs a complete sequence culminating in a warning. In this report we will be addressing the primary detection of a wire via a CCD as well as the requirements upon the organization of data by the scanning configuration. The specific pattern recognition problem will only be introduced to help define the detection statistics required to succeed in the task.

The technical approach used in this study is to define the overall system requirements for a WODS sensor in a realistic mission, use this information to characterize component technology issues, and lastly, perform a trade-off analysis for the purpose of choosing an optimum system.

The next section will describe the system requirements for wire object detection.

2.1 REVIEW OF WIRE OBJECT DETECTION

In operation, a potential WODS device would be mounted on a helicopter and would be used to scan the forward field-of-view along the flight path to detect the presence of a wire object. The laser actively illuminates the wire object and the backscatter is detected in a suitable way to identify the range to the wire as well as spatial location with respect to the flight vector of the helicopter (azimuth and elevation).

The general system requirements for this task are shown in Table 2-1. Wire obstacles as small as 1/8" may be hazards and must be detected at ranges of 300 meters to 1 kilometer.*

A gating pulse duration of 300 nSEC is considered as the maximum useful gating time consistent with WODS requirements. This gating time would allow detection of a wire in a slug of space corresponding to 90 meters. Ideally, however, the WODS system may be required to work in situations with much better range discrimination. In this study we will determine the achievable gating times for various detectors.

The output from the WODS sensor pertains to the presence of wires within a 10 Deg x 15 Deg FOV. Therefore, assuming total areal coverage the total number of pixels, N to be explored to test for a 1/8" wire at one KM is given by

---

* The factors described in Table 2-1 are consistent with a nap-of-the earth (NOE) helicopter mission.

$$N = \frac{(.175 \text{ radians})\ (.262 \text{ radians})}{(3.175 \times 10^{-6} \text{radians})^2} \qquad (2.1)$$

$$= 4.53 \times 10^9 \text{ pixels}$$

This large number of pixels imposes severe penalties upon bandwidth, resolution, and processing, and is beyond any reasonable detector at the present time. Therefore, it is clear that the WODS task requires techniques outside of traditional imaging methods.

A second approach that is useful for the WODS task is based upon non-resolved detection. This case is to be contrasted with imaging because the non-resolved datum of the wire is localized to only one pixel and cannot be further decomposed because it has no spatial structure. Thus for a resolution of 0.1 MRAD as given in Table 2-1 all the energy returned from the wire (of about 3 microradian subtance) will fall in one pixel. This is true as long as the point spread function of the optics and detector is small with respect to the pixel size. In fact, this localization of energy leads to activation of only a single pixel site and so is a suitable criteria for the presence of a hit to determine a resolution object. In a separate contract "Single Site Activation Logic And Display" FISD has characterized the computer processing scheme that results from this approach.

For a linear CCD array aligned in the vertical direction, the required number of pixels at 0.1 MRAD resolution is 1745 elements. The minimum wire subtends only 3% of the resolution cell by projection. However, the total number of pixels is given as before,

$$N = \frac{(.175)(.26)}{(.1 \times 10^{-3})^2} \quad = \quad 4.56 \times 10^6 \qquad (2.2)$$

TABLE 2-1

WIRE OBSTACLE DETECTION SYSTEM

SYSTEM REQUIREMENTS

OBSTACLE:	1/8" to 1" WIRE-LIKE OBJECT	
	SIGNATURE TO BE SPECIFIED	
PLATFORM:	HELICOPTER	
TYPE OF SYSTEM:	OPTICAL RADAR (NON IMAGING)	
OUTPUT:	ELECTRO-OPTICAL SUBSYSTEM-	
	BINARY DECISION OF PRESENCE OF WIRE OBSTACLE	
	PROCESSING SUBSYSTEM-ALARM/CONTROL	
ILLUMINATION SOURCE:	GATED SOURCE	
	TO BE SPECIFIED	
SCAN FACTORS:	SCAN VOLUME: 10 DEG HOR X 15 DEG VER	
	RESOLUTION: 0.1 MRAD	
	FRAME RATE: 1 PER SECOND TO 2 PER SECOND	
RADAR FACTORS:	OPERATIONAL RANGE:	300 M - 1 KM
	RANGE DISCRIMINATION:	≤ 90 M
	GATING TIME:	≤ 300 n SEC

For frame rates of 1-2 seconds, the resulting pixel rates are well within state-of-the-art.

The general principles of optical radar has been examined in detail in Appendix A. This approach differs from usual imaging or gated low light level TV in that integration over consecutive laser pulses is not allowed. Detection of wires in each pixel must be accomplished by processing a single pulse return.

Secondly, a wire object will be "recognized" by a suitable algorithm (digital processing) by tracking the spatial characteristics of the single site activations across the scanned frame. In Section 2.3 the scanning requirements are discussed.

It is the goal of this contract to investigate the utility of CCD devices for the WODS task because they appear to offer significant advantages for wire detection systems. These advantages include:

- Low weight, small size
- Low cost in production
- High near IR sensitivity
- Possibilities for "on chip" gating
- High metricity
- Compatibility with digital processing
- High reliability
- Flexibility in choice of formats
  Sequential video data accessibility

This report will emphasize the choice of formats and gating characteristics.

2.2. DETECTION REQUIREMENTS

This section defines the wire-like object detection problem in terms of optical radar principles.

The exact single site detection statistics are defined in terms of the probabilities of detection and false alarm for signals governed by the Poisson probability function. The process of detecting a wire segment is explored and characterized in terms of the noise in each pixel. An estimate of the number of scans required to detect a wire-like object is made when such noise is present.

Finally the general signal-to-noise ratios are presented for the WODS task.

2.2.1 Input To The Processing Algorithm

Assume that the input to the processor is a matrix of binary ones-or-zeros representing the detection of events in the "scene". Specifically, assume that the video information at each pixel location has been thresholded. Pixels where the energy density from the "scene" is higher than some predetermined value produce a "1" condition, otherwise a "0" condition. Due to the presence of the threshold and the binary decision the "image" with its associated grey levels is replaced by a unit contrast "image" with zero dynamic range. This is, in fact, probably necessary if a realistic processing algorithm is to be used. Consequently, the manner in which the "image" is treated is not like conventional image analysis but more akin to the point source detection treatment of optical radar applications. Therefore, we assume that each pixel input is characterized by:

1. State, 1 or 0
2. Minimum probability of detection, Pd
3. Maximum false alarm, Pfa
4. Location in a raster

2.2.2 Review Of Poisson Detection Statistics

We will assume that the signals are represented by the Poisson probability density function. At large flux densities the proper distribution may be Gaussian (for example) but the fact remains that the statistics of detection cannot be better than Poisson. Given a mean value of signal from the target wire, Nt, and from the background, Nb, the mean value is still Poisson. Therefore, the probability of detection is given by:

$$Pd = \frac{\sum_{x=\lambda}^{\infty} \frac{(N)^x e^{-N}}{N!}}{\sum_{x=0}^{\infty} \frac{(N)^x e^{-N}}{N!}} \qquad \text{Where } N = Nt + Nb \tag{2.3}$$

Where λ = threshold yielding the cummulative probability of detection. The value λ must be determined numerically. Once set (in equivalent electrons) λ will determine the reliability of the detection. Further, when the background level Nb is known λ will determine the value of N that must be received from the target.

The probability of false alarm is now defined by the probability of detecting noise alone (nb) when the threshold is set.

$$Pfa = \frac{\sum_{x=\lambda}^{\infty} \frac{(Nb)^x e^{-Nb}}{(Nb)!}}{\sum_{x=0}^{\infty} \frac{(Nb)^x e^{-Nb}}{(Nb)!}} \tag{2.4}$$

For given signal (Nb + Nt) the threshold is chosen according to a suitable criteria. For the WODS task the consequence of not detecting a wire-like object when it is present is very serious so that the Pd must be set as high as possible while allowing some tolerable background level. The set of parameters Pd and Pfa (with threshold value implicit) defines the single site statistics.

2.2.3 Wire Detection - Definition

In a wire detection system the stream of binary inputs to the processor must be searched for configurations of "ones" which indicate a wire. Specifically in the following we will assume that the data stream is organized into a raster and that a wire will consist of a string of "ones" in a curve basically described as a catenary ($Y = a \cosh (x/a)$). However, it is realized that the wire "hits" can take on a large number of shapes due to optical blurring, the angle of the wire, the steepness of the wire curve, and the probabilities that the wire crosses the intersection of cells providing dropouts or multiple hits. Secondly, the wire may be very long or very short. For these reasons the number of steps required in the processor may be large and in general, a real time processor may be required to operate at many times the sampling rate of the sensor if reasonable refresh rates are required.

We will search an MXL array of pixels for a short line segment. The length of the short line segment is strictly a function of the Pd in each single site. For example, if the minimum length of a wire segment is 7 pixels long and the single site Pd = .9986, the probability of detecting a wire when present is $(Pd)^7 = .990$. The conclusion is that the threshold must be chosen as low as possible to guarantee high confidence in detecting a short line segment.

For complete coverage of the FOV due to various optical effects, the single site hits may appear in contiguous (touching) or proximate (near but not touching) patterns. For this study we restrict ourself to the following conditions:

1. Hits are contiguous
2. The wire segment is a straight line
3. W contiguous hits are required to detect a wire.

These assumptions can be extended as required or specialized to other scan patterns.

2.2.4 Estimate of Spurious Detections

Once the pattern that would be interpreted as a wire-like object is defined, it is possible to estimate how often false alarms only would randomly occur in such a pattern. This estimate, nf, is given as:

$$nf = a \cdot b \cdot c \cdot (Pfa)^W \qquad (2.5)$$

a = number of configurations of a W-long line segment that are contiguous and linear

b = number of ways of counting a W-long line segment in a M x L array in one direction only

c = number of rotations that must be explored to determine if a wire-like object is present

$(Pfa)^W$ is the probability of occurrence of a W-long line segment due to false alarms only

W = Number of contiguous hits required for detection.

Estimates of these factors are as follows:

Configurations:

From the above definition of a line segment the line must occur in a 2 x W array where either site in each 2 x 1 must be a "1". Then the number of such configurations is $\approx 2^W/2$.

Therefore,

$$a = 2^{W-1} \tag{2.6}$$

Displacements

Consider a L x L sub-array of the M x L array. The number of ways a W long-line segment can be counted in the L x L array is

$$L \quad (L + 1 - W) \tag{2.7}$$

in the parallel direction only

and, for the entire M x L array we have

$$b = \left(\frac{M}{L}\right) \quad (L) \quad (L + 1 - W) \text{ parallel only} \tag{2.8}$$

Rotations

Consider one pixel in the middle of a L x L array. The number of angles that can be defined is simply the circumference of the array divided by the minimum definable increment along the circumference. Therefore,

$$c = \frac{4L}{(\theta_{MIN} \quad L)} = \frac{4L}{L \tan^{-1}\left(\frac{1}{L}\right)} = 4L \tag{2.9}$$

for large L

Therefore, the final expression is:

$$nf = 2^{W-1} \quad (4L) \quad L \quad (L + 1 - W) \left(\frac{M}{L}\right) (Pfa)^W \tag{2.10}$$

Now we assume that W = L and find an expression when the length of the line segment is equal to the number of scans made by an M x L array.

$$nf \approx 2^{L-1} \ (4LM) \ \ (Pfa)^{L} \qquad (2.11)$$

This is a simple expression that has important consequences. Figure 2-1 shows the plot of probability of false alarm, Pfa versus the number of scans required to detect the object with given false alarm.

Figure 2-1 shows the number of scans required versus false alarm rate (single site). As expected, the algorithm is more efficient in discriminating against "spurious wires" when the initial noise is low. On the other hand, as the noise becomes very high the burden upon the algorithm becomes severe and in the extreme may not converge at all. This curve gives us the basis for a trade-off between the number of scans required and the Pfa. In the rest of this report we will assume that Pfa = .02 and Pd = .9976 is a good compromise for detection with 7 raster lines.

2.2.5 Effect Of False Alarm Rate

The time, T, it takes to get one false alarm is given by:

$$T = \left[nf \ . \Delta \ . \ \frac{L'}{L} \ . \ 3600 \right]^{-1} \ \text{Hours} \qquad (2.12)$$

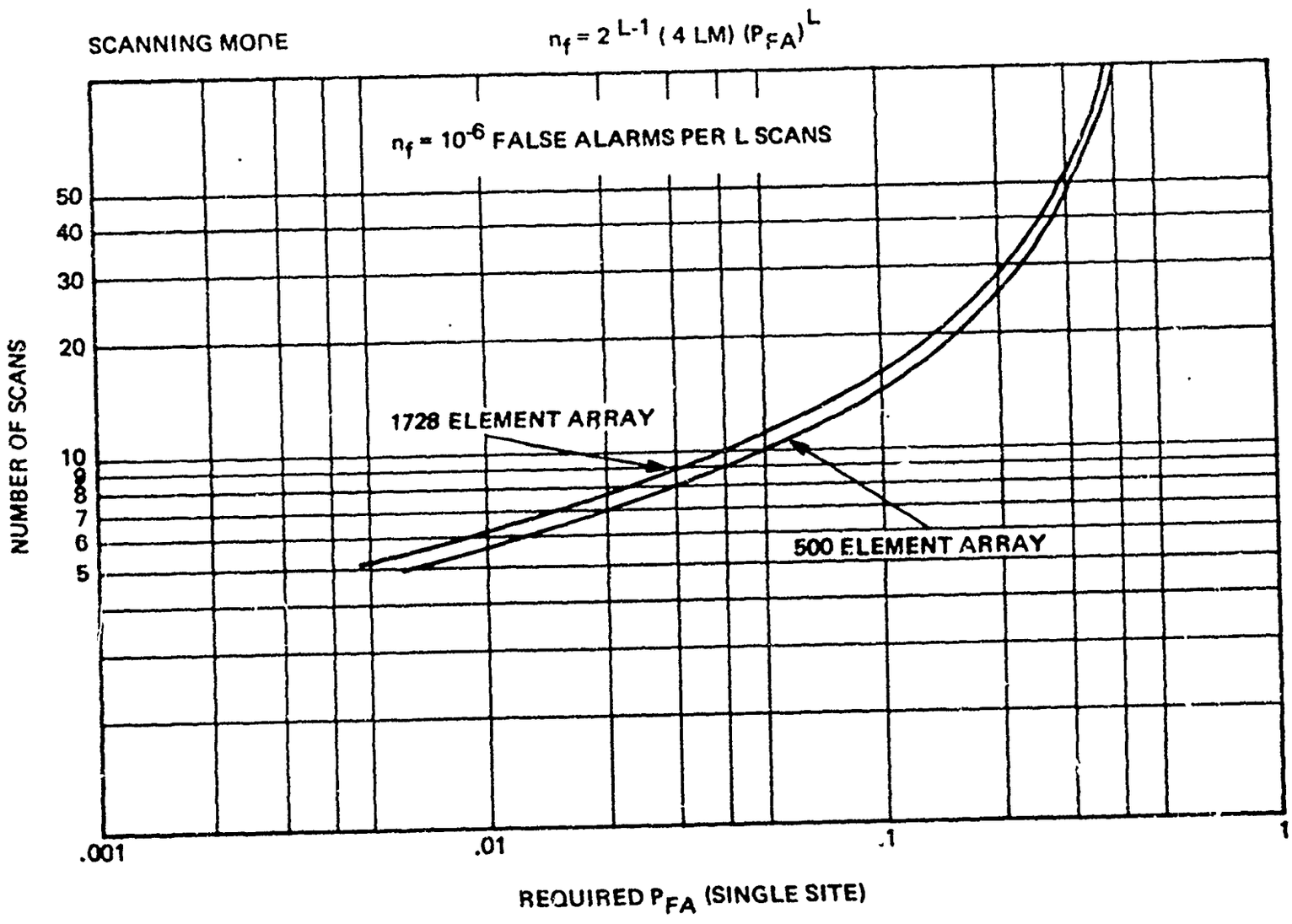

FIGURE 2-1 NUMBER OF SCANS REQUIRED vs P_{FA}

76-850

Where

nf = Spurious detection per L scans (calculated above)
Δf = Refresh rate (H_z) ($.5H_z$)
L' = Total number of scans (200 to 2000 per second)
L = Number of scans to detect wire-like object

For typical values we have

$$T = \left[10^{-6} \ (.5) \ \frac{(2000)}{7} \ (3600)\right]^{-1} = .94 \text{ Hours} \qquad (2.13)$$

The value, T, is to be interpreted as a "computed time before false alarm". In other words, the algorithm is very efficient in discriminating against false alarms due to the random alignment of noise patterns in the configuration expected for real wires.

2.2.6.1 Generalized Requirements for WODS

The previous arguments have established reasonable values for the probability of detection Pd = .9986 and Pfa = .02 as based upon a random detection process and a generalized algorithm. We will use this information to establish the minimum values of electrons due to the background, Nb. The results can be expressed as minimum contrast values and as signal-to-noise ratios for the phenomena which will allow detection. These requirements can be expanded to include a non-ideal sensor to determine the actual limits on performance as a function of sensor paramenters.

Table 2-2 shows the minimum requirements for wire detection based upon noiseless sensor and random statistics. The table is obtained by a numerical solution to equations (2.3) and (2.4)

For every value of background level a threshold can be chosen to yield the required Pfa against background. Given this threshold condition a minimum value of target return is required to yield the high Pd. As we see, the exact threshold is a function of the background level itself. Conversely, once the threshold is set, the value of target return required will allow us to scale the laser illuminator in a practical way.

Figure 2-2 shows a plot of the mean value of target return versus the mean noise in equivalent electrons at the input. This curve can be particularized to a CCD by using the CCD noise equivalent signal NES, to define the total noise. In this treatment the NES is the square root of the total noise of the detection process. The values of 20 and 50 electrons shown on the curve are characteristic of state-of-the-art linear arrays with floating gate amplifiers (see Section 3). Also on this plot the required linear and log SNR is shown for comparison.

Figure 2-3 shows a typical radar detection case which emphasizes that our analysis is consistent with radar principles.

2.2.6.2 Extension To Practical Cases

We have defined the exact SNR required for detection of wire-like object to achieve specific detection reliability. We must interpret these SNR values as that required at the moment of threshold. However, practical radar systems may be degraded by a number of factors including:

1. Target signature
2. Atmospheric channel
3. Platform motion
4. Detector internal noise
5. Transmitter characteristics
6. Background (scene) factors

TABLE 2-2

MINIMUM REQUIREMENTS FOR OBJECT DETECTION (1,2)

SINGLE SITE

Pd .998

Pfa .02

SIGNAL (Nt+Nb)	THRESHOLD Pd = .998	ALLOWABLE BACKGROUND	MINIMUM TARGET Nt	MINIMUM CONTRAST	MINIMUM SNR
10	2	.21	9.79	.979	3.09
20	8	3.3	16.7	.835	3.75
50	31	20	30	.60	4.24
80	56	41	39	.4875	4.36
100	72	55	45	.45	4.5
150	116	95	55	.366	4.49
200	161	135	65	.325	4.59
1,000	909	847	153	.153	4.84
10,000	9,712	9,508	471	.049	4.90
100,000	99,089	98,440	1,559	.0159	4.93
1,000,000	997,120	995,063	4,937	.0049	4.94

Reference (1) "Tables of the Individual and Cumulative Terms of the Poisson Distribution" 1962 D. Van Nostrand Company, Inc.

(2) "Handbook of Mathematical Functions" U.S. Govt. Publications, 1970

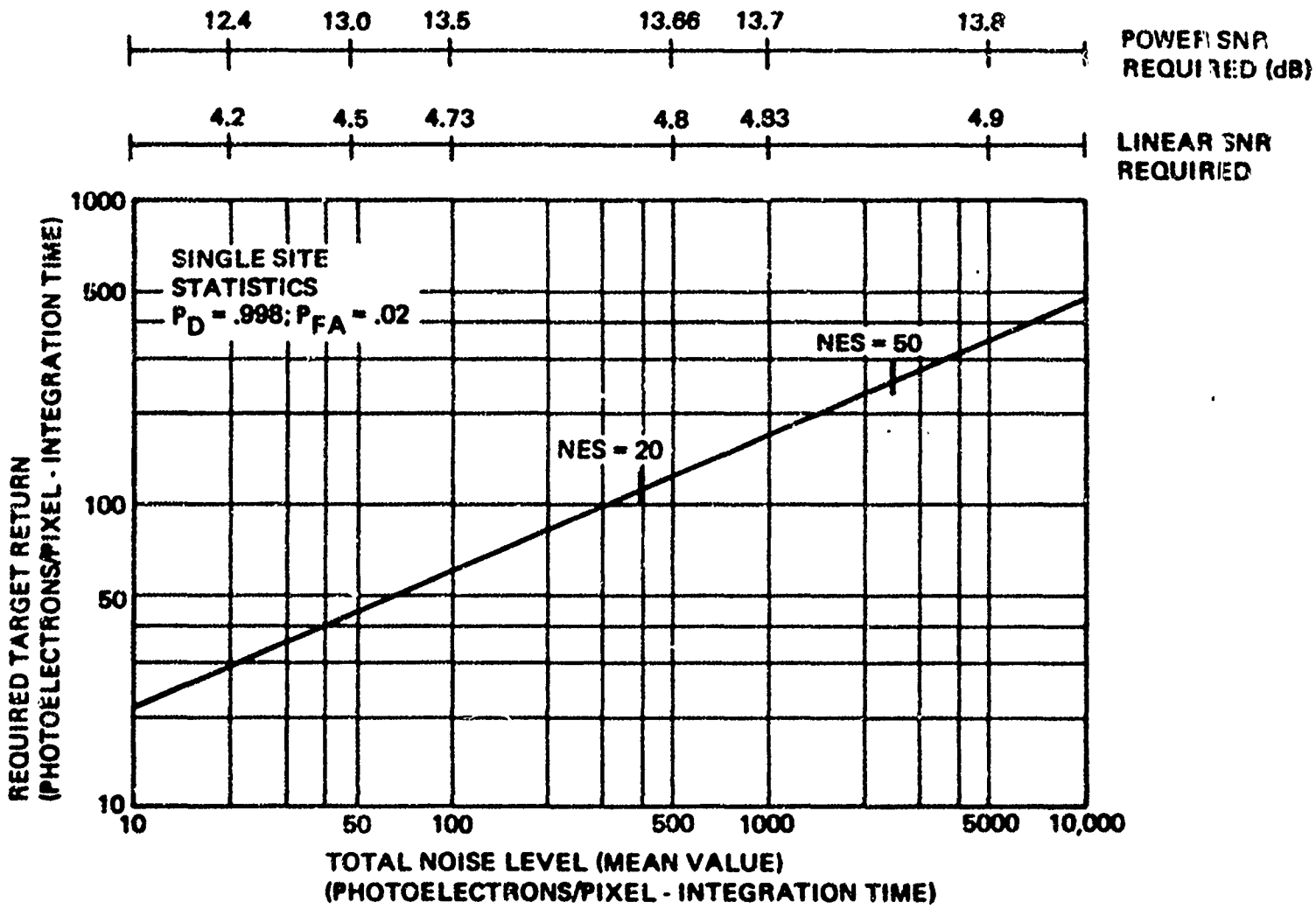

FIGURE 2-2 SNR REQUIREMENTS FOR WIRE DETECTION

(SINGLE SITE STATISTICS P_D = .998, P_{FA} = .02)

76-858

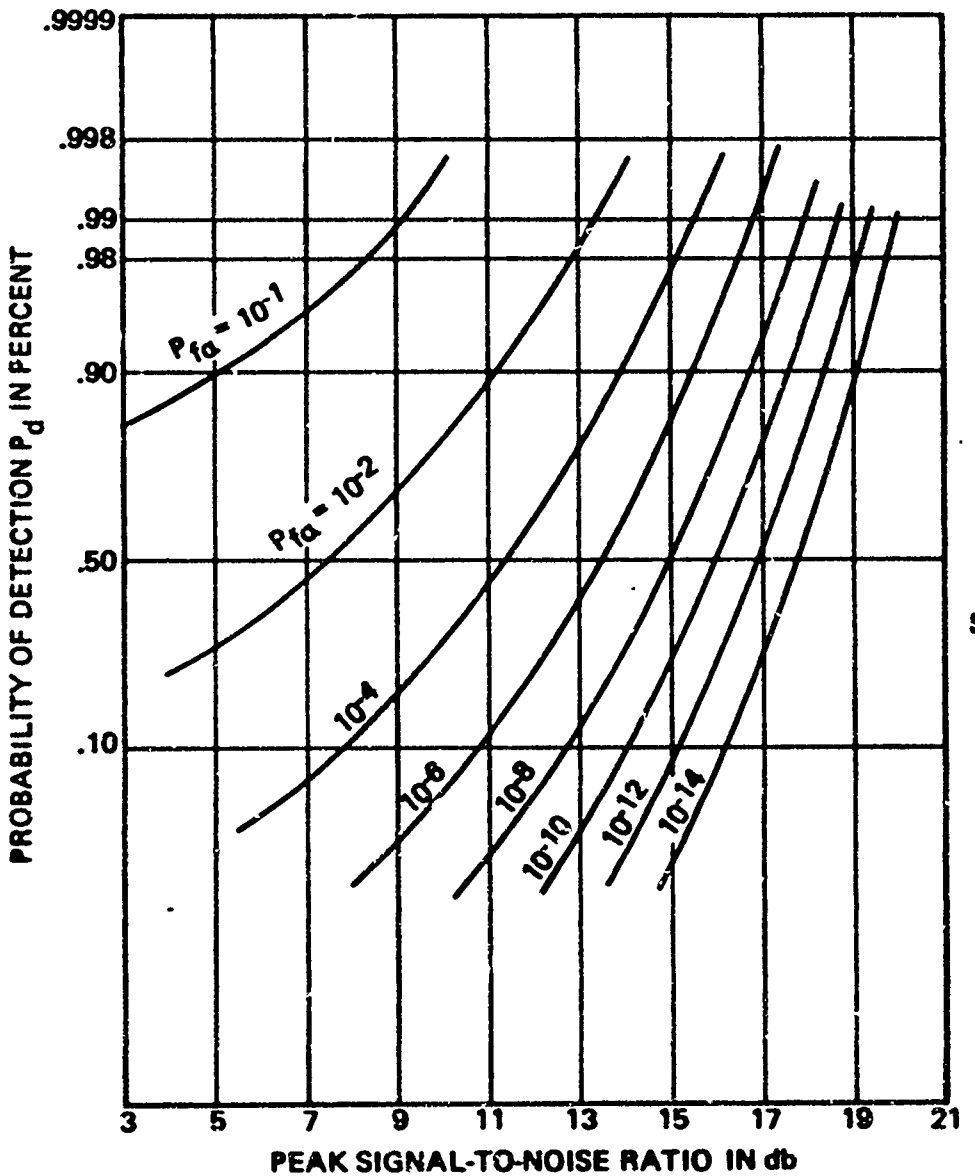

SNR_{db} = 20 LOG (LINEAR SNR)

FIGURE 2-3

DETECTION CHARACTERISTICS FOR EXACTLY KNOWN SIGNAL

The effect of each of these factors is to limit the achievable SNR. We are now in a position to consider each of these factors in order to define the overall system requirements.

2.2.7 Background Noise Effects

In the wire object detection task, single pixel activations that are not due to wire objects may contribute to false alarms. The sources of such false alarms can be due to scene related effects or to internal detector noise. Scene effects may include ambient illumination characteristics such as sky/terrain transitions, or laser backscatter from ground terrain. Internal noise may include detector dark signature, amplifier noise and fixed pattern noise. Both these types may be termed background noise effects.

The manner in which these background effects are handled is an important subject which affects the reliability of the WODS sensor. The effect of background noise is discussed from the point of view of signal-to-noise ratio and errors caused when the background noise has sharp transitions.

An optimum smoothing technique is outlined that can reduce some of these difficulties. The signal-to-noise ratio for cases including smoothed background estimates is derived.

This analysis shows how the required laser power in the WODS task can be minimized for both quantum noise and detector limited systems.

Finally, a background smoothing technique is explored in terms of detection error due to sharp transitions in the scene background.

2.2.7.1 Signal-To-Noise-Ratio

Consider the case where a background estimate is obtained from a linear average of n pixels (excluding the pixel that conditionally includes the target return). We include the effect of mean sensor noise equivalent input, N, and form the relevant parameters as follows:

Mean Value of Background Estimate

$$\bar{N}_b = \left[nN + nN\right] /n = N_b + N \tag{2.14}$$

The averaged RMS noise is given as

$$(\bar{N}_b)_{RMS} = \frac{1}{n}\left[n(N_b + N)\right]^{1/2}$$

$$= \left[\frac{(N + N)}{n}\right]^{1/2} \tag{2.15}$$

The assumed contents of the pixel including the target return NS, is given by

$$N_s = (N_t + N_b + N)$$

Subtraction of the "target pixel" from the background estimate yields the estimate of "target" electrons

$$(N_t + N_b + N) - (N_b + N) = N_t \tag{2.16}$$

The noise after the subtraction process is given by the RMS value

$$(\bar{N}_s)_{RMS} = \left[\frac{(N_b + N)}{n} + (N_t + N_b + N)\right]^{1/2}$$

$$(\bar{N}_s)_{RMS} = \left[(N_t + (1 + \frac{1}{n}) (N_b + N)\right]^{1/2} \tag{2.17}$$

Where the conventional noise without averaging is given as

$$(\bar{N}_s)_{RMS} = \left[(N_t + 2 (N_b + N)\right]^{1/2} \tag{2.18}$$

Therefore, we see that some theoretical advantage is obtained as the background estimate is made more reliable by the use of more samples. For small target returns the maximum ratio of the noise "enhancement" is given by the ratio of EQN. (2.17) and EQN. (2.18). This ratio is:

$$\frac{(\bar{N}_s)_{RMS}}{(N_s)_{RMS}} \quad \text{or} \quad \frac{(1 + 1/n)}{2} \quad \text{for } N_t \neq 0 \qquad (2.19)$$

for large N the maximum reduction of noise = $(0.5)^{1/2} \approx 0.707$
Note that the noise in the estimate of the background, N , goes as the square root of the number of pixels integrated-as expected for an incoherent integration process. However, the noise reduction in the subtraction process can never be better than a factor of 0.707. The SNR ratio after detection is given by the following:

$$SNR = \frac{m N_t}{(N_s)_{RMS}} = \frac{m N_t}{\left[m N_t + (1 + \frac{1}{n})(N_b + N)\right]^{1/2}} \qquad (2.20)$$

Where m = modulation transfer function
N = internal noise of detector element
Setting the SNR output equal to the SNR required to detect with suitable single site statistics (SNR) req, we can solve for N_t as a function of the (SNR) req and the noise in the system. The exact solution to the resulting quadratic equation is:

$$N_t = \frac{(SNR)^2_{req}}{2m}\left[1 + \left\{1 + \frac{4\left(1 + \frac{1}{n}\right)(N_b + N)}{(SNR)^2_{req}}\right\}^{1/2}\right] \qquad (2.21)$$

This equation allows us to determine the exact laser energy required for any set of parameters. We see that the estimation of the background level by integration can lead to some improvement in the SNR - or reduction in laser transmitter power.

We distinguish two important cases

Case 1) SENSOR NOISE LIMITED

For example, in a CCD with a floating gate amplifier the noise equivalent signal (NES) is typically on the order of 50 electrons. Thus,

$$NES = \sqrt{N} = 50$$
$$N = 2500$$
$$N_t = 55 \text{ for } t = 0.3 \text{ usec}$$
$$N_t << N$$

Consequently, equation (2.21) reduces to

$$N = \frac{(SNR)req \cdot (NES) \cdot \left(1 + \frac{1}{n}\right)^{1/2}}{m} \qquad (2.22)$$

and the detection process is CCD noise limited.
Averaging over many pixels will tend to reduce the effect of NES variation from pixel to pixel (by factor of $(1 + {}^{1}/_{n})^{1/2}$) but the value of the threshold will be essentially the same.

Case 2) SIGNAL NOISE LIMITED

When the internal noise is very small - as is true of many image intensifiers, equation (2.21) becomes

$$N_t = \frac{(SNR)req \cdot \sqrt{N_b + N_t} \cdot \left(1 + \frac{1}{n}\right)^{1/2}}{m} \qquad (2.23)$$

Where N_t replaces the value of N because it contributes to noise.

In this case the detection process is quantum noise limited. Fruthermore, the averaging process described above will be very sensitive to the level of the background itself. In this case the estimate of N_b can be used to define the optimum threshold. It is useful to consider an adaptive threshold to optimize the detection process.

2.2.7.2 Fluctuations

In addition to the noise reduction inherent in smoothing properly chosen implementation can help to adaptively discriminate against background effects such as change of level or edge gradients.

The mathematical procedure outlined below is included in this analysis in order to provide a definitive way to establish the mean value of the background return. Once established, this estimate of background can be used to calculate a threshold required to achieve a specific signal to noise ratio by simple multiplication. This procedure allows the WCDS algorithm to be relatively immune to terrain features such as leaves, tree branches, and similar effects. In this way a true single site activation can be obtained and the smoothing/threshold setting proceedure becomes a vital link in converting the analog single to a valid binary (0 or 1) output.

We will define a transversal filter which offers utility in optimizing the background estimate in many situations. This type of filter has had great success in smoothing and peak detection for many applications including spectroscopy. (3)

(3) Golay and Savitsky, Analytic Chemistry, Vol. 36, 1964 "Smoothing and Differentiation of Data by Simplified Least Squares Procedures."

Secondly, we will display numerical examples demonstrating the accuracy when edge gradients are in the FOV.

DEFINITION OF FILTER

A general transversal filter can be constructed to operate on the incoming data stream. The filter is assumed to have the following form:

$$\bar{A}_n = \frac{1}{N}\sum_{-m}^{+m} W_m \cdot A_{n-m} \; ; \quad (m<n) \qquad (2.24)$$

Where An-m is the detected level at pixel n delayed (advanced) by index m

W_m = The coefficient (weight) multiplying the pixel contents at the (n-m) position.

$\bar{A}_n$ = The estimate of the contents of pixel at location n.

N = normalizing constant.

A simple interpretation of this equation is that the transversal filter is a 2m-element delay line where the W_m are the weights of the taps. This filter is operating in the spatial domain. The result is that the new estimate of A_n will be smoothed by a factor $\sqrt{2m}$ which is due to incoherent addition.

Figure 2-4 shows a simplified block diagram describing how such a filter operates on the incoming data for a 5 element filter. The output of the filter is used to set an accurate threshold - possible by means of a look-up table.

The coefficients W_m control the accuracy of the estimate. In the simplest case, all the coefficients can be set to unity leading to a moving average.

On the other hand the coefficients can be chosen to extract the best fit to a polynomial in a least square sense. For most types of noise this procedure will lead to an optimum estimate of the value.

The paper of Reference 1 shows how to set the coefficients to simple integer number for high order least square functions. The following summarizes the coefficients calculated in the reference.

TYPE	LENGTH	CO EFFIEIENTS
Quadratic	5-elements	-3,12,17,12,-3
Smooth		Norm = 35
Cubic	7-elements	5,-30,75,131,75,-30,5
Smooth		Norm = 231

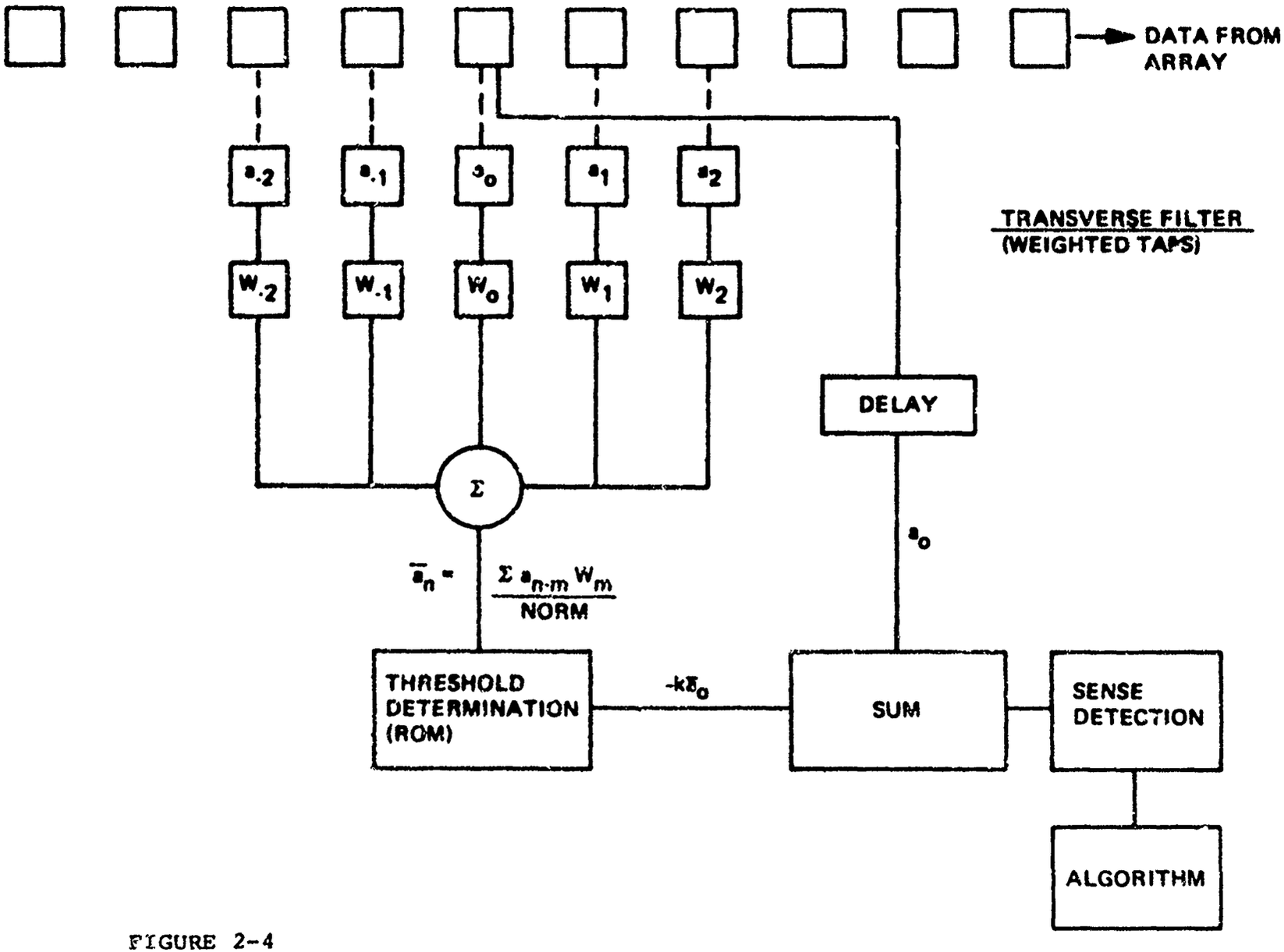

FIGURE 2-4

BACKGROUND ESTIMATION - SIMPLIFIED BLOCK DIAGRAM

Table 2-3 shows the result of these smoothing filters when a sharp edge transition is within the FOV. The value Nb represents the contents of each pixel. Two transitions, from 20 to 60, and 60 to 200 are assumed to be within the FOV. The linear, quadratic, and cubic smoothed values are shown. The error, the true value minus the estimated value, is also shown.

As an example of the power of this technique we note that the error for the linear fit is very high near the transition considering the transition at pixel position 7-8. The true value is 40. The linear value will be 40 / 2 because four points are used in the fit. The theoretical error for the quadratic and cubic fit is 17.8 and 15.1, respectively. However, the calculated error is almost a factor of two less. The reason is that the mathematical constraint of "least square" forces the error at any particular point to distribute itself along the whole curve. Therefore, the estimate will be truly optimized.

A practical advantage of such a filter, other than its simplicity, is that it is suitable for use with signal levels which vary over many magnitudes - as is expected in the WODS application.

The least square procedure will be effective as long as the data does not rapidly fluctuate in the length of the filter.

In an application of this technique to the WODS task we must reorganize the algorithm somewhat so that the pixels including the assumed target are not included in the smoothing. This can be achieved by setting the weight (Wo) of the center tap in the filter equal to zero and renormalizing the entire set of weights.

TABLE 2-3

EFFECT OF SHARP TRANSITION UPON BACKGROUND ESTIMATE

		LINEAR		LEAST SQUARE CURVE FIT			
		$\overline{4}$		Quadratic (5)		Cubic (7)	
Pixel Position	An	- An	Error	- An	Error	- An	Error
1	20	20	0	20	0	20	0
2	20	20	0	20	0	20	0
3	20	20	0	20	0	20	0
4	20	20	0	20	0	20	0
5	20	20	0	20	0	20.86	-0.86
6	20	30	-10	16.57	+3.4	15.67	+4.32
7	20	40	-20	30.28	-10.3	28.65	-8.65
8	60	40	+20	49.71	+10.3	51.34	+8.65
9	60	50	+10	63.42	-3.4	64.33	-4.33
10	60	60	0	60	0	59.13	+0.86
11	60	60	0	60	0	60	0
12	60	60	0	60	0	63.03	-3.03
13	60	95	-35	48	+12	44.84	+15.13
14	60	130	-70	96	-36	90.30	-30.31
15	200	130	+70	164	+36	169.69	+30.31
16	200	165	+35	212	-16	215.15	-15.13
17	200	200	0	200	0	196.96	+3.0
18	200	200	0	200	0	200	0
19	200	200	0	200	0	200	0
20	200	200	0	200	0	200	0

In summary, the least square curve fitting procedure outlined above can be used to provide an optimum estimate of background levels (or reduce the effects of sensor noise). The smoothing can be implemented by a relatively simple transverse filter operating on the data stream itself which can provide an adaptive system. Furthermore, the effect upon noise and signal-to-noise-ratios during the WODS task has been derived.

2.3 SCANNING REQUIREMENTS

Of the large number of potential scanning methods we have selected various promising types for further definition and study during the initial phase of the program. At the outset, we considered the interaction between the laser-transmitter and the receiver functions in an optical radar approach, the detector geometry, and the effect of finite gating times on the system performance. In the WODS task, the array geometry is governed by the need for simultaneous detection over a large number of detector elements in order to cover the specified field-of-view. Typical parameters most directly related to scanning methods are as follows:

Scan Volume: 10 DEG x 15 DEG
Angular Resolution: 0.1 MRAD
Frame Update: One per two seconds, minimum

Scanning methods fall into two broad categories, mechanical and electronic. Mechanical methods are generally the simplest when large systems are considered. One mechanical technique would be to place a scanning mirror in front of the lens. Placing the mirror in front of the lens means that its effective aperture has to be somewhat larger than the lens entrance pupil. The mirror aperture can be considerably reduced by placing it behind the lens, close to the CCD. However, in this case the location of the plane of best

image focus at the CCD will vary relative to the plane of the CCD photosites. The high speed, that is, low relative aperture of the lens (F/#) coupled with the high resolution of the CCD does not permit sufficient depth of focus to overcome the focal plane variation during the mirror scan.

A multifaceted polygon mirror could be rotated at constant speed to achieve the scanning. However, the small field of view (15°) coupled with the objective of keeping the dead time between successive scans to a minimum would result in a polygon with a large number of facets; 48 estimated facets total. Furthermore, the size of this polygon would be huge as each face would require a clear aperture somewhat greater than the lens entrance pupil divided by the Cosine of 45° if the line of sight is deviated by 90°. The effective pupil diameter for a 130 mm F/1.4 lens is 93 mm or 3.65 inches. Obviously, a slow scan fast flyback mirror is more suitable.

The mirror will have to be larger if it is called upon to simultaneously scan the illuminator over the FOV. Boresighting the camera lens and the illuminator lens through the same mirror and maintaining the boresighted condition throughtout the scan poses some additional complexity. One can take advantage of the long scan time and relatively small scan angle by mounting both the illuminator and the camera, boresighted together on the same assembly and oscillating the entire assembly to achieve the scan. This eliminates the mirror but the mass to be scanned is considerably larger. The flyback part of the scan cycle will impose the most stringent requirements on the scanning mechanism.

It is possible to reduce the severe requirement of the scanner by altering the scan cycle to be equal in both directions, i.e., scan the scene in one direction and instead of the fast flyback, scan the scene slowly in the return direction generating data all the time.

Electronic scanning techniques would be strongly dependent on the type of CCD utilized. In some instances the CCD selected may be influenced by the feasibility of scanning technique. For example an area array is electronically self-scanned in two directions. On the other hand a group of parallel linear arrays could be be scanned electronically if gaps are permissible in the FOV perpendicular to the wire direction. A mechanical flip-flop type image shifter could be combined with multiple linear or area arrays to fill in gaps in the FOV. Such a scanner could be considered as a combined electronic and mechanical scanner.

Another method of electronically scanning the CCD would be to use an image dissection tube. The tube could be altered with the linear 1 x 1728 CCD inside so that the electron beam image could scan across the CCD. Furthermore, gating could be added in the same tube. Again this avenue of approach appears to require a development program of its own.

It is clear that the final scan approach must have a high transmission in both the receiver and transmitter channels, must boresight both channels coincidently, and must be compatible with gating. That is, it must have a high receiver transmission during gate-on and a high rejection ratio during gate-off.

2.3.1 Review of Scanning Methods

2.3.1.1 Laser Illumination Pattern

The fundamental nature of optical radar limits the candidate scanning approaches to those which can be used to range gate. Range gating is a technique for precisely defining - and limiting - the position in space that contributes to the target return. Given the extended detector for the WODS task we can extract the azimuth and elevation position of the wire obstacle. Given the timing of the gating pulse and detection it is possible to determine uniquely the position in space that generates the detection. Without such a "range gate" the spatial information would be useless in real time operation.

The equations governing the range resolution are:

$$\text{Detection Range} \qquad Ro = \frac{C(\Delta t)}{2} \tag{2.25}$$

$$\text{Range Resolution} \qquad \Delta R = \frac{C(\Delta T)}{2} \tag{2.26}$$

Where Δt = Delay time - set at detector

ΔT = Pulse width - set at laser transmitter

C = Velocity of light

For example, if detection at 1 KM is required and a pulse width of 300 nsec is assumed, the delay is 6.66 microseconds and the range resolution is 45 meters. In order to increase the range discrimination it is necessary to decrease the laser pulse width. In this way it will be possible to detect a wire within 50 feet of a background such as trees if a 50 nsec pulse can be employed.

The maximum pulse repetition rate imposed by the two-way path will be 1 over (Δt + ΔT), or about 140KHz.

From the above discussion it is seen that the chief constraint imposed upon the scanning requirements is that the entire laser pulse can occur only over a time period on the order of 50-300 nsec in order that range discrimination be valid.

Secondly, the entire field-of-view subtended by the detector must be illuminated by the laser source during the gating time. This places strict constraints upon the system analysis. We have emphasized scanning systems in terms of the following factors:

- Angular scan rate
- Laser power
- Scan coverage
- Gating compatibility
- Registration accuracy
- Range discrimination
- Sensitivity
- Algorithm efficiency

2.3.1.2 Flying Spot Scanner

One approach to laser illuminator that may use laser power in an optimum way is the flying spot scanner. In this technique, the laser is focused (or collimated) into a spot with a divergence on the order of the spatial resolution required. We will consider here a raster scan although complex patterns could also be generated.

2.3.1.3 Polygon Scanner

Consider a raster scan where the total angular displacement is 10 Deg. Choose the beam size consistant with a .1 MRAD IFOV. Therefore, the minimum optical aperture diameter must be on the order of:

$$D = \frac{2.44\lambda}{\Delta\theta} \qquad (2.27)$$

(Rayleigh Criteria)
For typical parameters, λ = 1µm, a clear aperture diameter of at least about 2.0cm is required when working near the diffraction limit. One laser scanning geometry that would be useable is a collimated beam (of 2.0cm diameter) followed by a polygon scanner with a clear aperture of slightly greater than 3.0cm. The scanning speed per facet, V , will be:

$$V = \frac{10\ \text{DEG}}{(300 \times 10^{-9}\ \text{sec})} = 33.3 \times 10^{6} \times \frac{\text{DEG}}{\text{SEC}} \qquad (2.28)$$

This type of scan could also be achieved with other optics such as a rotating wedge or refractive polygons. The fact that the reflecting (or refracting) element is after the lens alleviates problems due to curved focal planes. Also note that the effective focal length of this type of illuminator is very large being on the order of the range to the object divided by the spot size (10,000 to 1). In general, the minimum facet size, L_{min}, is given as:

$$L_{MIN} = \frac{D\sqrt{2}}{\text{Sin}\left(\frac{\pi}{N}\right)} \qquad (2.29)$$

Where N = the number of sides of the polygon. For a 180 DEG scan N = 2 The minimum aperture is just 1.4D. For a 90 DEG scan L_{MIN} = 2D. For a 10 DEG required for WODS the number of sides = 36 and the L_{MIN} = 16.2D. This type of scanner is not suitable for narrow angles.

Moreover, we note that the WODS task does not require - and, in fact, is inconsistent with-the close packed continuous raster scan technique associated with a conventional polygon scanner. The "Radar Delay" prevents the adjacent facets from being used since it is evident that a WODS system will transmit a pulse only every MSEC or so. Therefore, the only requirement on the mirror scanner is that it sweep out a raster in 50-300 nsec. Therefore, a simple scanning or nutating mirror could be used.

2.3.1.4 Mirror Behind Lens

Consider the case where a nutating mirror is located between the collector aperture and a flat focal plane. The focal plane becomes a curved surface at the effective radius of curvature of the primary lens. As the mirror scans away from the optical axis, the true focal plane and the detector surface deviate by an amount called the saggita. This saggita, S, is given by the approximation:

$$S = \frac{X^2}{2R} \quad \text{(meters)} \qquad (2.30)$$

X = Linear distance off axis
R = Radius of curvature

However the depth of focus, d, of an optical system is given by:

$$d = \lambda \, (F/\#)^2 \qquad (2.31)$$

F/# = Aperture ratio
λ = Mean Wavelength

The saggita is to be less than the depth of focus for optimum detection to take place.[4] For example, let

$$S = d/2$$

Then $$\frac{x^2}{2R} = \frac{\lambda(F/\#)^2}{2} \qquad (2.32)$$

$$\therefore \quad x^2 = \lambda(F/\#)^2 \cdot (R)$$

For WODS $\lambda = .85 \times 10^{-4}$cm

R = 6.5cm (one half the focal length)

F/# = 1.4

Then $x^2 = 1.0 \times 10^{-3}\text{cm}^2$

$x = .033$ cm

Therefore, the mirror can be allowed to scan off axis only .33mm ($\theta = 0.14$ Degrees) before focus is lost. This is an entirely untenable system that will only work at full field F/numbers approaching 500.

In practice, we can allow the blur size to be equal to, but no larger than, the angular resolution. In the WODS task this is 0.1 MRAD. Therefore, behind the lens scanning is not possible for the WODS task for CCD devices with flat image planes. Other scanning techniques that have been investigated and rejected for the WODS application include focal plane/slit scanning, raster scan patterns, refractive wedges, refractive polygons, and combinations of circular plus linear generating functions.

---

(4) Principles Of Optics, P. 441, Born & Wolf, Pergamon Press, third edition, 1964

2.3.1.5 Bandwidth Considerations

In many situations the readout bandwidth is the limiting parameter that determines system utility. A general expression for the bandwidth, is:

$$\Delta f = \frac{\Omega}{2NWT} \qquad (2.33)$$

Δf = Readout bandwidth (H_z)
Ω = Total field-of-view (Steradians)
W = Instantaneous field-of-view (Steradians)
T = Field time (for update) (Seconds)
N = Number of detectors

The readout bandwidth is directly proportional to the total number of pixels (Ω/W) and is inversely proportional to the field time and number of detector elements.

For a given scan rate and coverage, the only way to reduce bandwidth is to utilize as many detectors as possible. A direct comparison, everything else being equal, of a point detector (flying spot scanner) versus a 2000 element CCD shows that the CCD would operate with a readout bandwidth lowered by a factor of 2000. Therefore, an optimum system will operate with as many detector elements as possible. However, the possible number of detector elements is limited by other factors including present availability, transmitter-receiver compatibility, laser power scanning technique, and gating compatibility.

2.3.2 Charge Coupled Imaging Devices (CCD)[5,6]

A charge Coupled Device, CCD, is a metal-oxide-semiconductor (MOS) structure which can collect and store minority carrier charge packets in localized potential wells. The charge packets, in the

case of imaging devices, are formed by impinging photons subsequently absorbed in a suitable diffusion layer below the surface releasing minority carriers which collect in localized potential wells at the silicon-silicon oxide interface near the surface.

After a suitable integration period the charge packets are transferred into analog shift registers located in the same MOS structure. These shift registers are used to transport the charge packets in an orderly fashion to an on-chip output section. The analog shift registers and transfer gate consist of electrodes which can control the potential at the silicon-silicon oxide interface. Proper manipulation of the voltages on these electrodes causes the potential wells to move toward the output with the charge packets following the potential wells.

Several types of on-chip output preamplifiers have been used with the various CCD imaging devices, i.e., gated charge detector (GCD), single stage floating gate amplifiers (SFGA), and distributed floating gate amplifier (DFGA). These different preamplifier configurations offer different levels of sensitivity performance.

Charge coupled devices fall into two geometric categories, i.e., area and linear arrays. The area arrays can be thought of as a replication of an "n" element linear array "m" times to form an "nXm" element area array. Three types of arrays have been developed by Fairchild; they are 100 x 100, 190 x 244 and 380 x 488 element arrays. The latter is equivalent to a four-fold replication of the 190 x 244 array. Another version of the 1 x 1728 linear array is the Charge Coupled Interlaced Linear Imaging Device (CCILID). It is described in greater detail in Section III because it has the potential of being gated vis-a-vis an electronic exposure control electrode, and this provides the basis for a gating feasibility experiment.

All of the CCD devices discussed have responsivities that favor the GaAs injection laser spectral region; they range between 200 and 350m Amps per watt in the region between 0.8 and 0.9μm.

The next three paragraphs discuss the applicability of the area CCD array (380 x 488). The linear CCD arary (1 x 1728), and the interlaced linear CCD array (1 x 1728).

2.3.2.1 Application of Area CCD Arrays

The largest Fairchild area array currently developed is the 380 x 488 device. Its photoelement arrangement and dimensions are 380 elements horizontally (18μm wide on 30μm centers) by 488 elements vertically (14μm high on 18μm centers). If one sets the photo element vertical IFOV, $\Delta\theta_V$, equal to 0.1 m radian, then the total vertical FOV, θ_V, is 0.1 m Radian x 488 or 62.7 m Radian (3.59°). Similarly the horizontal FOV, θ_H, is 81.4 m Radian, (4.67°). Therefore, without scanning the total FOV for this device falls short of that required, namely 10° x 15°.

One could hypothesize, however, the use of 9 area arrays in a 3 x 3 boresighted mode to cover the whole field except that the area CCD's are not presently gateable. Thus, the use of external gating devices together with the task of boresighting 9 area arrays seems complicated. On the other hand, a single CCD covering the 10° x 15° FOV could be considered as an approach. It is of interest to compare these two schemes in some analytic manner.

---

(5) Amelio, G.F. "Charge Coupled Devices", Scientific American 230, 22 Feb. 1974

(6) Sequin & Tompsett Charge Coupled Devices, Academic Press N.Y., 1975

A geometrical figure of merit can be defined by examining equation (23) of Appendix A, which gives the ratio of detected target energy to reflected background. In this equation, the parameters that depend on the CCD characteristics (and illuminator) are θ_H, θ_V, and $\Delta\theta_V$; the balance of the parameters remains constant for a given situation. Thus, the figure of merit is defined as:

$$M = \frac{1}{\theta H\ \theta V\ \Delta\theta V} \tag{2.34}$$

One wants this figure to be as high as possible since that would correspond to the maximum energy returned from the target relative to the ambient energy reflected. However, before choosing a particular device, the S/N ratio and average laser power must be considered as well as the decision making process for deciding that a wire obstacle is present in the field of view.

Consider now three situations:

a. One 380 x 488 CCD with 0.1 m Rad. resolution.
The figure of merit is found from equation (24) Appendix A, by substituting θ_H = 0.081 Rad, θ_V = 0.063 Rad and $\Delta\theta_V$ = 0.0001 Rad so that

$$M_{1A,\ HR} = \frac{1}{(0.081)(0.063)(10^{-4})} = 1.96 \times 10^6$$

Where the subscript 1A means one array area and HR means high resolution or 0.1 mRad.

b. Nine 380 x 488 CCD's with 0.1 mRad resolution.
In this case θ_H = 3(0.081) = 0.243 Rad,
$\Delta\theta_V$ = 0.1 mRad. Therefore, the figure of merit is:

$$M_{9A,HR} = \frac{1}{(0.243)(0.189)(10^{-4})} = 2.18 \times 10^5$$

c. One 380 x 488 CCD with 10° x 15° FOV.
For this case θ_H = 15° (0.262 Rad) and
θ_V = 10° * (0.175 Rad); also $\Delta\theta_V$ = 0.278 u Rad.

The figure of merit is

$$M_{1A,\ LR} = \frac{1}{(0.262)(0.175)(2.78)(10^{-4})} = 7.85 \times 10^4$$

The figure of merit really indicates how well the laser illumination of a single pulse is utilized for various configurations of a particular CCD. It does not take into account frame rate or, as in the case of linear CCD's the number of laser pulses required to complete a frame. For the area CCD a single laser pulse will illuminate the full field after which all of the elements could be swept out. If a conventional TV display is considered, the laser pulse, would occur 30 times per second. One could slow the laser rate down consistent with the data handling. This would lower the average laser power but the extent of this slow down would be limited by the maximum allowable integrated dark current in the CCD's.

Another factor to consider in the case of area arrays is the area utilization of the device, that is, a certain percentage of the device ($\approx$ 50%) is insensitive to light because those areas contain the vertical shift registers and are masked off.

2.3.2.2 Application of Linear CCD Arrays

The CCD 121 introcuced above is a 1 x 1728 element linear array. Its photo-elements are 17 μM wide by 13 μM long on 13 μM centers. With proper image scanning its area utilization is virtually 100%. Various methods of applying this device are described below. However, all of these methods require some external gating device, e.g., Kerr cell shutter or gated intensifier, and

non-conventional sensing and/or display techniques. Two of the methods require mechanical scanning to cover the field of view.

2.3.2.3 Linear array

If the laser is allowed to illuminate the entire 10° x 15° field the figure of merit is found as follows:

$$\Theta_V = 10° = 0.175 \text{ Rad}$$
$$\Theta_H = 15° = 0.262 \text{ Rad}$$
$$\Delta\Theta_V = 0.175/1728 = 0.101 \text{ mRad}$$

Therefore:

$$M_{VL} = \frac{1}{(0.175)(0.262)(0.010 \times 10^{-3})} = 2.16 \times 10^5$$

where the the subscript VL stands for vertical linear array. This is no better than the figure of merit for nine area arrays which is 2.18×10^5.

However, by focussing the illuminator on the instantaneous area seen by the CCD and scanning the two simultaneously an advantage can be gained. In this case Θ_H approaches $\Delta\Theta_H$ which is (17μM/13μM) $\Delta\Theta_V$ or 0.132 mRad.

The figure of merit is therefore,

$$M_{VL,\ HS} = \frac{1}{(0.175)(0.132 \times 10^{-3})(0.101 \times 10^{-3})} = 4.29 \times 10^8$$

The subscript VL denotes vertical linear array and subscript HS denotes horizontal scan.

2.3.2.4 Horizontal Array (Vertical Scan)

The figure of merit in this case is found as follows:

$$\theta_H = 0.262$$
$$\Delta\theta_V = (0.262/1728)(17/13) = 0.198 \text{ mRad.}$$

and the substitution

$$\theta_V = \Delta\theta_V \text{ is made in equation (2.34)}$$

Thus, the figure of merit is

$$M_{HL,\ VS} = \frac{1}{(0.262)(0.187 \times 10^{-3})(0.198 \times 10^{-3})} = 1.03 \times 10^{8}$$

which is one-quarter of that for a vertical linear array.

2.4 GATING TECHNIQUES

In the sections that follow, three generic gating techniques are described, i.e., electro-optic, gated image tubes and direct exposure control of the photosites of a CCD array.

2.4.1 Electro-Optic Gating

There are a great number of electro-optic (and magneto-optic) effects that can be used to gate or shutter a light beam. The most popular of these have resulted in such devices as the Kerr cell, Pockels cell and lately, PLZT (lead-lantharium-zirconium titanate) which is a ceramic material.

In general, the active material is placed between a pair of crossed polarizers. The crossed polarizers block the light very effectively until a voltage is applied to the active material. When voltage is applied to the material, it becomes optically active or birefringent. If the material is properly oriented with respect to the first polarizer, the polarized light passing through the material becomes elliptically polarized. Under these conditions some of the light is allowed to pass through the second polarizer.

The Kerr cell requires the highest voltage level to operate (∿35 Kv) but it is extremely fast and can easily handle a 20° angular field. Its pulse repetition rate is generally limited by the recovery of the hydrogen thyratron used to drive the Kerr cell. One manufacturer offers an off-the-shelf Kerr cell shutter system which has a clear aperture of 0.8" x 1.5", will accept a 20° angular field and can be pulsed at 60 pps with durations ranging from 5 nsec to 10μsec. Its open transmission is 20% while closed it is 0.005% which is an extinction ratio of 4000:1.

A high insertion loss, that is, low open transmission is characteristic of the electro-optical shutters. It should be noted that the polarizers will reduce randomly polarized light by 50% exclusive of any other losses.

The Pockels cell will operate on lower voltages (∿2 Kv) and at high pulse rates but cannot handle a wide angular field. Typically, its extinction ratio is down to 100:1 with a 2° field angle.

PLZT electro-optic shutter devices can handle the angular fields at repetition rates sufficient for this application but switching times between 4 and 14 μsec have been demonstrated.[7] However, a close examination of this material is warranted for its potential of achieving faster switching. Present insertion loss is about 10%.

(7) Cutchen, J.T., Harris, J.O., Jr., Laguna, G.R., "Electro-Optic Devices Utilizing Quadratic PLZT Ceramic Elements", Sandia Laboratories, SLA-73-0777, August 1973.

2.4.2 Gated Image Tubes

A gated image intensifier can be used as a shutter in front of a CCD. If the output face plate of the intensifier is fiberoptic, the CCD can be butted to this face plate with good optical efficiency. However, one of the chief advantages of the CCD which is its high responsivity (300 ma/W) would be lessened when coupled to an intensifier. Typically, the image intensifier photocathode response at 0.85 μm is 15 ma/W average for an extended red S-20 surface; the phosphor is usually P-20 which is green. In this region the response of a CCD linear imaging array is down to approximately 100 ma/watt.

2.4.3 "On Chip" CCD Gating

An attractive candidate for a WODS sensor is a CCD array with specialized architecture so that "On-Chip" gating could be achieved by programable logic commands. This type of CCD could be used directly with laser pulses in the spectral range 0.8 to 0.9 micro meters. Potential advantages of such a WODS sensor are listed below:

- Low Cost (In Production)
- High Infrared Responsivity
- Perfect Geometrical Registration
- Directly Controlllable via Clocks & Logic
- Lightweight
- Inherently Rugged
- Long Life
- No Lag

To be useful for the WODS task, this device would have to be suitable for fast range gating on the order of 50 NSEC total on-time. Therefore, in order to avoid loss due to "shutter" effects, the rising and falling edges of the temporal window must be kept to a fraction of the total gating time. Typically, rise and fall times of less than 10 NSEC would be needed. This fast switching

speed may be compromised by various CCD effects such as propagation delays and attenuation along electrodes which can have dispursive delay line characteristics.

Secondly, long wavelength radiation may be absorbed below the useful depletion layer of the CCD resulting in signal "lost" from the photowell. The effects of such "lost" signal may appear as poor transfer efficiency, or, as spurious signal (crosstalk) from adjacent pixels during the Gate-On time. This "lost" signal may redistribute itself in such a way so as to be detected directly in the registers. During the Gate-Off time the effect would appear to limit the gating rejection ratio achievable with a CCD device.

The performance of such a gatable CCD array can only be discussed in context of a specific design. At the present time no area arrays suitable for fast gating have been designed or produced. However, a linear array, the Fairchild ILID 1728, does appear to be suitable for further characterization in the gating mode due to its large number of pixel elements, low noise, and the presence of an on-chip exposure control electrode. The characteristics of this array will be used in the following trade-off analysis.

2.5 TRADE-OFF ANALYSIS

One systematic approach to the WODS task is to choose the optimum detector based upon criteria that minimizes the required laser power. This section will compare and contrast the required laser power per pulse for a bare CCD array versus an Image Intensifier front end. A general comparison of these candidate approaches is given as a function of laser wavelength.

2.5.1 Background Calculation

The expression for the number of photoelectrons per pixel per exposure time has been developed from equation 17b of Appendix A. This equation is shown below:

$$Nb = \frac{RP_a(\Delta\lambda)(\Delta t)r_b(\Delta\theta h)(\Delta\theta v)T_L\ T_f F^2 \exp\{-\alpha R_b\}}{16e\sqrt{2}\ (F/\#)^2} \qquad (2.35)$$

Where

R = Responsivity
P_a = Background Spectral Radiance
$750\ W/M^2\ .\mu m; \lambda = .85\mu m$
$\Delta\lambda$ = Wavelength band
Δ_t = Exposure time
r_b = Background reflectivity
$\Delta\theta_h$ = Detect IFOV Horizontal
$\Delta\theta_v$ = Detect IFOV Vertical
T_L = Lens transmission
T_F = Filter transmission
α = Extinction coeff.
R_b = Range to background plane
$e = 1.6 \times 10^{-19}$ coul/electron
$F/\#$ = F - number
F = Focal length of lens

Previous calculations have established that the maximum expected background in a range-grated system is on the order of 55 photo-electrons. This was based upon a gate on time of 0.3 microseconds with a high reflecting background at 2KM range filling the field-of-view. We will restrict this discussion to background levels of this magnitude in order to use the minimum laser power per pulse necessary to achieve detection.

2.5.2 Range Equation

The range equation has been developed from equation 4 of Appendix A. We extend the equation in order to describe a MXN array. This is given as follows:

$$\frac{E_o \exp\{-2\alpha R_0\}}{(R_o)^3} = \frac{4e(MXN)d_v' d_h' (F/\#)^2 N_t''}{R \; r_t \; F^3 \; D d_h T_f T_o} \qquad (2.36)$$

Where

E_o = Laser power (joules/pulse)
R_o = Slant range to target (meters)
r_t = Target reflectivity
N_t'' = Required electrons per pixel per exposure (see below)
D = Wire diameters (M)
M = Vertical length of array (pixel number)
N = Horizontal length of array (pixel number)
d_h = Horizontal detector active length (M)
d_h' = Horizontal detector CTC length (M)
d_v' = Vertical detector CTC length (M)

Assumption: The laser illumination angle is exactly equal to the FOV of the MXN array.

2.5.3 Linear Versus Area CCD

We will assume the presence of a bright hill, solar illuminated, at 300M. This puts an upper bound on the background level. Therefore, the analysis will be "worst case" as far as background level is concerned. Furthermore, we will choose the minimum gating time condition. (Δ_t = .3u sec) so that the laser power required will be minimum against a bright background. Figure 2-5 shows the required energy per pulse versus range for area CCD arrays having 100 x 100 and 488 x 380 pixels. The angular relations have been computed from published information about Fairchild area CCD's.

The general conclusion from reviewing the Section 2.3.5 and equation (2.35) is that the dominant factor determining laser energy comparisons is the area of the array.

Present area arrays are not quotable. Secondly, they will incur a loss of power by a factor of two due to deadspace. For utilization of equal laser energy a single 1728 array is equivalent to a 30 x 30 element array (same SNR at each detector). For scanning a FOV of 10 Deg. x 15 Deb. the linear array is preferred because of practicality of a simple scanning system and optimum utilization of laser power.

2.5.4 CCD Versus Image Intensifiers (II)

The next figure (Figure 2-6) shows the solution to the range equation for achievable values of device parameters. Specifically, the chief degrading factor for the CCD is the loss of signal due to crosstalk, and that for the II is the finite MTF of the phosphor and fiber optics combination. Table 2-4 lists the parameters used in this calculation.

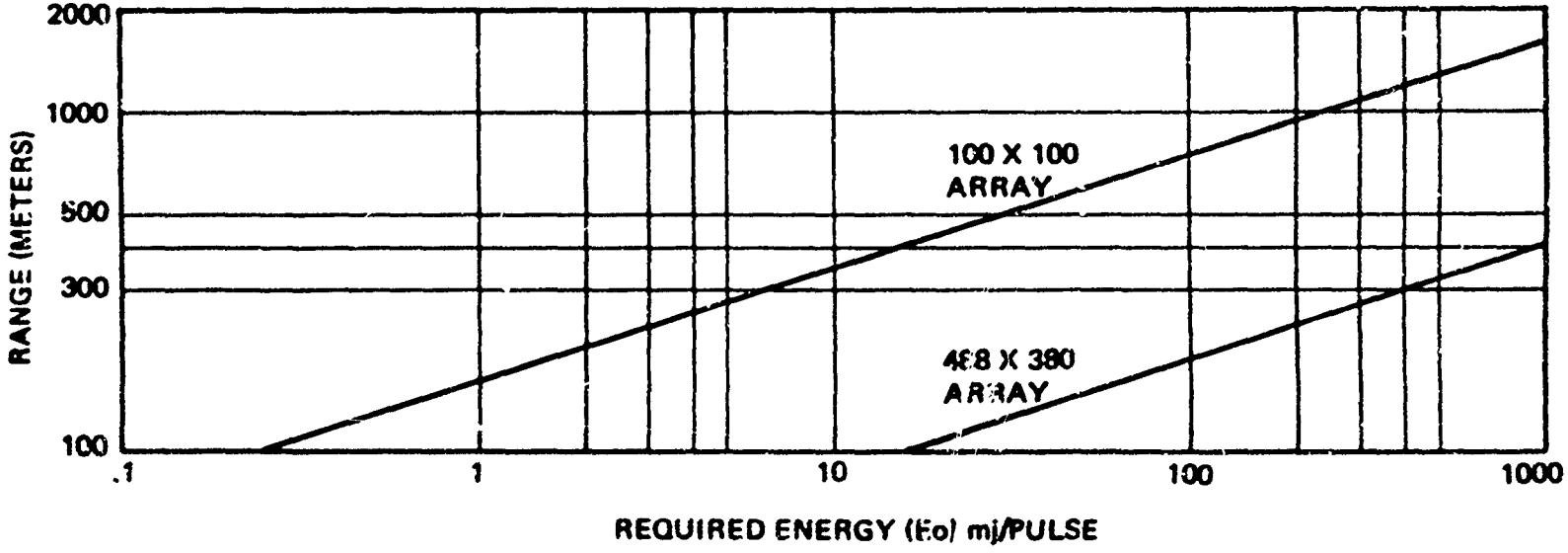

FIGURE 2-5 AREA ARRAY TRADE-OFF

The CCD approach is found to be superior in terms of achievable detection range if such an array can be gated. The chief penalty that is incurred in using the II is that the laser energy per pulse must be higher than in the bare CCD approach by a factor of 4. The disadvantage of the II is a consequence of the relatively low responsivity of photocathodes at λ = .85uM and the MTF due to the fiber optics and phosphor. These MTF degrading factors appear to be unavoidable for the II and cannot easily be overcome in the near future.

A further argument for the use of the bare CCD is that the CCD operates about equivalently in the laser spectral range of .85 to .90 uM and therefore can be operated with (non cryogenic) GA As lasers throughout this range.

Furthermore, present Image Intensifier Devices are already at their practical limit at λ= .85uM and cannot be expected to operate as reliably at λ= .90uM.

Table 2-5 and Table 2-6 summarize the factors involved in the trade-off (at λ= .85uM). In the laser application we are considering the pulse energy requirements favors the CCD approach because of the high responsivity achievable with the CCD. In summary, the bare CCD concept offers the best device to implement the WODS task in terms of required laser power (.9 mj/pulse required at 300M against a low reflectivity 1/8" wire), flexibility of laser wavelength of operation and compatability with virtually any scan configuration.

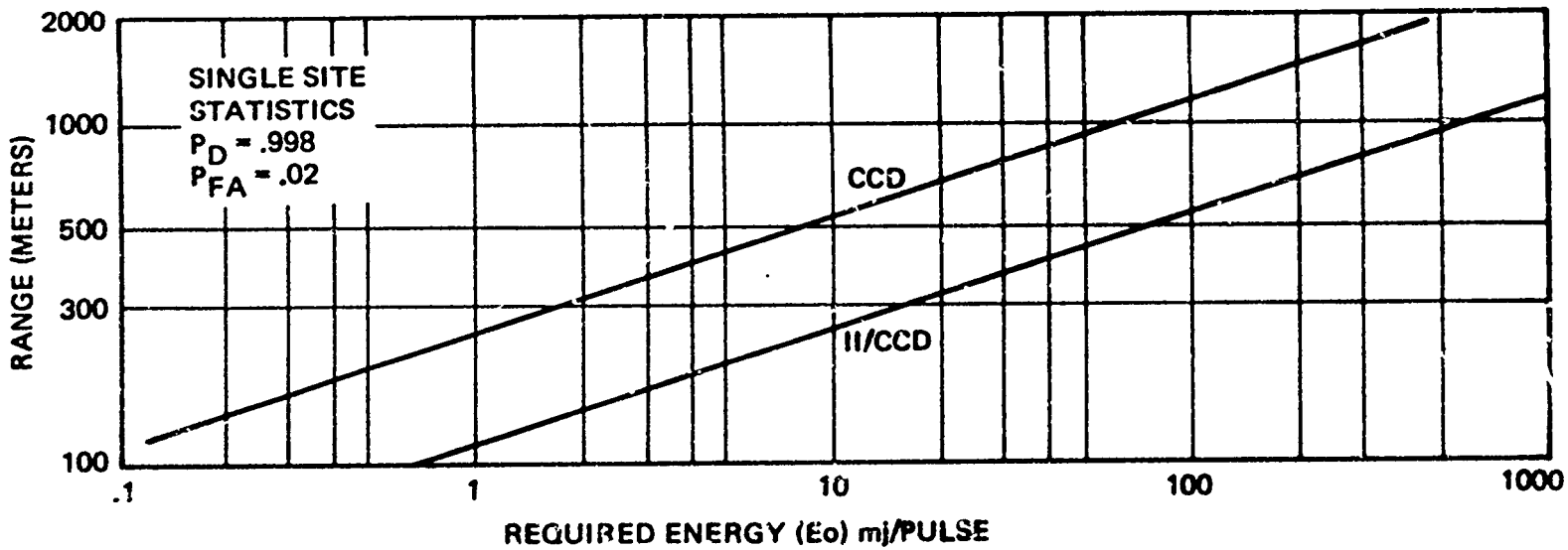

FIGURE 2-6 CCD vs II/CCD (λ=.85uM)

TABLE 2-4 SYSTEM PARAMETERS

CCD

d_h = 17 uM,

d_v = 13 uM,

d'_h = 17 uM

d'_v = 13 uM

$\Delta\theta_h$ = 1.3×10^{-4} Rad

$\Delta\theta_v$ = 1.0×10^{-4} Rad

θ_v = 9.9 Deg (1728 pixels)

Δt = .3μ sec.

R = .36 A/W; λ = .85 uM

MTF = .7 (due to crosstalk) at 38.5 LP/MM

Target

D = 1/8"

r_t = .2

IMAGE INTENSIFIER

40 mm Input/Output format

FO coupled

R = .02 A/W, λ = .85 uM

3 to 1 magnification

MTF = 0.3 at 38.5 LP/MM (Inverter Type)

Due to phosphor and fibers only

Ideal pickup device

Optics and Atmosphere

F = .13M

F/# = 1.4

T filter = .8

T optics = .9

$\Delta\lambda$ = ±.025 uM

α = .34 (good seeing; λ = .85)

Pa = 750 W/M^2 uM

R_b = 300M (Hill barrier)

r_b = .71

TABLE 2-5 SILICON ARRAY VERSUS IMAGE INTENSIFIER - CHARACTERISTICS

FACTOR	CCD	II/CCD
RESPONSIVITY	R = .36 a/W	R = .015a/W
NEAR IR WAVELENGTH RANGE	0.7 - 1.1 μM	0.7 -0.85 μM
INTERNAL NOISE	NES=50 FGA 20 DFGA (GOALS)	NEGLIGIBLE
GATING CAPABILITY	DEVELOPMENT OF GATED ARRAY NEEDED	SUB MICROSECOND RANGE AVAILABLE
MTF	0.7 AT 38.5 $\frac{LP}{MM}$	0.3 AT 38.5 $\frac{LP}{MM}$

TABLE 2-6 TRADE-OFF
$\lambda = 0.85\mu M$
SILICON ARRAY VERSUS IMAGE INTENSIFIER
(300 NSEC EXPOSURE)

(300 METER RANGE)

FACTOR	SILICON ARRAY	IMAGE INTENSIFIER*
LIMITING NOISE	NES	QUANTUM
DETECTION STATISTICS	$SNR = N_t/NES$ $4.5 = N_t/50$ $N_t = 225$	$SNR = N_t/(N_t + N_B)^{1/2}$ $4.5 = N_t/(N_t + 3)^{1/2}$ $N_t = 22.4$
MODULATION TRANSFER FUNCTION	SOURCE: CROSSTALK $m = 0.7$ $N_t' = \frac{N_t}{m} = 320 \quad (N_B = 55)$	SOURCE: FIBER OPTIC AND PHOSPHOR GRANULARITY $m = 0.3$ $N_t' = \frac{N_t}{m} = 75 \quad (N_B = 3.0)$
RANGE EQUATION	$E_o = k \cdot N_t'/RESPONSIVITY$ $R = .36$ a/W $E_o = 0.90$ mj/PULSE	$E_o = k.N_t'/$ RESPONSIVITY $R = .02$ a/W $E_o = 3.8$ mj/PULSE

*Assumes ideal pickup device.

TABLE 2-7 WAVELENGTH TRADE-OFF - PARAMETERS

	λ=.53		λ=.6943		λ=.85		λ=1.06		COMMENTS	SOURCE
	II	CCD	II	CCD	II	CCD	II	CCD		
Ambient Background ($\frac{W}{M^2 \cdot \mu M}$)	1400		1300		750		525		Solar Illuminated	RCA Handbook
Extinction Coefficient (km^{-1})	0.5		0.4		0.38		0.34		Light Haze	"
Responsivity ($\frac{A}{W}$)	.055	.10	.066	.27	.02	.36	.004	.03	"Best Available"	ITT(Photocathodes Fairchild (CCD)
Received Background Level (Photoelectrons) 0.3KM	7.6	14	12	46	3.0	55	.21	1.6	• Within Range Cell $^{*}r_t$ = .71	Equation 2.35
MTF At 38.5 LP/MM	.3	.9	.3	.77	.3	.70	.3	.24	CCD:Crosstalk II:FO + Phosphor	Section 2.4.4
Required Laser Return (Photoelectrons)	87	250	96	292	75	320	70	938	To guarantee High Reliability	Equation 2.21
Required Laser Energy (mj/pulse) 300M	1.75	2.8	1.5	1.1	3.8	.9	18	32	Transmit Energy (300 NSEC)	Equation 2.36

2.5.5 Extension To Other Wavelengths

It is possible to consider other than Ga As solid state lasers as the transmitter in the WODS approach. In order to characterize the WODS device at other laser wavelengths, we have extended our analysis to include the following high power lasers which can produce short pulses.

- λ = .53 Micrometer; Frequency doubled YAG
- λ = .6943 Micrometer; RUBY
- λ = 1.06 Micrometer; YAG

Table 2-7 displays the entire set of parameters used in this calculation. The calculation was performed for gating pulses of 300 NSEC and detection ranges of 300-500 meters. The results must be compared with State-Of-The-Art laser output powers to determine feasibility.

In order to clarify the utility of a CCD versus an Image Intensifier as a function of wavelength, we have done a parametric study. Table 2-7 shows the factors used in this analysis. The following comments are appropriate.

1. RESPONSIVITY

For the Image Intensifier the responsivity values shown are best available at each wavelength. The criteria of availability and compatability with Image Intensifier processing limits the photocathodes to S-20, S-20ER and S-1 types. For the CCD the responsivity value used is best available. A single CCD has not been found that has simultaneously the high responsivity values across the spectrum. Figure 2-7 shows measured values for the CCD and S-25 multialkali photocathode.

2. MTF

II - The MTF for a typical Image Intensifier is chiefly due to the spreading involved in the use of fiber optics at the input and output as well as the spread function of the phosphor itself. We assume an overall value of 0.3 at 38.4 LP/MM which is independent of wavelength. Figure 2-8 shows typical MTF associated with phosphor granularity and fiber optic.

CCD - The MTF of the CCD is due to crosstalk. The level of crosstalk used here has been derived from published results[8] for the ILID 1728. This crosstalk is characterized in Figure 2-9.

3. ATMOSPHERIC/BACKGROUND CONDITIONS

Light haze was assumed for the system calculations. The extinction coefficient and the ambient background level was taken from the RCA handbook on electro-optics.[9]

4. The background range used in the calculation is $R_b = R_o + C\Delta_t$ which allows for background return within one range cell. We assume that this will be "worst case".

Figure 2-10 displays the required energy per pulse versus operating wavelength for both the image intensifier and bare CCD although the device characteristics may not be smoothly varying as a function of wavelength. The curves are shown connected to clarify the wavelength dependency. Note that the bare CCD requires less laser energy throughout the entire near IR spectral region.

(8) M.V. Harris "Slow Scan Operation of Long Linear CCD Arrays" presented at Jet Propulsion Lab, Pasadena, Calif., 7 Mar 75

(9) RCA Electro-Optics Handbook, EOH-11, RCA Commercial Engineering, Harrison, N.J. 1974

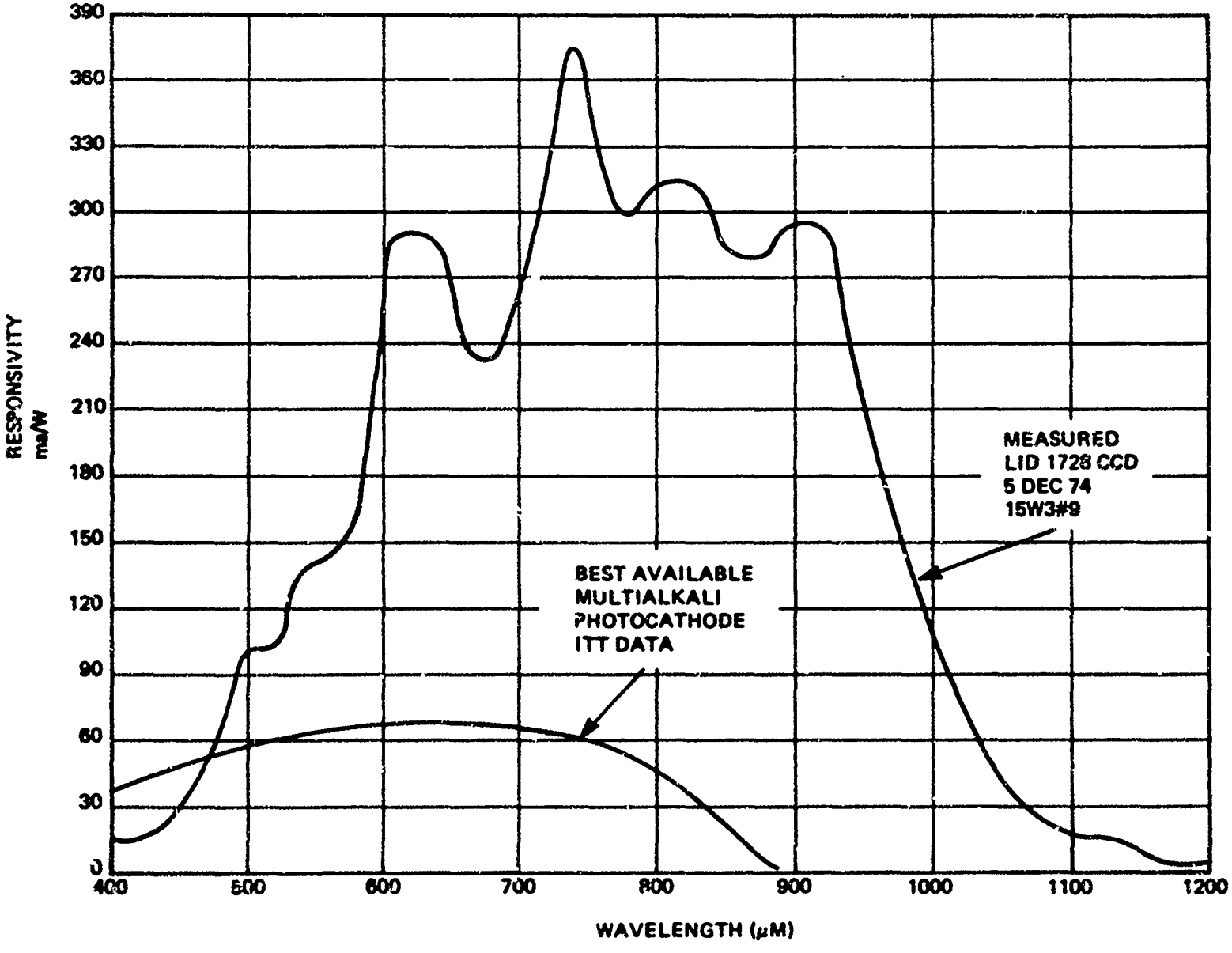

FIGURE 2-7 RESPONSIVITY COMPARISON OF CCD AND II

78-862

FIBER OPTIC:

D = FIBER DIAMETER

HEXAGONAL PACKING

PHOSPHOR: P-20 TYPE

AVERAGE BRIGHTNESS

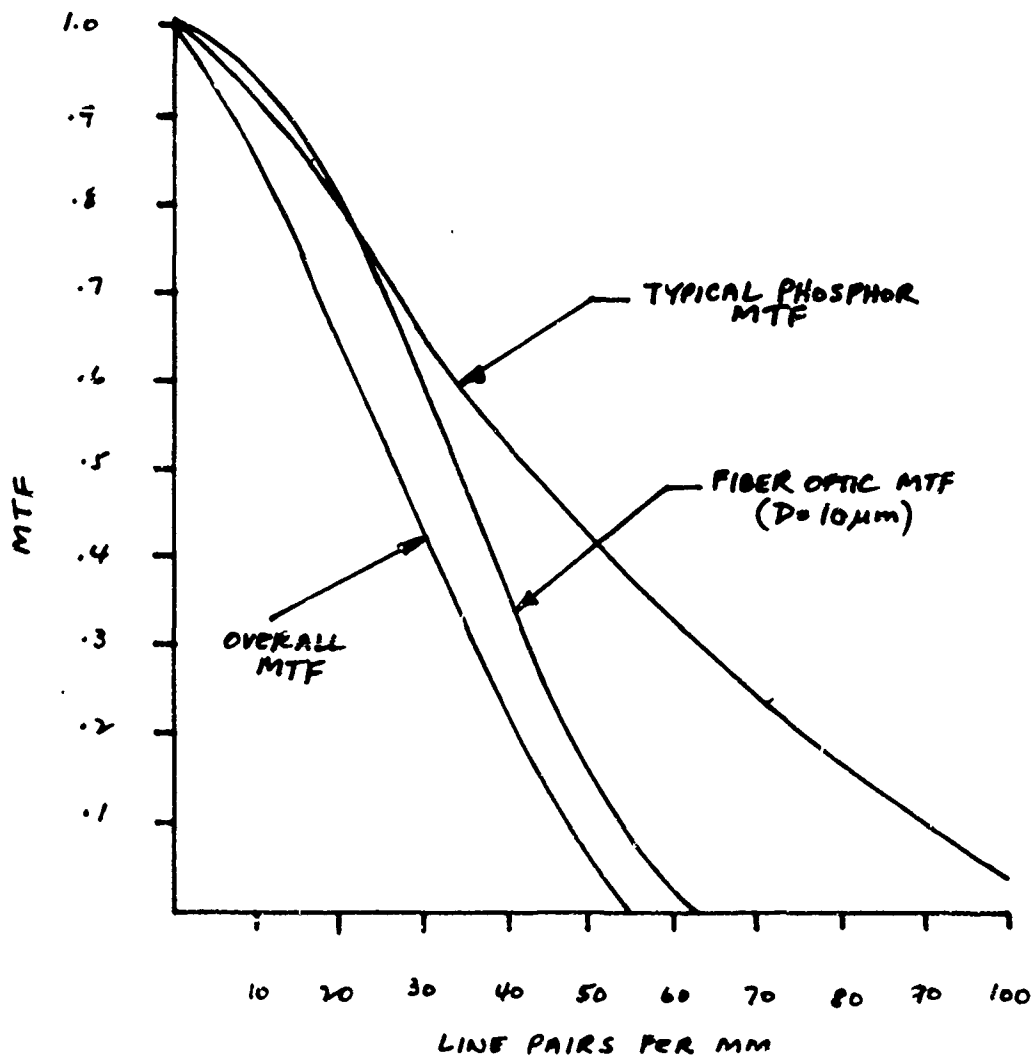

FIGURE 2-8 SYSTEM MTF-IMAGE INTENSIFIER

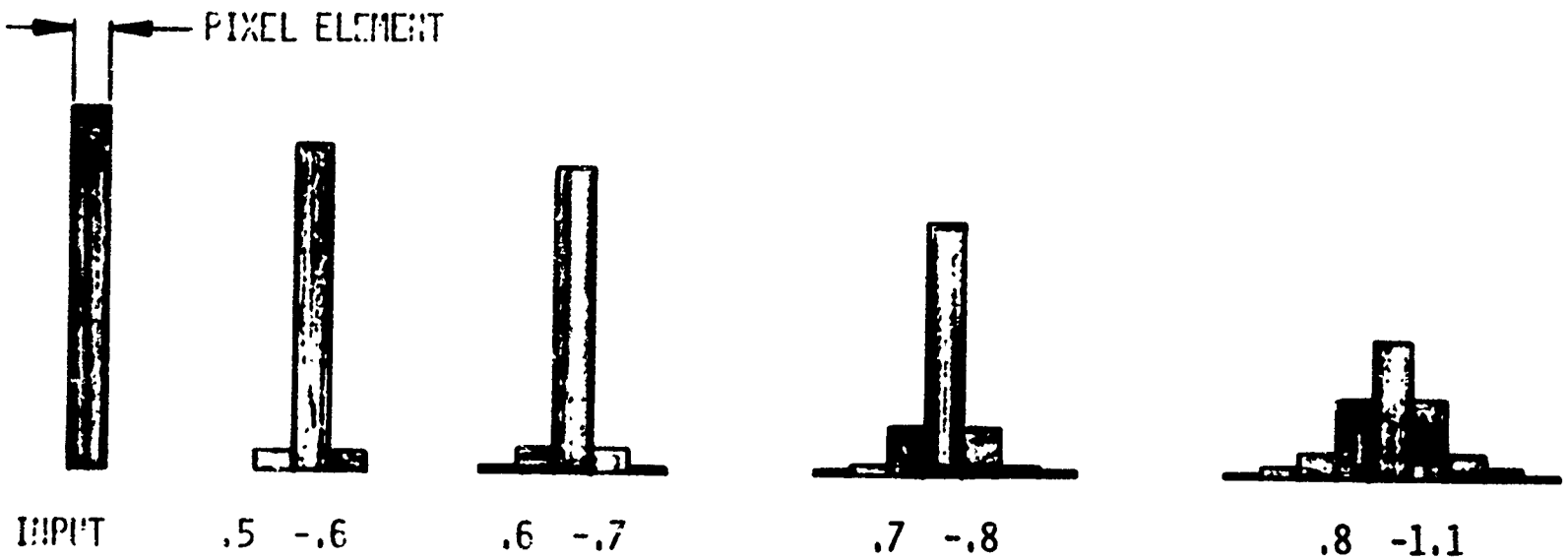

FROM M.VICARS-HARRIS PAPER
"SLOW SCAN OPERATION OF LONG LINEAR ARRAYS" SYMPOSIUM ON CCD TECHNOLOGY FOR SCIENTIFIC IMAGING APPLICATIONS, JPL, 1975

FIGURE 2-9 CROSSTALK CHARACTERIZATION OF 1728 ELEMENT CCD

LINEAR ARRAY (10 DEG. X 0.1 MRAD)

GATED TO 300 NSEC.

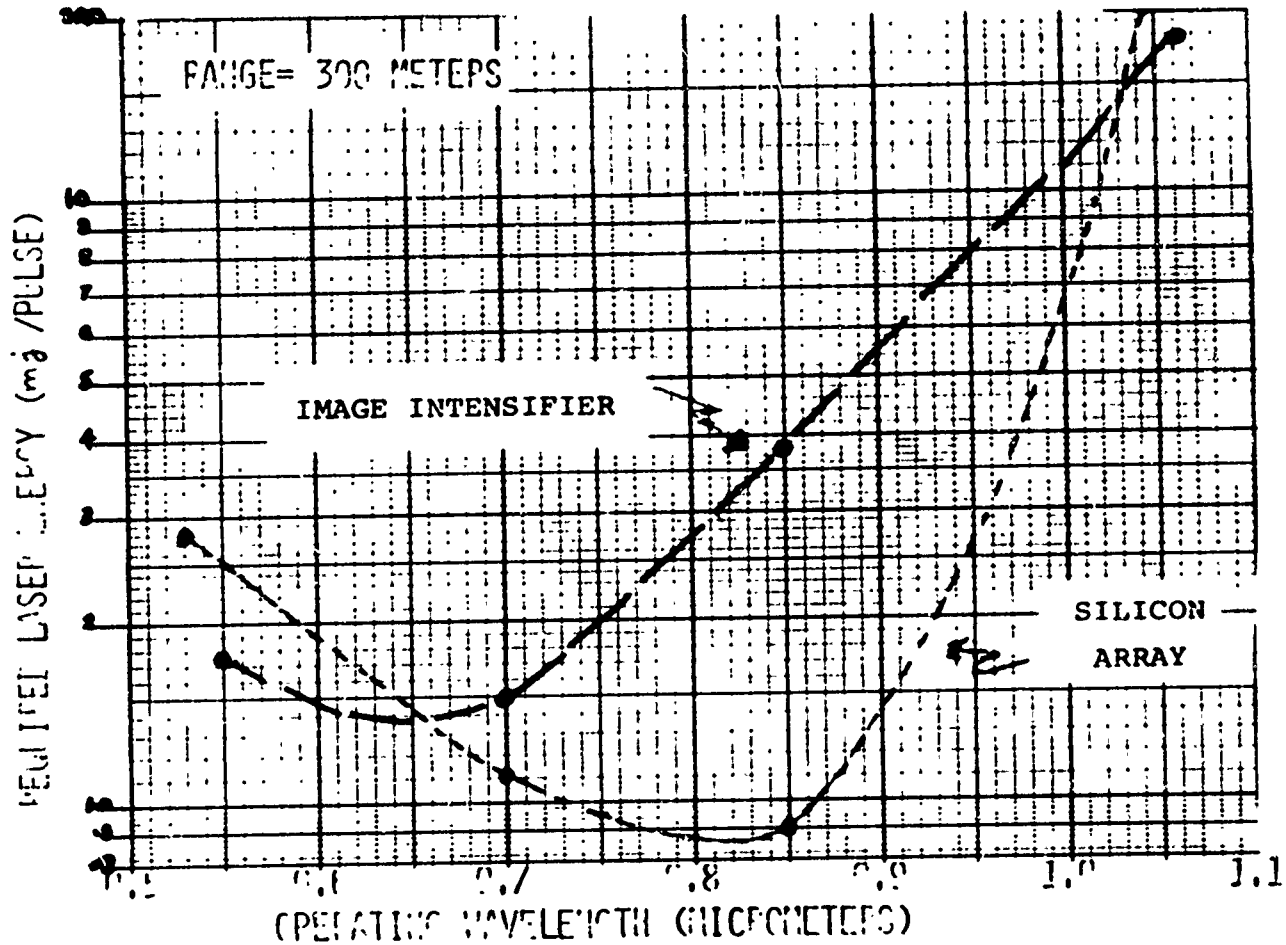

FIGURE 2-10 WAVELENGTH TRADEOFF

2.5.6 Summary

We have performed a system analysis for the Wire Object Detection Task. This analysis has emphasized the basic detection statistics particularized to wire objects, scanning techniques, and gating techniques. A review of component technology has disclosed advantages and disadvantages for each candidate. An evaluation and trade-off analysis has been performed based upon these technology issues. The baseline device that emerges as optimum has the following characteristics.

• DETECTOR:	CCD Linear Array 1745 elements
• WAVELENGTH OF OPERATION:	Near IR: 0.8 - 0.9μm (covert)
• GATING TECHNIQUE:	On chip
• GATING TIME:	50 NSEC - 300 NSEC
• SCANNING TECHNIQUE:	Line scan
• OPTICAL APPROACH:	Dual boresighted transmit and receive channels

The direct CCD approach is chosen because it offers the simplest optical system with high reliability, compatibility with near IR laser wavelengths and formats with large numbers of elements are available. The CCD itself is light weight and compact, thereby making the system requirements for ruggedization relatively easy to accomplish.

In addition, the long linear array approach utilizes laser transmitted energy in the most optimum way. This is particularly true if long array solid state arrays are used as the transmitter.

The unaswered technology issue in this apprcach is the capability of a CCD to perform in the "On-Chip" gating mode hypothecated. Since this is a crucial issue, we have devised a feasibility experiment to test this capability. At present, the only CCD which can be utilized in a gated mode is the Fairchild CCILID 1728. This experimental array posesses an exposure control electrode which may be used to examine che gating characteristics.

Secondly, this array can be used to satisfy the second aspect of the feasibility experiment - namely, demonstration of single site activation.

In the next section, we describe in detail the ILID 1728 array and the camera circuits which constitute the basis for the feasibility experiment.

3.0 CAMERA DESIGN

3.1 GENERAL DISCUSSION

An experimental camera has been designed and fabricated incorporating the Fairchild ILID 1728 array which has been delivered to the U.S. Army Electronics Command. The camera inlcudes the following subsystems:

1. Logic board
2. Array driver board
3. CCD socket board
4. Video processor board
5. Galvanometer mirror scanner
6. Mirror driver and controller
7. Hughes scan converter
8. Scan conversion interface board

We will discuss below the details of the camera electronics followed by the experiment description.

3.2 CCD ARRAY DESCRIPTION

The Fairchild ILID 1728 has been selected as the detector in the WODS camera for two reasons. First, the ILID 1728 has resolution and sensitivity consistent with the WODS task by virture of the 1728 resolution elements and the low noise floating gate amplifier used on this array. Secondly, the array is an experimental type that is unique in having a built-in exposure control function. This exposure control feature is presently the best candidate for gating with available components and, therefore, provides a suitable device for feasibility studies.

Therefore, the ILID 1728 array is a suitable choice for operation in the standard detection mode as well as the gating mode required by the WODS contract. Our approach has been to design the logic and camera controls so that either of these modes of operation can be achieved with the same camera.

The next section outlines the principles of the ILID 1728 which form the basis for camera design.

3.2.1 Technical Description

A schematic diagram of the CCILID-1728 is shown in Figure 3-1. In operation, electrons generated by incident light are collected at the 1728 photosites in the silicon under the photograte ϕ_p. The transfer gate, ϕ_x, is then turned on to transfer these electrons as charge packets in the neighboring two phase CCD shift register. Since only one of the two clock phases in the shift register is held high at this time, only half of the charge packets are transferred, as illustrated in Figure 3-2. These charge packets are then transferred through the shift register and detected by the output amplifiers. After the shift register is cleared, ϕ_x is turned on again to read out the remaining charge packets.

Since only one shift register is required to read out the video information from the photosites using this interlaced mode of operation, an "exposure gate" ϕ_{EC} and a sink diode are incorporated along the other side of the photogate to obtain element antiblooming and electronic exposure control. A low-noise floating gate amplifier (FGA) is provided as the on-chip charge detector in addition to a conventional gated-charge detector (GCD) circuit. An electrical input circuit (EI) is located at one end of the shift register for testing purposes.

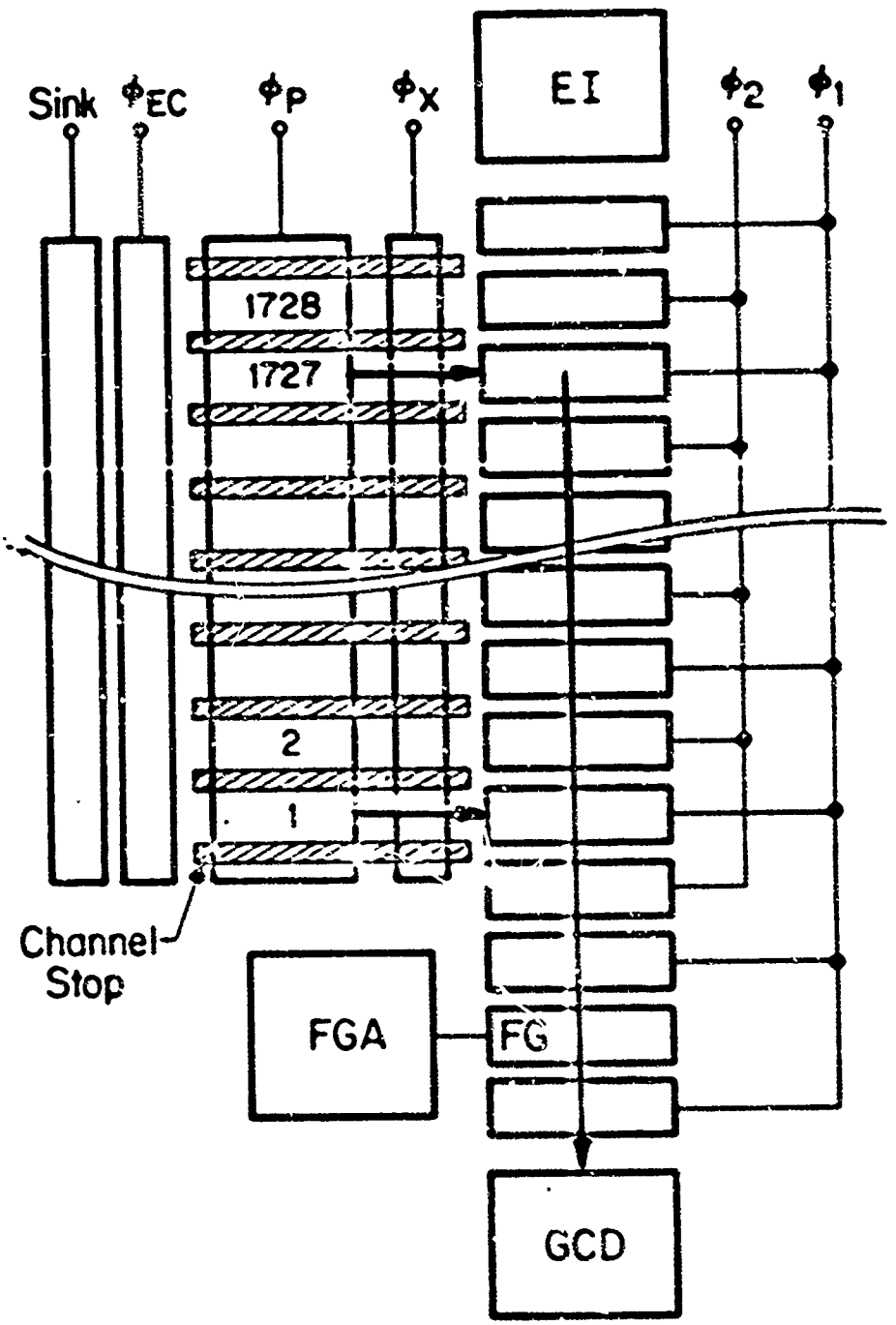

FIGURE 3-1 CCD ILID 1728 SCHEMATIC ODD FIELD READOUT

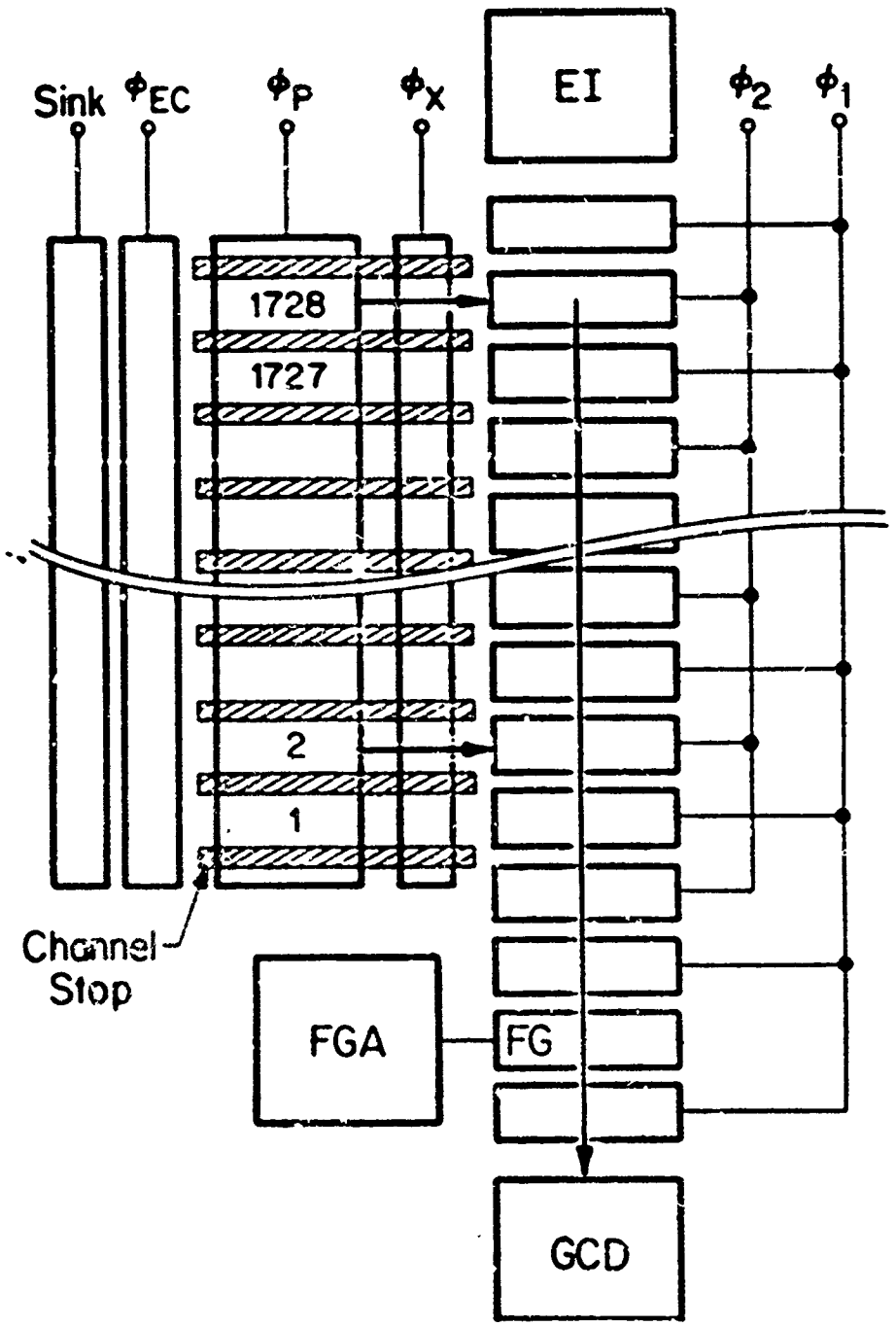

FIGURE 3-2 CCD ILID 1728 SCHEMATIC EVEN FIELD READOUT

3.2.2 Shift Register Design

The shift register is constructed using two layers of polysilicon with self-aligned implanted barriers. After the first polysilicon gates have been defined and oxidized, they are used as the mask to define the barrier (boron) implant. The second polysilicon layer is then deposited and defined to cover the gaps between the first polysilicon gates.

3.2.3 Photocell Design

An aluminum layer is deposited to block incident light except in the photogate area. A positive dc voltage is applied to the photogate to collect the photoelectrons in the potential well under it. A channel stop diffusion under the photogate separates the 1728 photosites distinctly. The center-to-center spacing of the photosites is 13 um.

3.2.4 On-Chip Amplifier

As an experimental device the ILID 1728 incorporates two separate on-chip amplifiers as shown in Figure 3-3. The conventional differential gated charge integrator DGCI has a processing gain of approximately 0.02 microvolts/electron and a noise equivalent signal of about 200 RMS electrons by design. In contrast, the floating gate amplifier (FGA) is designed for a gain of about 1.4 microvolts/electron and an NES of about 50 electrons. The camera will be designed to use the FGA because of its superior performance.

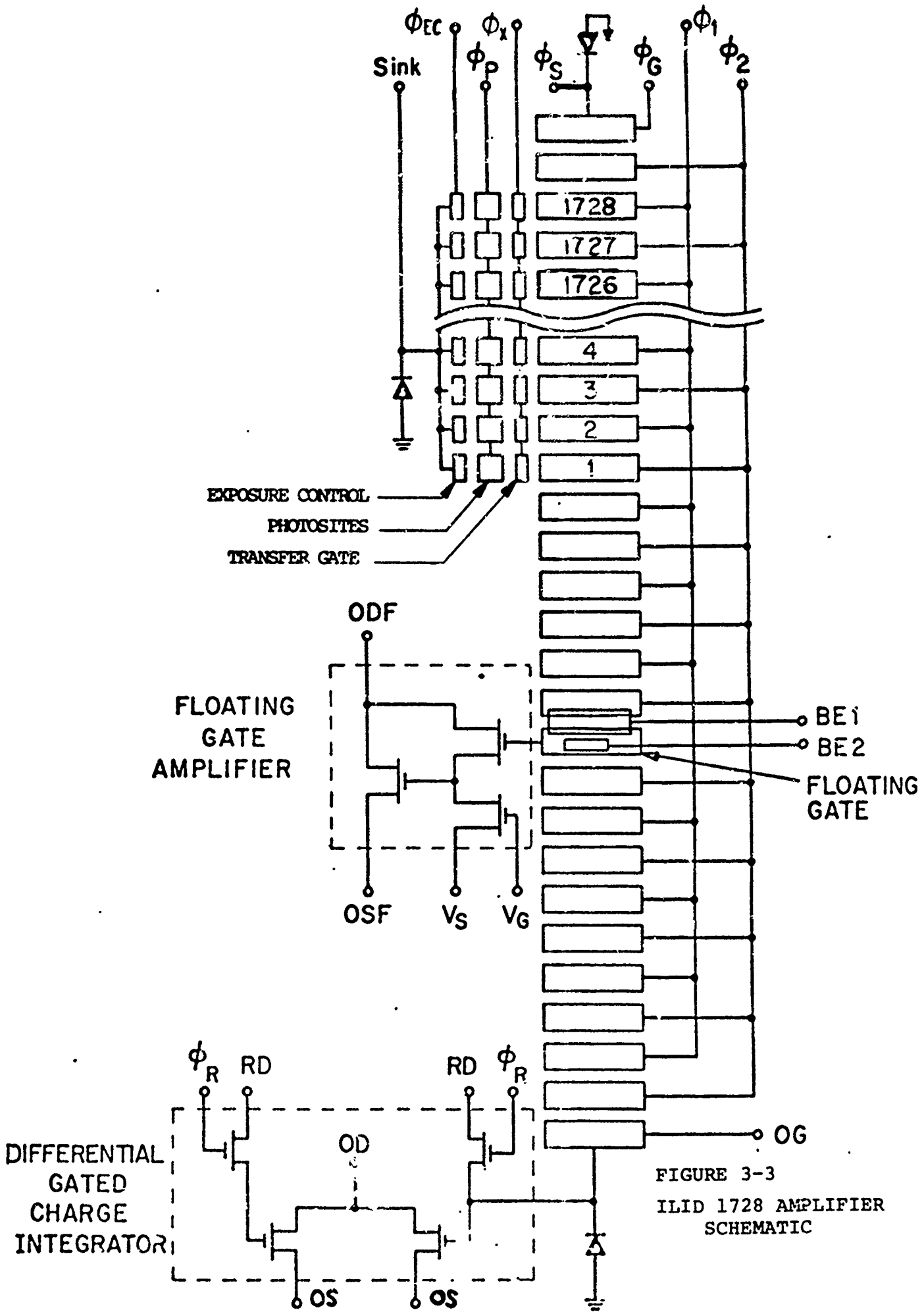

FIGURE 3-3

ILID 1728 AMPLIFIER SCHEMATIC

The charge packet to be sensed is brought under a conductive floating gate by manipulation of the potentials of the adjacent charge-coupling electrodes. It can be seen that the floating gate provides a capacitive coupling between the signal charge in the CCD channel and the current in the MOS channel without making physical contact to either of them. Because the signal charge is not destroyed by the FGA, it can be transferred further in the CCD register and be detected again by the GCI. A cross-sectional view of an FGA is shown in Figure 3-4. From this figure, C1 is the capacitance between the signal electrons and the floating gate, C2 is the capacitance between the floating gate and the bias electrode, C3 is the depletion capacitance between the signal electrons and the substrate (ground), and C4 is the stray capacitance from the floating gate to the channel stop (ground). The MOS transistor is represented by its input capacitance C_{in} where its value depends on the bias conditions of the circuit. If a charge, ΔQ, coulombs is placed under the floating gate, the change in voltage it produces between the floating gate and ground is

$$\Delta V_{FG} = \frac{\Delta Q}{C_{FG}} \qquad (3\text{-}1)$$

where C_{FG} is defined as the floating gate capacitance and is given by

$$C_{FG} = C_2 + C_4 + C_{in} + \frac{C3}{C_1}\ (C_1 + C_2 + C_4 + C_{in}) \qquad (3\text{-}2)$$

The sensitivity of the floating gate for this device was designed to be 1.4 uV per electron.

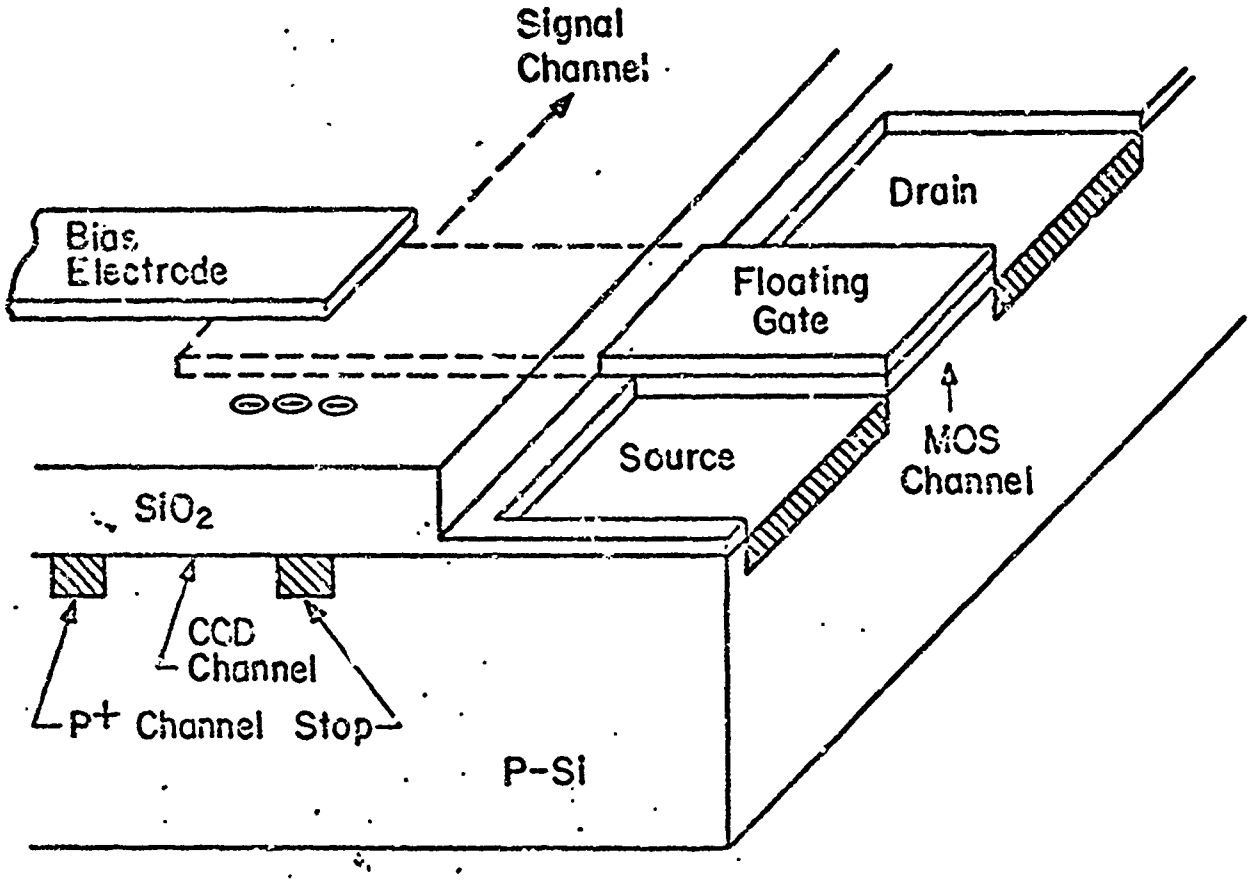

FIGURE 3-4 FLOATING GATE AMPLIFIER

It is implied by equation (3.2) that in order to maximize the FGA sensitivity, a minimum device geometry is desired. A small transistor, however, has low trans-conductance that results in a small voltage swing at the output. A two stage amplifier circuit, as shown in Figure 3-5, was therefore designed. In this figure, T_1 is a minimum geometry "floating gate" transistor, T_2 provides a high load impedance for T_1, and T_3 is a large geometry output buffer transistor. Typically, T_3 is biased as a source follower by connecting an external load resistor Rs to its source. With this circuit, a 1.4 to 2.0 uV per electron sensitivity at the output terminal can be achieved.

Since no resetting of the FGA is necessary, the reset noise associated with the GCI does not exist with the FGA. The dominant noise sources of the FGA are the 1/f noise and the thermal noise of the transistors. The magnitude of these can be estimated by measuring the noise spectral density of an MOS transistor with the same geometry and process sequence as the FGA transistor. These measurements predict an RMS noise equivalent signal of approximately 40 to 50 electrons for a 300 KHz bandwidth at room temperature.

The floating gate amplifier is a non-destructive configuration that samples the charge but allows it to be transferred further down the shift register to the second output amplifier. In the array schematic, Figure 3-3, it is seen that the floating gate takes the place of a shift register electrode. This missing electrode would normally be excited with a clock signal Ø1. In order to maintain charge transfer through the region of the floating gate, two electrodes have been added. Electrode BE1 is clocked with Ø1 (the voltage of this clock is critical for operation of the WODS camera). Electrode BE2 is a DC bias.

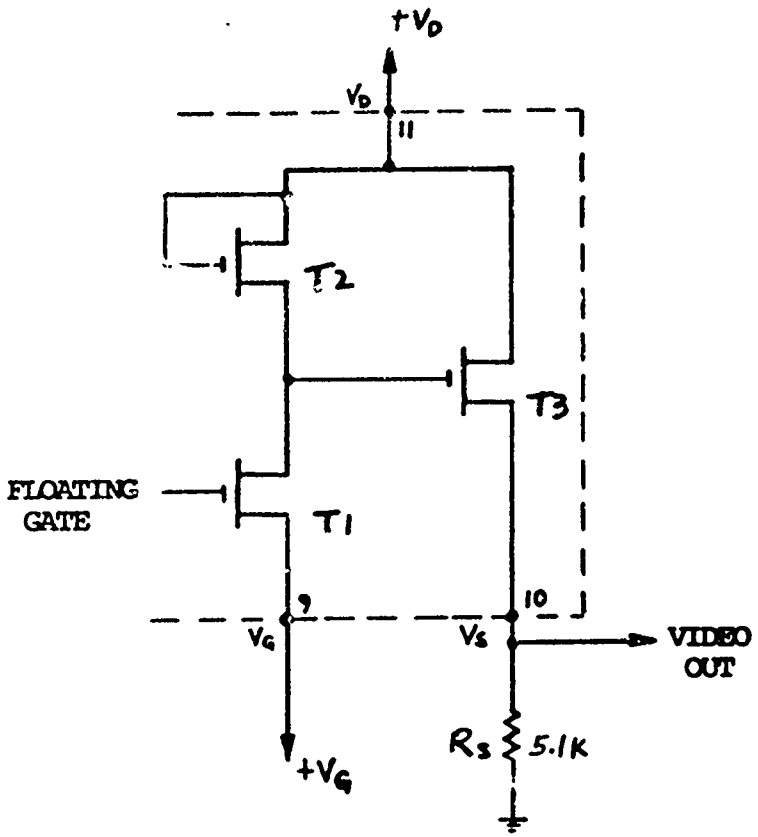

OCILID 1728

FIGURE 3-5
FLOATING GATE AMPLIFIER CONFIGURATION

3.2.5 CCD Gating

As noted, the chosen CCD incorporates an exposure control electrode and sink which are located physically on one side of the photo-elements as shown in Figure 3-6. The exposure control feature allows that all, or some, of the electrons created under the photosite, can be transferred to the sink through the exposure control electrode. Therefore, these signals electrons which are transferred to the sink are not available and are not present in the video which is read out by the usual transfer method.

This exposure control feature has been successfully employed in an "anti bloom" mode. In this mode, the exposure control voltage, ØEC, is kept constant at some intermediate value, say -5 volts. This creates a control so that the contents of the photosite will be "drained" only when the contents exceed some value determined by ØEC. In this mode sharply defined bright zones in the image do not create crosstalk or blooming conditions.

For the WODS application we can use the exposure control electrode in such a way so as to achieve gating. Consider the sequence of events shown in Figure 3-6 through Figure 3-8.

Figure 3-7 shows the exposure control electrode with a zero or negative voltage. In this case, the integration will proceed normally. In Figure 3-8 read out occurs by clocking pulses applied to Øx, Ø1 and Ø2. Figure 3-6 shows the condition when ØEC is set positive. In this case the contents of the photosite is not integrated but flows to the electrical sink. We can arrange to pulse the potential ØEC to integrate for only a short time. Figure 3-9 shows the associated waveforms for Øx (transfer), ØEC, and the resulting exposure time. The exposure time is defined from the negative going edge of ØEC to the positive going edge of Øx when the contents of the photosite are transferred. The

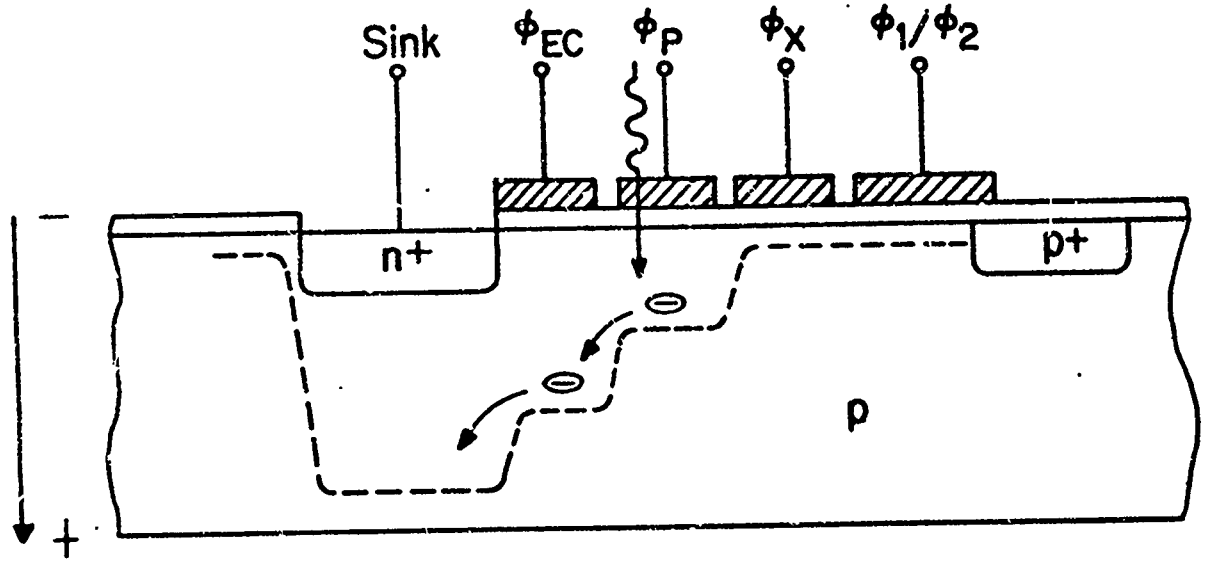

FIGURE 3-6 EXPOSURE CONTROL OPERATION-DRAIN

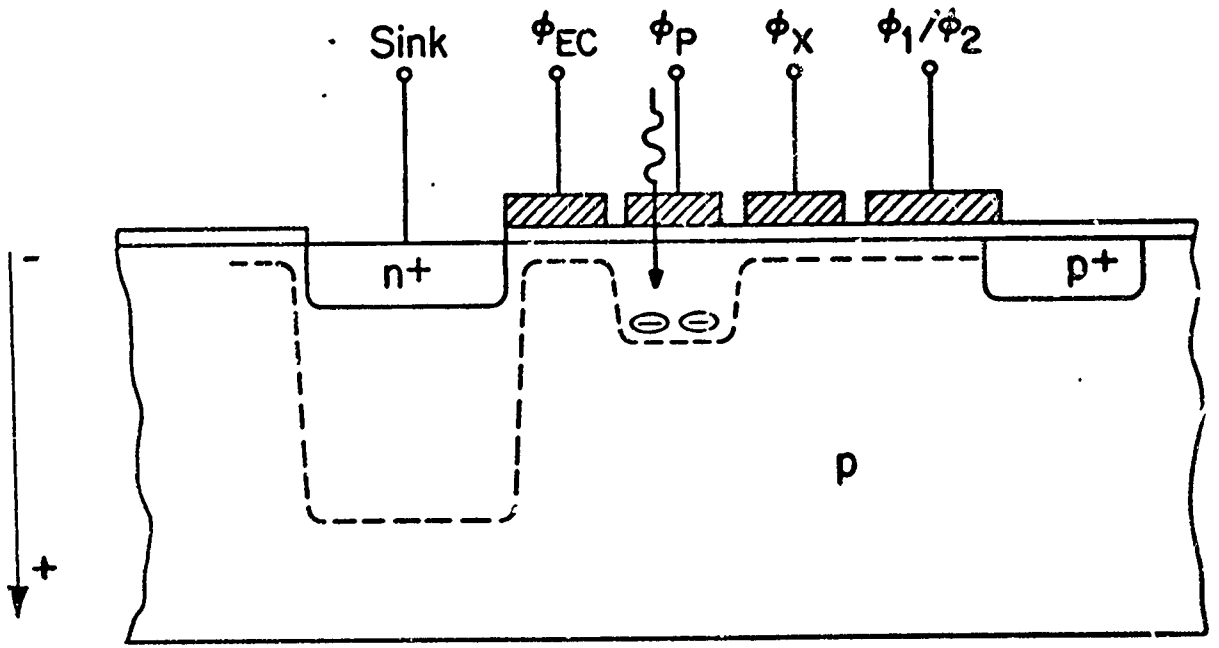

FIGURE 3-7 EXPOSURE CONTROL OPERATION-INTEGRATION

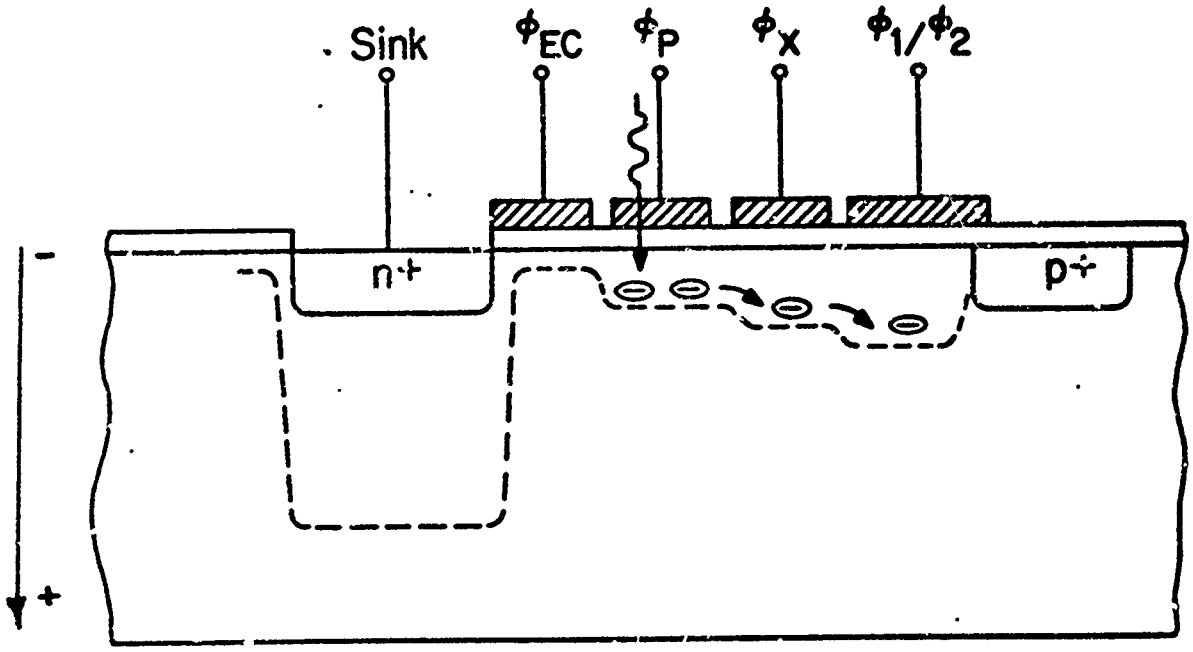

FIGURE 3-8 EXPOSURE CONTROL OPERATION-READOUT

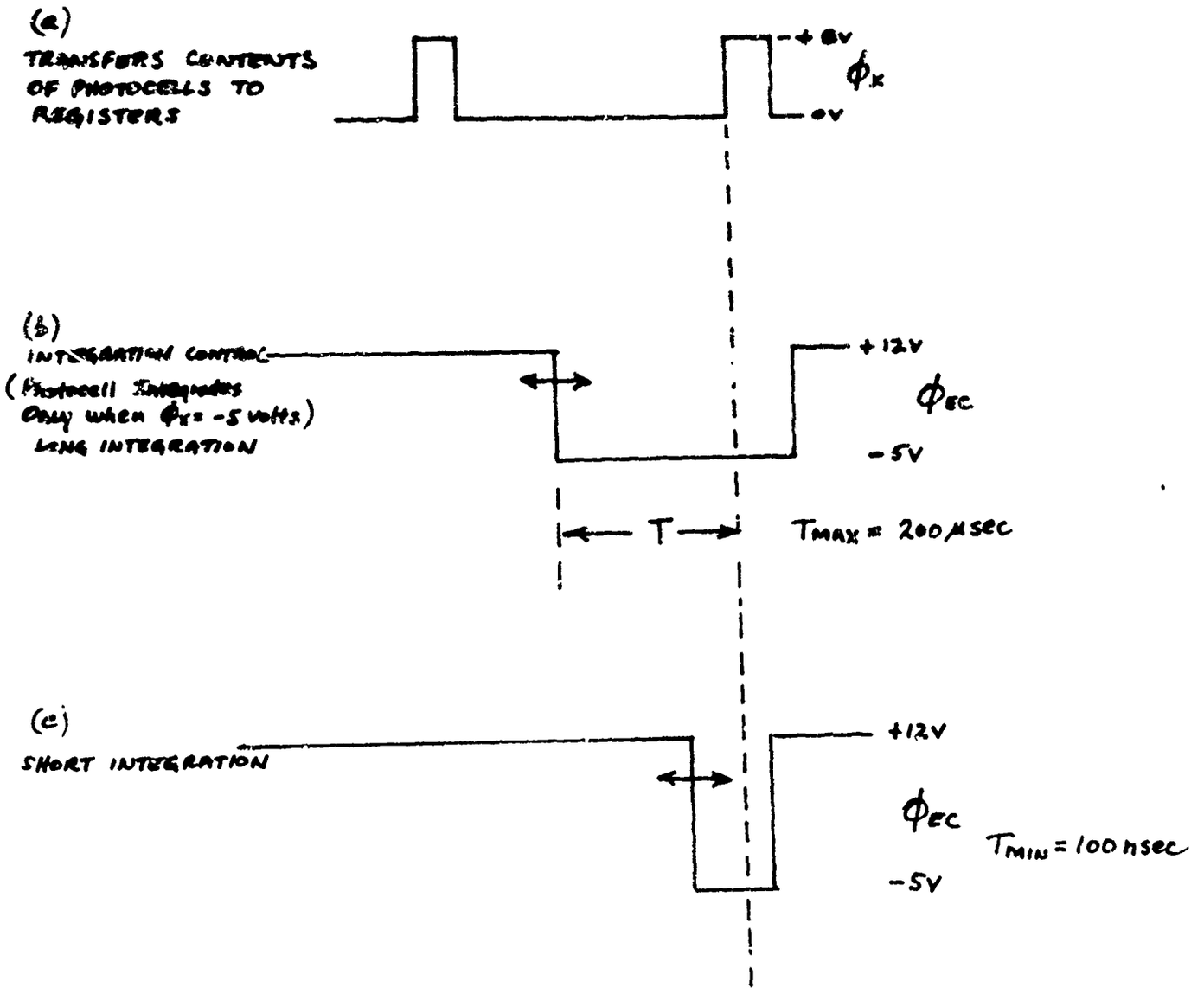

FIGURE 3-9 WAVEFORMS

camera logic has been designed to operate between 100-NSEC to 255 microseconds in the gating mode. A constant exposure time of about 500 microseconds is used in the standard mode. Changing between these modes is accomplished by the use of jumper 3 to 2 (SSA mode) or 1 to 2 (gating mode), on the driver PCB.

Table 3-1 shows the pin numbers of the ILID1728 and the corresponding symbols used in Figure 3-3 with the description of function. Also shown are typical voltages measured at the socket for gating for two arrays typical of that supplied to U.S. Army Electronics Command as part of the deliverable hardware.

This table can be used to reset the voltages after an experiment.

TABLE 3-1 CCD 1728 PINOUT DESCRIPTION

PIN [1]	SYMBOL	FUNCTION	ARRAY 14W2-N021		ARRAY 14W2-N023	
			NORMAL (2)	GATED (3)	NORMAL (2)	GATED (3)
1	Øp	Photowell	6	18	10	16
2	ØEC	Exposure Control	-6		-4	
* 3	Øx	Transfer	8	4.8	8	2.5
L	EC SINK	Exposure Control Sink	18	18	18	7
S	SD	Sink Drain	5	0.6	10	0.23
6	GND		-	-	-	-
* 7	BE1	Floating	5-10	3.5-7	5-10	2-8
8	BE2	Gate	-10	-3.2	-15	3.6
9	Vg	Amplifier	10	10	12	3.5
10	Vs		-	-	-	-
11	Vd		18	18	18	6.5
12	Nc		-	-	-	-
13	OS	Differential	0	0	0	0
14	OD	Gated	10	18	8	8
15	CS	Charge	0	0	0	0
16	RD	Integrator	10	18	15	7.5
* 17	ØR		-5-(+15)	11	-5-(+18)	0-15
18	Ø6		5	2.5	18	6.5
19	GND		-	-	-	-
* 20	Ø2		0-10	-2-(+7.3)	-1-(+9)	-1-(+10)
* 21	Ø1		0-10	-2-(+7.3)	-1-(+9)	-1-(+10)
22	Øg	Electrical Input	-	-	-	-
23	Øs	(Not used)	-	-	-	-
24	GND		-	-	-	-

*Waveforms

1. Pin numbers are measured clockwise from left when pins facing up and notch in dip at bottom.
2. Jumper 3-2 on Driver DCB.
3. Jumper 1-2 on Driver PCB.

3.2.6 Image Display

The video output of the ILID 1728 array is an interlaced field consisting of the odd pixels (864 elements) followed by the even pixels (864 elements). The visual TV presentation will be a checkerboard as shown in Figure 3-10(a). The advantage of this readout is that it preserves the resolution. The disadvantage is that the brightness of the display is low. If a sample and hold circuit is used, the pixels can be extended resulting in a loss of resolution but improved brightness as shown in Figure 3-10 (b). We will not implement the later "hold" technique because of the WODS resolution requirement.

3.3 DESCRIPTION OF THE WODS CAMERA

The high resolution WODS camera uses an interlaced linear image sensor with 1728 photosites which has been discussed above. For this array, white is positive. For array pin connections, refer to Table 3-1 which shows the functions and the voltages associated with normal and gated modes. Only the higher sensitivity floating gate amplifier is used. In operation, the potential on electrode $\emptyset_p$ is normally high. As long as this potential is high, electrons generated by incident light are collected at the photosites. When $\emptyset_p$ goes low and the potential on the transfer gate ØX goes high, charge is transferred from photosites to adjacent shift register sites only if the potential at the site is high. Since only half the shift register site potentials are high at one time (either Ø1 or Ø2 is high), charge from only the odd or only the even numbered photosites is tranferred at one time. This leads to the normal interlaced operation of the device in which alternating odd and even half lines are provided at the output. This mode of operation is used in the WODS camera. Once transfer from array to shift register has been completed, charge integration begins again and the data is shifted out to the amplifiers which

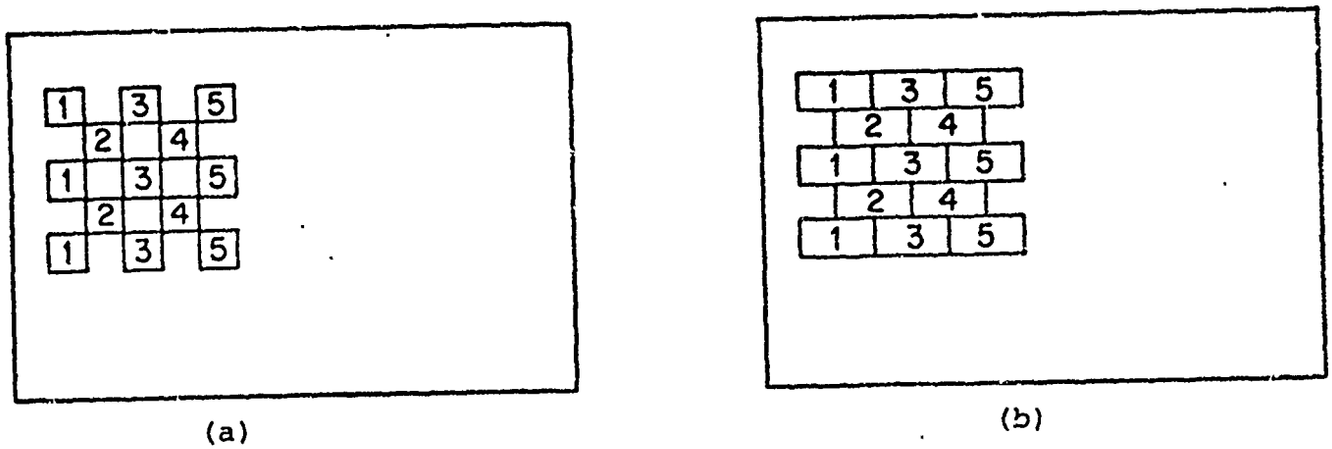

FIGURE 3-10 METHOD OF OUTPUT DISPLAY

convert charge to the output voltage. The integration time (time in which charge is accumulated) in this mode is the time required to shift out two half lines.

NORMAL OPERATION

Figure 3-11 shows the timing signals required for the normal mode. It should be noted that it is the polarity of the shift register clock signals (Ø1 and Ø2) that determine whether the charge in the odd or in the even photosensor elements are transferred to the shift register. Phototransfer occurs when ØX is high. Thus in the half resolution mode where two photo-transfers are made for each line, ØX goes high twice per line.

3.3.1 Video Processor

A simplified Block Diagram of the video processor is shown in Figure 3-12. This video processor has been specifically designed for the ILID 1728 CCD array.

The video processor input is the raw video from the CCD array's floating gate amplifier. The format of this video dictates to a large degree the configuration of the video processor. Signal charge packets are transferred to the region under the floating gate when Ø1 is high. When Ø2 is high there is no charge under the gate and the output voltage returns to the interelement level This level does not necessarily correspond to the black signal level. Instead, it is determined by the potential gradient established by electrodes in the vicinity of the floating gate and by leakage paths in the semiconductor material. Bias control is required in the processor since the interelement level is used as a reference in the DC coupled portions of the processor.

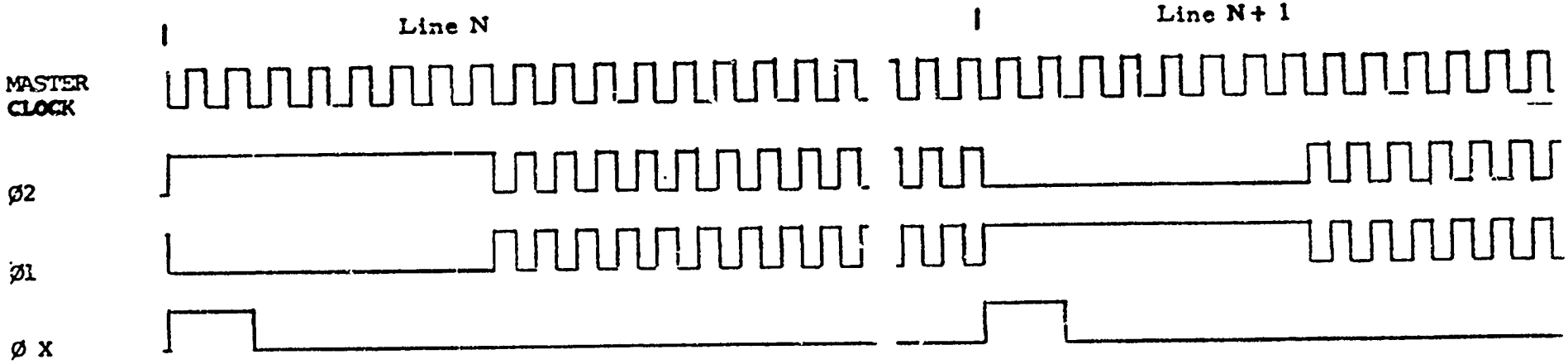

FIGURE 3-11 SIMPLIFIED ARRAY TIMING DIAGRAM

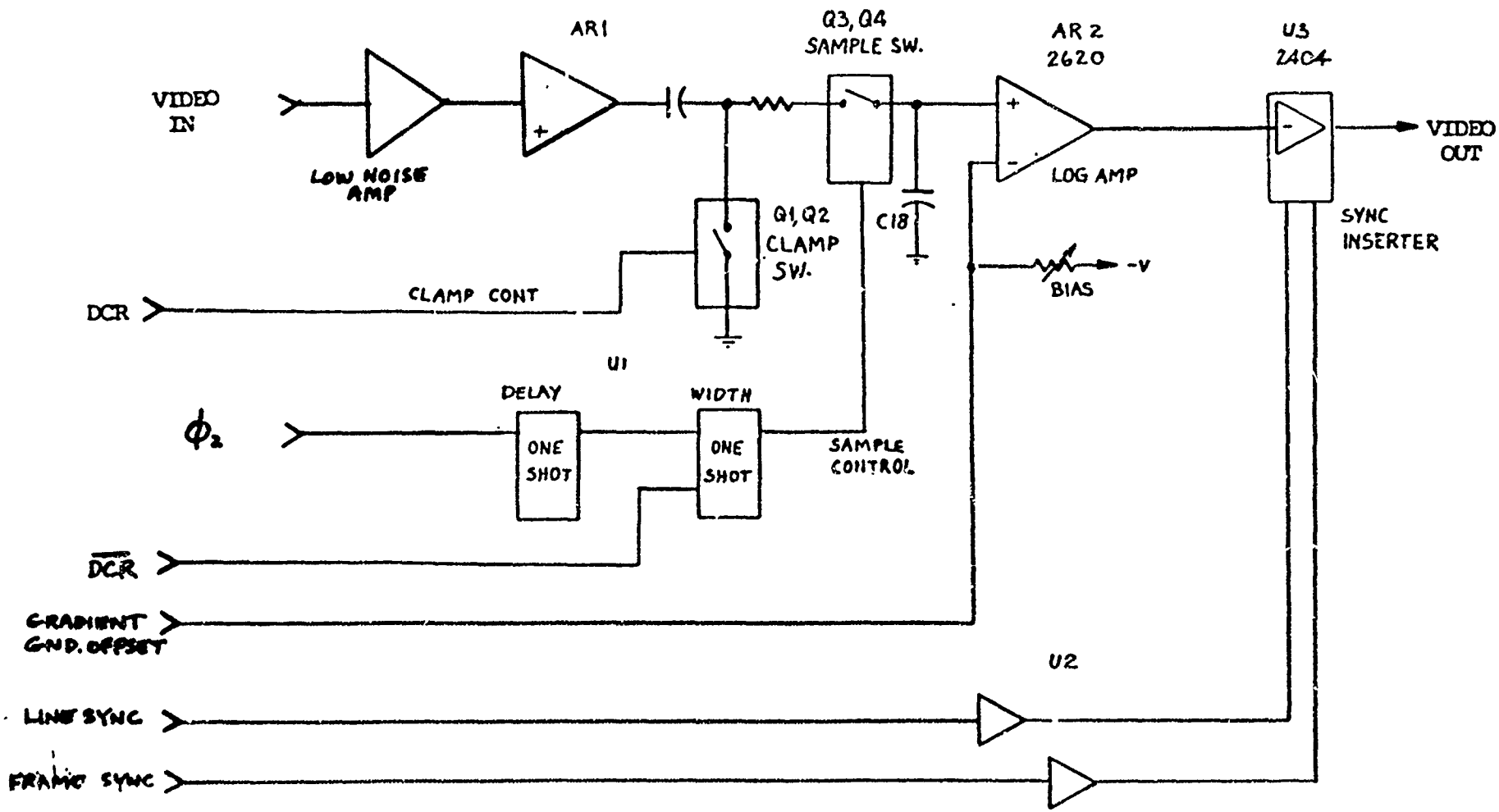

FIGURE 3-12 VIDEO PROCESSOR

Offset compensation was required since arrays used in the full resolution mode demonstrated a DC offset between odd and even half lines.

For the CCD 1728 Camera, where the video is positive going, it is first applied to a low noise inverting amplifier with a nominal gain of 4. The video is then applied to AR1 which is an AC coupled amplifier designed for a nominal gain of 10. The output of AR1 has sufficient amplitude for DC restoration. This is accomplished on an element-by-element basis. The clamp switch (consisting of FET's Q1 and Q2) closes at the center of the interelement interval and thus clamps the interelement level to ground.

The clamped video is applied to a sample and hold circuit consisting of FET's Q3 and Q4 and capacitor C18. The sample switch closes at the peak signal and charges the holding capacitor. When the switch opens the peak value is stored. In the WODS Camera, the switch is operated twice per element, once at the signal peak and once during the clamping time. This results in a chopped signal with approximately a 50% duty cycle. It is similar to the unsampled signal, however, due to the dual sampling action, it is squarer and comparatively noise free. The dead zones between elements permits a true interlaced display of the camera video.

The logic Augat circuit card also contains the voltage dividers used to provide the DC biases to the array and the DC levels to the clock drivers.

3.3.2 Logic

The logic for this camera is located on the Control Logic Board. CMOS is used in this design throughout in order to guarantee fast rise times and fall times for the gating experiment.

The master clock is generated on the Oscillator Driver Board. In the WODS Camera, the master clock is 2.0 MHz. A dual one shot is also located on this board. It generates the element-by-element clamping pulses for the video processor.

The master clock is applied to the line logic generating circuitry on the Control Logic Board. This section includes a 12 stage counter. A count of 1028 is decoded. Half a clock period later, the decode is used to set a flip-flop which resets the counter. Half a clock after the 1029th pulse, the flip-flop is reset and the cycle begins again. Thus a divide by 1029 is established. The line sync pulse is developed from the basic cycle in a flip-flop formed by cross-coupled gates. The decode of 1028 sets the flip-flop while a count of 8 resets it. Thus the line sync pulse is 9 clock intervals long.

The array clocking logic and the multiplexer develop the logic signal ϕ2 which is used for the ϕ1, ϕ2 and ϕBE1 clocks. This signal changes phase during the interline period allowing the combination of charge from adjacent odd and even photosites.

3.3.3 Clock Drivers

The CCD arrays present a capacitive load to the clock signal. This is analogous to the load presented by MOS memories and shift registers. Thus clock drivers must be used to interface between the logic and the arrays. The drivers must be capable of rapidly charging and discharging the array capacitance. The camera uses CMOS bilateral switches configured as single pole-double throw switches. There are four separate switch sections on each IC. Two sections are used to form each single pole-double throw switch. A logic input switches the output to either ground or the clock supply voltage. The switches can either invert or not invert the sense of the logic depending upon how they are connected.

In the WODS Camera, the BE1 clock is AC coupled and clamped to a DC voltage to provide clocking between two positive levels.

3.3.4 X-Y Sweep Generation

The video output from the ILID 1728 CCD array is written onto the storage target of a Hughes 639 scan converter. This device requires sweep voltages of 0 to 1 volt in both axis. For a total FOV of 10 x 15 degrees the total number of lines in both directions will be 1728 by 2600. Therefore, for this case, each line corresponds to a voltage deflection of less than 0.5 MV in both the X and Y direction. Furthermore, fluctuations in this voltage must be kept to a fraction of this voltage in order to prevent scan irregularities that may lead to an unacceptable presentation.

In the WODS application the video line scan is written in the Y direction, while the angular mirror displacement is written in the X direction. These voltages are derived by means of the scan interface circuits.

The voltages are derived from a low noise OP amp configuration used in an integration mode. These ramps are synchronized by the master logic and by the TTL sync output of the galvanometer mirror control.

3.3.5 Exposure Control Logic Setting

The logic control has been discussed in detail in Section 3-6. The swtiches for exposure control are located from U8 to U10 on the Logic Augat Board. The width of the pulse ØEC is directly controlled by those switches. In other words, the setting of the exposure time (integration time) for the array depends on whether the switches are open or closed.

Table 3-2 is the list for different exposure time settings. Table 3-3 shows the layout for each switch on the Logic Board. These switches are directly visible with the camera top removed. A photograph of the WODS Camera with the top removed is shown in Figure 3-13. The logic switches are found on the lower left portion of the Augat Board.

TABLE 3-2 EXPOSURE CONTROL SETTINGS

EXPOSURE TIME (μsec)	LOGIC SETTINGS									
	10	9	8	7	6	5	4	3	2	1
0	0	0	0	0	0	1	0	1	1	1
.5	0	0	0	0	0	1	0	1	0	1
1	0	0	0	0	0	1	0	1	0	0
2	0	0	0	0	0	1	0	0	1	0
3	0	0	0	0	0	0	1	1	1	1
4	0	0	0	0	0	0	1	1	0	1
5	0	0	0	0	0	0	1	0	1	0
10	0	0	0	0	0	0	0	0	0	0
20	1	1	1	1	1	0	1	0	0	0
30	1	1	1	1	0	1	0	0	1	1
40	1	1	1	0	1	1	1	1	1	0
50	1	1	1	0	1	0	0	1	1	0
100	1	1	0	0	1	1	0	1	0	0
150	1	0	1	1	0	0	1	1	1	1
200	1	0	0	1	1	1	1	1	1	1

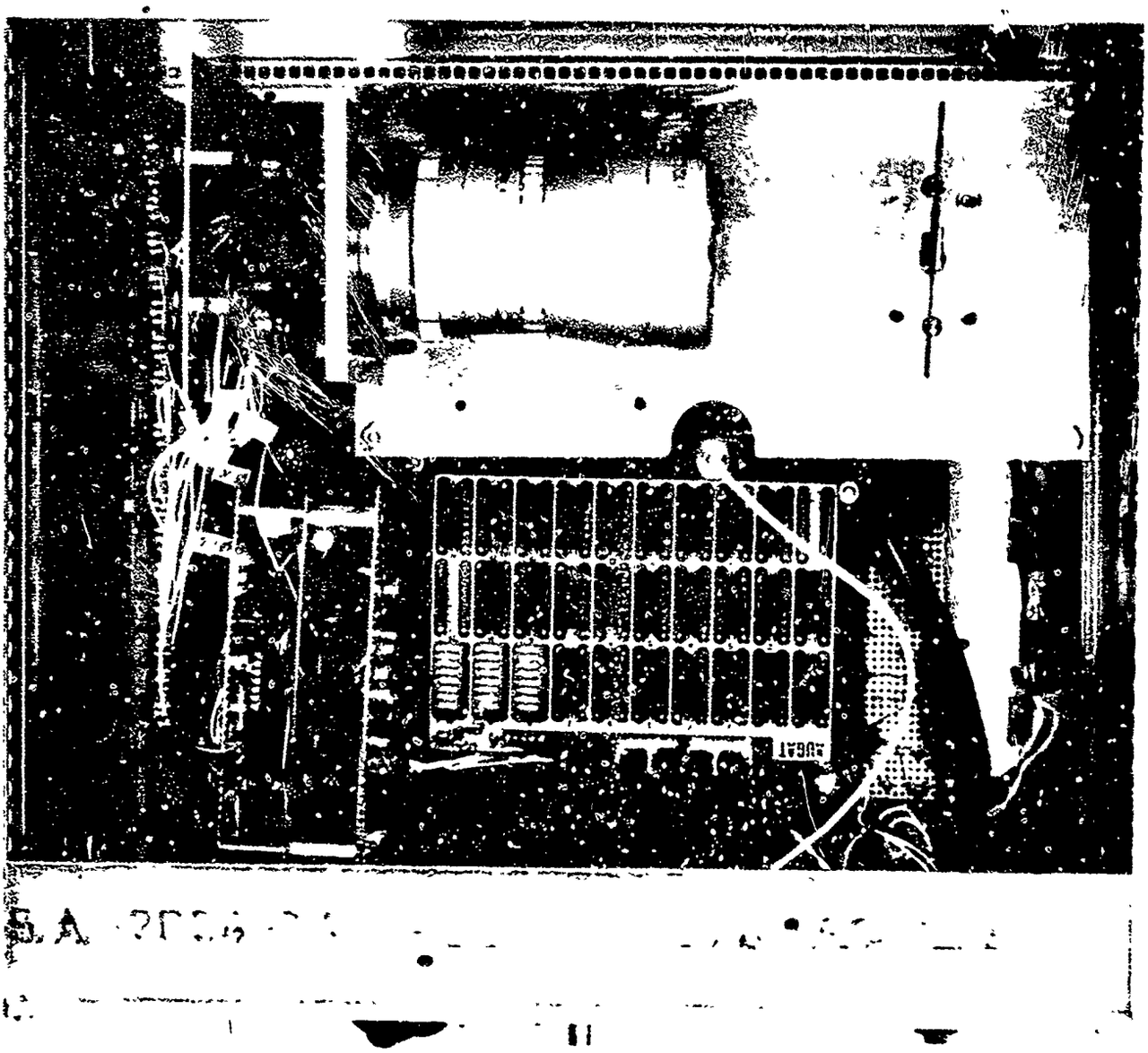

FIGURE 3-13. WIRE OBJECT DETECTION SIMULATOR (WODS) TOP VIEW

TABLE 3-3 LOGIC LAYOUT

POSITION	U8	U9	U10
1	EC3	S3	EC1
2	EC4	S4	EC2
3	EC5	S5	---
4	EC6	S6	EC POLARITY
5	EC7	S7	---
6	EC8	S8	---
7	EC9	S9	S1
8	EC10	S10	S2

EC = EXPOSURE CONTROL

S = STROBE PULSE TRIGGER (5V TTL)

OPEN = 0

CLOSED = 1

3.4 OPERATING PROCEDURE

In this section we establish a procedure for system setup and adjustments.

3.4.1 Components

The system consists of the following:

3.4.1.1 WODS Scanner

This unit consists of a Fairchild 1728 CCD Array, socket board, logic board, driver board, various sweep generator boards, and system interface. The unit also contains a galvanometer scanner motor, General Scanning Model C-300PD plus mirror. Three-self-contained power supplies are designed into unit. All interface signals enter and leave the unit through the rear panel. One toggle switch activates the scan for the entire system. The rear panel is shown in Figure 3-14.

3.4.1.2 Scan Converter

A Hughes 639 scan converter is used in the high resolution mode (1029 TVL) to convert the line scan output to a 1029 TV standard. The scan converter can be used to display the image for up to 1/2 hour without serious degradation. Front panel adjustments are brightness and contrast which control levels during writing. By panel control, the unit may be in zoom or normal modes.

3.4.1.3 Scan Controller

A general scanning driver controller (Model CCX-102) is used to provide sweep signals to the galvanometer scanner in the WODS

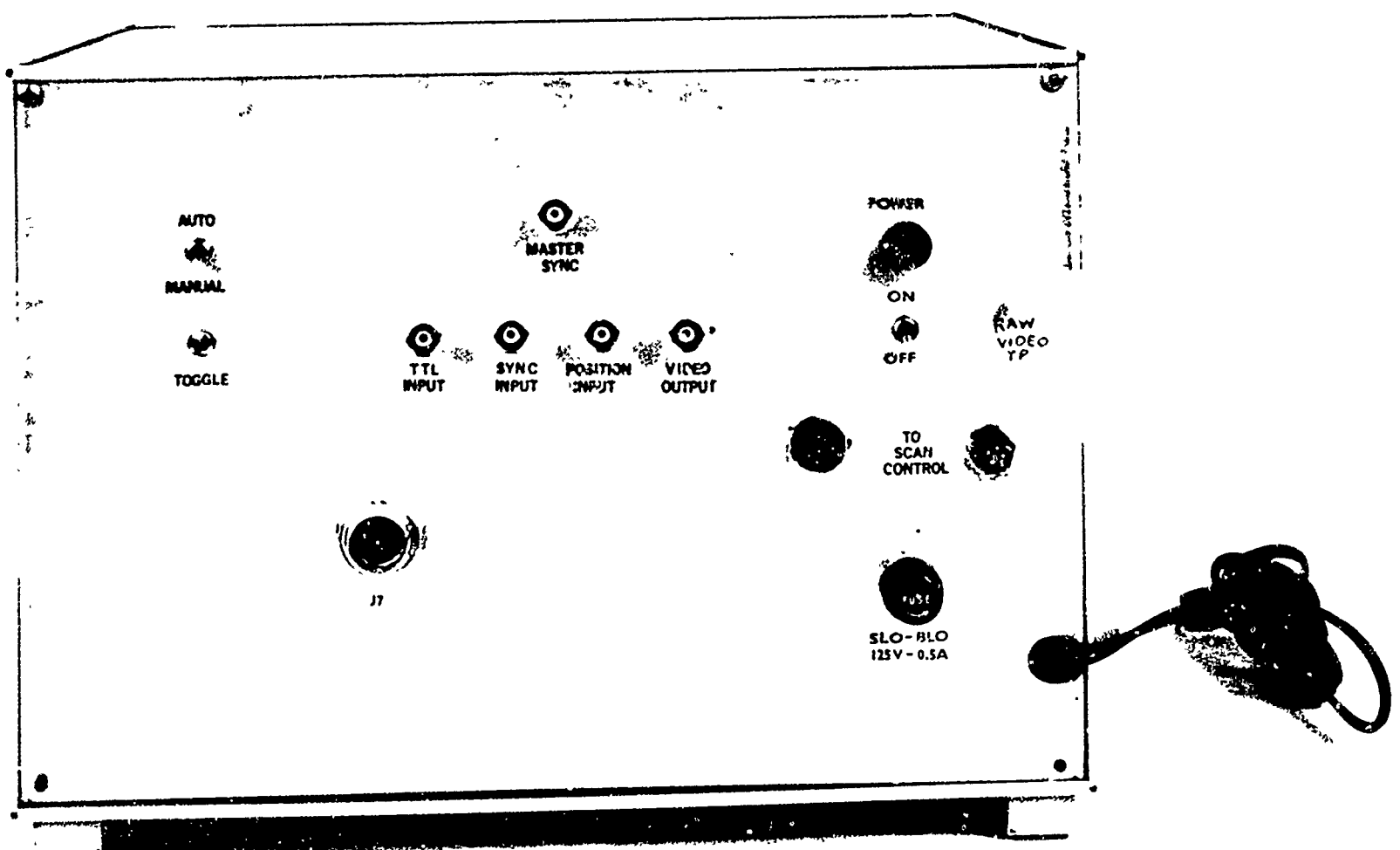

FIGURE 3-14. WIRE OBJECT DETECTION SIMULATOR (WODS) REAR PANEL

camera. The output of this unit is a TTL signal which defines "beginning of frame".

Front panel adjustments include "ramp frequency" which controls the duration of the mirror sweep, "offset" which controls the position of the mirror axis, and "amplitude" which sets the scan angle. The front panel includes a mode control which allows selection of internal or external sweep generators.

3.4.2 Wods Scanner Test

3.4.2.1 Scanner Setup

Before turning on the WODS Scanner, verify the following:

a. Power switch - off.
b. Control source set to "manual"
c. Video output (BNC) connected to scan converter video input.
d. TTL sync output of scan controller connected to sync input of WODS Scanner.
e. Command connector from WODS Scanner to scan converter (Cannon Plug J7) is in place.
f. Driver cable from scan controller to WODS Scanner is in place
g. Monitor is "on".
h. Monitor is connected to video output of scan converter.

3.4.2.2 Turn-On

After suitable warmup delay for scan converter (5 minutes) system is ready for operation. Remove top cover of scanner by loosening side screws and sliding back top panel.

3.4.2.3.1 Operational Test

For the next tests, it is suggested to use a standard TV test target or any other photograph that can be interpreted with respect to grey tones, resolution, and aspect ratio. Set the test target along the optical axis at about 5-8 feet. Illuminate this test object from the side so that no glint or surface irregularities can be seen. Establish the following conditions:

a. Attach oscilliscope to video output via a BNC connector.

b. For oscilliscope external trigger use BNC from master sync at rear of WODS scanner.

c. Set focusing ring of lens to approximate distance.

d. Observe video output on oscilliscope. Adjust f/ number of lens so that signal is in range of 0-1 volt. Readjust focusing to peak fine structure in video.

e. On scan converter front panel, set zoom control to "off" and position brightness and contrast to typical values.

   Brightness: 3 divisions from left stop
   Contrast: 6 divisions from left stop
   (Ten divisions total each control)

f. Turn on 1029 TVL monitor and set to maximum brightness.

g. On scanner control, set signal source to internal. Verify sweep by viewing oscilliscope. Set 10 turn pot of ramp frequency to 1.60. Sweep is now let for approximately 0.5 Hz.

System is now ready to initiate scan commands. Depress toggle at rear of scanner momentarily. Image should appear on monitor at end of second full frame period (from 2 to 4 seconds delay). To optimize image:

- Adjust monitor brightness
- Adjust f/number of lens
- Adjust brightness of scan converter
- Adjust contrast of scan converter (interactive with above)

It will be necessary to adjust horizontal and vertical position and scale on monitor to provide for proper aspect of image.

3.4.2.3.2 Zoom

Switch scan converter into "zoom" mode. Adjust zoom control to observe magnified portion of image. Move joystick to inspect different portions of image.

3.4.3 Replacement of CCD Array

The CCD array may be removed and replaced by following this procedure: (Refer to SDI of Appendix C)

a. Set up a test target with proper illumination. Record the level of video output that corresponds to peak.

b. Turn WODS scanner to "OFF". Disconnect power.

c. Open CCD case which contains replacement array. Note that pins of CCD are pressed into black foam. This is chosen to be conducting foam to prevent static charge buildup.
During the next step, the CCD must be protected from damage due to static charging.

d. Reach into the WODS scanner at the CCD. With one hand under the CCD and one above, release the socket by pushing the L-shaped bar downwards. Prior to removing CCD, place one hand on the electrically conducting foam to discharge any static buildup. Remove CCD and return to foam. Insert replacement

CCD array into socket reversing procedure. The notch in the CCD case is "UP".

e. Switch "ON" WODS scanner with oscilliscope monitoring video output while viewing previous test target.

f. If video level is same as before, no further adjustments are necessary. In this case, initiate scan and observe result on monitor.

g. If video level is low, adjust CCD amplifier gain (vg) which is done by rotating ten turn potentiometer on driver board (number 11) until video peak level is equal to or larger than previous level.

h. Video level may be optimized by adjustment of transfer clock voltages, at pot number 2 of the driver PCB.

i. Verify image quality by scanning image.

3.4.4 Verification of Gating and Synchronizing Signals

The following setup is required: Change jumper on driver PCB from position 3 to 2 (direct mode) to position 1 to 2 (gating mode). This connection must be soldered for proper performance.

3.4.4.1 Verification of Gating Pulse

The duration of the exposure time can be varied from less than 100 nsec to over 200 microseconds in the gating mode. This test verifies the signals input to the CCD. Gating time is defined from the falling edge of ØEC (+2 to -2 volt swing) to the leading edge of Øx. These waveforms are observed on the scope in separate

channels by placing pins in socket position number 2 (ØEC) and position number 3 (Øx). Exposure time settings are adjusted by utilizing switches EC1-EC10 on U10 of the logic board. For all positions, the leading edge of ØX is constant. Refer to Table 3-2 and 3-3 for settings and layout.

3.4.4.2 Verification of Illumination Source Position

In a similar manner we can trigger an external light pulse under switch control. Define the exposure pulse position on an oscilloscope by either Øx or Øec.

Set other oscilloscope probe at position "TP" on the driver PCB (refer to SD1 of Appendix C). The pulse will be zero, going positive 5 volts for a time of less than or equal to one clock pulse of 500 nsec duration.

With trigger pulse observed on oscilliscope, perform the following:

a. Adjust duration of pulse by ten-turn pot mounted on driver board. Duration can be set from 100 nsec to 500 nsec.

b. Adjust position of pulse with respect to exposure time by changing switches S1 through S10 on U8 through U10 of the logic board.

WODS scanner can now be utilized with external pulse light source (such as a laser). Use a TTL output pulse to trigger the laser pulse. Observe video output during preset exposure time under adjustment of EC1 - EC10. Switches S1 through S10 can be used to experimentally compensate for any delay in the laser pulse circuitry and range delay when present.

4.0 FEASIBILITY EXPERIMENT DESCRIPTION AND GOALS

The testing performed in this contract was for the purpose of defining the utility of the selected CCD array for gated operation and, secondly, to prove the capability of the array for the detection of high resolution wires (single site activation) in the scanning mode. The following sections describe the selection of the arrays and the performance achieved in the WODS scanner. This section justifies the selection of the array to be supplied as part of the WODS scanner which was delivered under this contract.

4.1 CCD ARRAY SELECTION

The purpose of this test phase was to select the best candidate CCD ILID 1728 arrays which will provide useful information concerning their performance in both a gated and normal mode of operation. After testing, several CCDILID 1728 have been chosen according to suitable criteria. The following are the test procedures:

4.1.1 Test Equipment

The test equipment was mounted on a 2-meter optical bench. A calibrated light source was mounted on one side of the bench. The light source operated at a color temperature of 2854°K and was controlled by a constant power supply. A CCDILID 1728 array exerciser could be mounted at any position of the bench. The CCD under test was plugged directly into a socket mounted in the exerciser. The video output was displayed on an oscilliscope and recorded via a polaroid scope camera.

4.1.2 Measurement Conditions

1) Measurements were performed at room temperature (25°C)
2) DC illumination was used.
3) Nominal clock frequency of 2MHz was used. This provides a transfer pulse frequency of 2 KC such that a normal integration time of 500 μsec for the normal mode operation was obtained. This clock frequency is consistent with high resolution imaging as required for this test.
4) Since these measurements were intended only to rank the available arrays, no source calibration was made. Uniformity of illumination across the array was provided by use of suitable geometry. The tungsten filament of the lamp was separated by up to 35 inches to simulate a point source. Secondly, an opal glass diffuser was used at the CCD plane to further create diffuse and uniform illumination.

4.1.3 Test Description

The test procedures utilized in this report are contained in Appendix B, "Experiment Test Plan", which was supplied to USAECOM for review as part of this contract.

Twenty one CCD 1728 arrays were made available by FISD for testing during this contract. The available arrays were screened for proper electrical and optical performance for both the normal and gating portions of the experiment. During this effort two series of tests have been made. In the first series of tests, the Electro-Optical performance of the arrays was characterized. In the second series of tests the performance of the entire WODS scanner was characterized.

4.1.4 Electro-Optical Performance

These tests were intended to characterize the CCD 1728 for various modes of operation. Testing was accomplished with a breadboard realization of the WODS scanner logic, driver, and socket boards only.

4.1.4.1 General Electrical Factors

Using DC illumination, the signal level was tested for both the gating and normal exposure mode. Table 4-1 shows the signal voltage level for useful in the normal integration mode. The signal level is a direct indication of the sensitivity in that mode of operation. This table includes all arrays that were suitable with respect to blemishes and uniformity. The relative sensitivity and ranking varies by over a factor of 100.

Table 4-2 shows the results of a preliminary check of the gating operation. The table shows the uncancelled signal when the exposure time was set for zero seconds. Also shown is the extinction ratio which is defined as the ratio of the signal obtained in the normal mode to the zero exposure signal in the gating mode. The lower the extinction ratio, the less suitable is the array with respect to gating.

All signal levels were measured with adjustments to applied voltages made to optimize performance for each array.

TABLE 4-1 SIGNAL OUTPUT - NORMAL MODE

ARRAY	SIGNAL (MV)
5C W1 NO17	850
5D W4 NO5	760
5C W1 NO24	600
4W W2 NO23	440
4W W2 NO21	400
5D W5 NO12	365
5B W2 NO16	200
4W W4 NO2	70
5B W1 NO5	35
5A W2 NO13	30
5B W1 NO7	24
5B W1 NO9	7

* FLOATING GATE AMPLIFIER
* 500 µSEC INTEGRATION

TABLE 4-2 SIGNAL OUTPUT - GATING MODE

ARRAY	UNCANCELLED SIGNAL * (MV)	EXTINCTION RATIO **
5C W1 NO17	120	7.1
5D W4 NO5	40	18.8
5C W1 NO24	70	8.6
4W W2 NO23	15	39.4
4W W2 NO21	5	80.
5D W5 NO12	35	19.5
5B W2 NO16	10	20.
4- W4 NO2	2	35.7
5B W1 NO5	3	17.5
5A W2 NO13	7	4.3
5B W1 NO9	0	--
5B W1 NO9	0	--

* FOR ZERO EXPOSURE TIME

** RATIO OF SIGNAL FOR ZERO EXPOSURE TIME TO 500 MICROSECOND EXPOSURE TIME. (SEE TABLE 4-1)

4.1.4.2 Signal Output Versus Exposure Time (Normal Mode)

When the array is operated in the normal mode of operation, the applied voltage, DC ØEC, governs the signal that is in the potential well available for readout. This voltage can be adjusted from a negative value (storage mode) through a positive value (full drain). Variation of this potential thereby accomplishes the exposure control function. Figure 4-1 shows the plot of signal output versus DC ØEC over the useful exposure control region.

4.1.4.3 Signal Output Versus Exposure Time (Gating Mode)

The video output of the CCD was measured over a range of exposure times from about 100 NSEC to several hundred microseconds. The procedure for adjustment of the exposure time has been outlined in Section 3.9.

Figure 4-2 is a plot of the output over the range of interest showing operation to 500 Nanoseconds. At about 500 Nanoseconds, there is a sharp drop in gating effectiveness. These results were obtained after optimization of applied voltages on the array. Therefore, we have found a definite lower limit on the gating time achievable for this array.

4.1.4.4 Propagation Characteristics

The gating capability of the ILID 1728 array was found to be limited by the propagation time along the polysilicon exposure control electrode. This effect is due to the dispursive delay line characteristics of this electrode causing both attenuation of the exposure control pulse as it propagates with finite velocity along the array. The effect has been measured by inverting the polarity of ØEC. Therefore, the voltage is pulsed from normally store level to drain level.

PARAMETERS:

- ARRAY: REDI - 4W2 #21
- CLOCK RATE: 2 MHz
- 2854°K COLOR TEMPERATURE
- INTEGRATION TIME: 500 µSEC
- LENS APERTURE: F/1.4
- AMBIENT TEMPERATURE

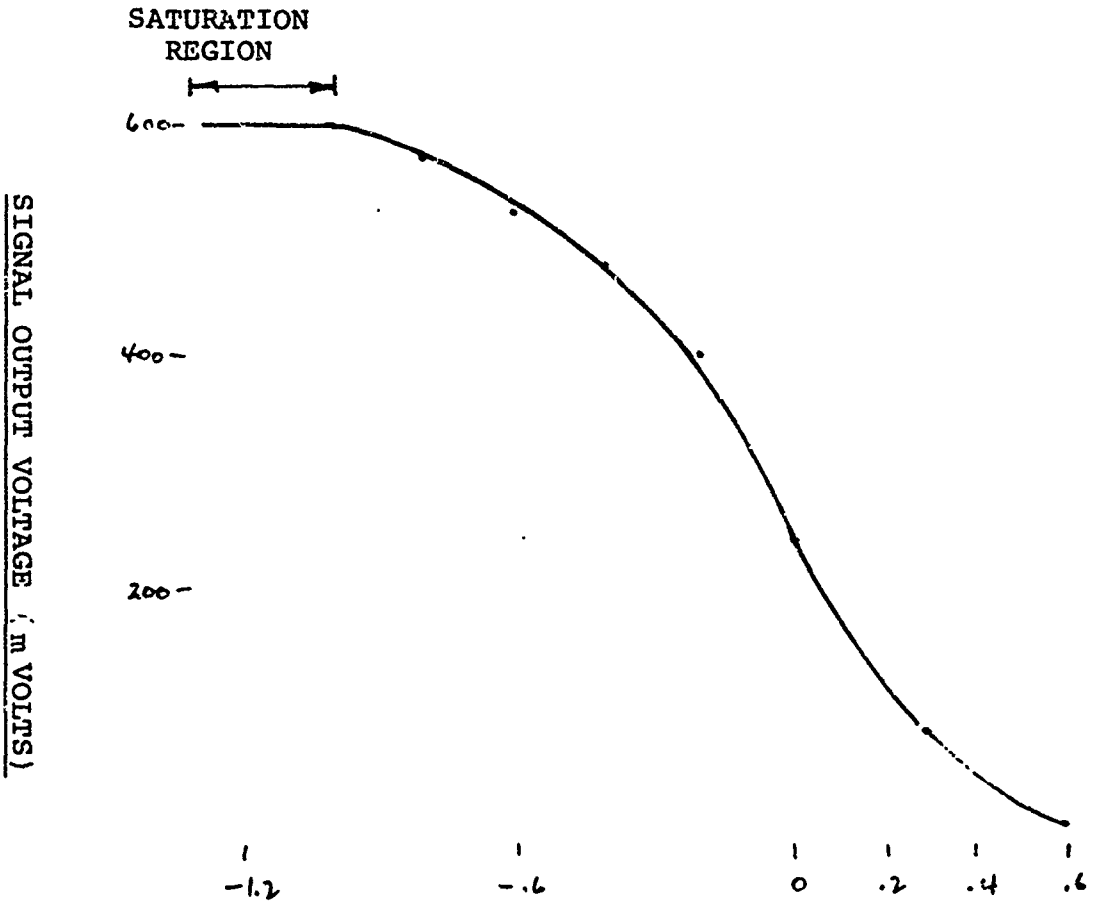

FIGURE 4-1 SIGNAL OUTPUT VERSUS EXPOSURE CONTROL VOLTAGE (NORMAL MODE)

PARAMETERS:

- ARRAY: REDI - 4W2 #21
- 2854°K COLOR TEMPERATURE
- ØEC HIGH +3.0 VOLTS
- LOW -5.4 VOLTS
- LENS APERTURE: AS SHOWN
- AMBIENT TEMPERATURE

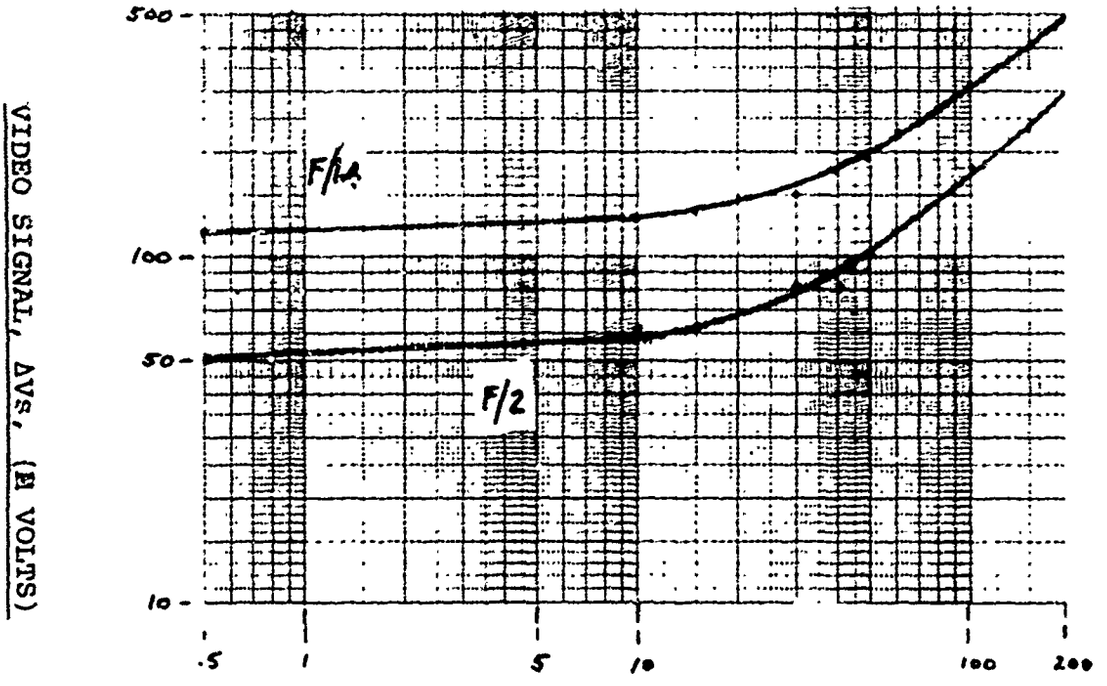

FIGURE 4-2 SIGNAL OUTPUT VERSUS EXPOSURE TIME (GATED MODE)

Figure 4-3 shows the operation of the ILID array in the gated mode for both the positive going (Figure a) exposure pulse and the negative going (Figure b) exposure pulse.

In Figure 4-3a the top oscilliscope channel shows the array output for one portion of the clock phase (odd only). From left to right the output consists of 864 pixels which are the alternate pairs of the full 1728 pixels. At the end of the record is an overscan with no video output simply due to the method of electronic timing. The bottom portion shows the exposure control pulse, ØEC, which is normally low (-5.4 volts) and is pulsed positive going (0.6 volts) with a 10 microsecond duration. During the exposure control pulse of -5.4 volts of the CCD is integrating. While it is positive, the CCD is dumping the charge.

Figure 4-3b shows incomplete and non uniform erasure of charge due to propagation delay of the 500 NSEC exposure pulse. The transition time from "off" to "on" becomes about 40 microseconds due to the RC time constant of the array.

4.1.4.5 Verification Of Gating Capability

The ILID array was operated in the gating mode with an external light pulse which was provided either by a strobe (Strobotac, Type 1531-A Zenon flash lamp) or an infrared emiting diode (Fairchild LED FPE 104) operating at 0.85 micrometers.

Figure 4-4 shows the temporal phasing among the exposure control, transfer pulse, and, light source trigger. Figure 4-4a shows the 500 NSEC transfer pulse (top) and the actual trigger output of the strobe unit (bottom) In this example, the light pulse occurs 13 microseconds before the transfer.

PARAMETERS: RED I - W2#21

TOP: FGA OUTPUT
BOTTOM: EXPOSURE CONTROL PULSE, ØEC

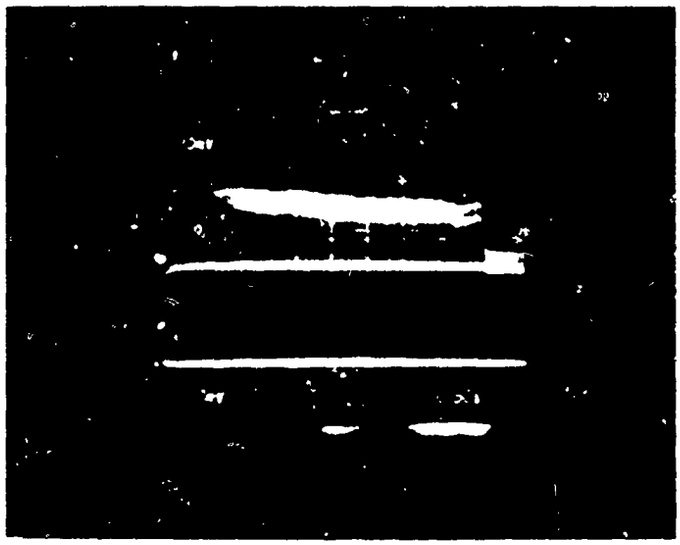

(a)

FULL STORAGE

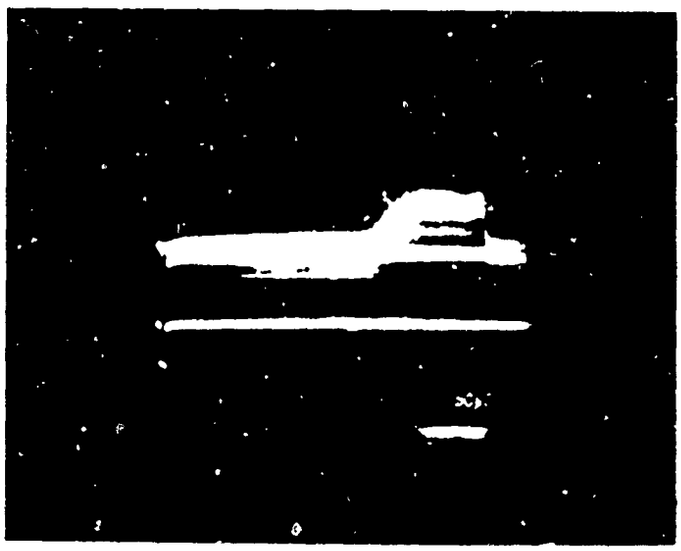

(b)

FULL DRAIN

FIGURE 4-3 GATING CHARACTERISTICS

PARAMETERS:

LIGHT SOURCE: XENON FLASH LAMP
STROBOTAC TYPE 1531-A
PULSE WIDTH 3 MICRO SEC.

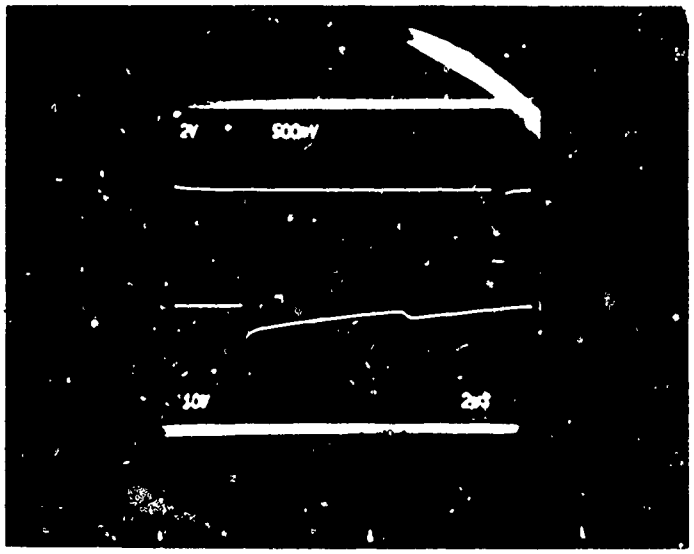

TOP:

TRANSFER PULSE
ØX (500 NSEC)

BOTTOM:

STROBE PULSE
13 µSEC DELAY

(a)

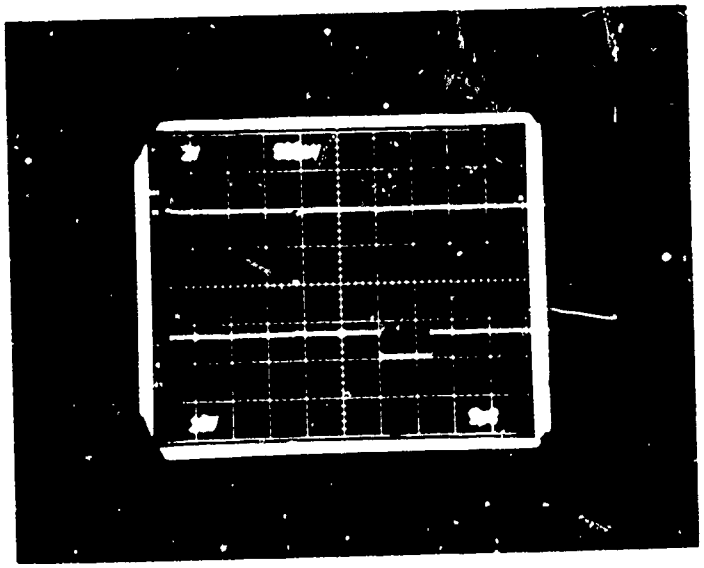

TOP:

TRANSFER PULSE
ØX (500 NSEC)

BOTTOM:
EXPOSURE CONTROL
ØEC

(b)

FIGURE 4-4 TEMPORAL PHASING

Figure 4-4b shows the relation between the exposure control pulse and the transfer.

Figure 4-5 shows the results of gating the ILID 1728 when an infrared emitting diode is focused onto the array. Prior to this experiment it was demonstrated that a similar light emitting diode could be imaged onto the array so that the video was confined to a small extent on the array. In this way, optical blur was estimated to be less than, or equal to, three pixels.

Figure 4-5a shows the video output of the array for a 500 NSEC integration time. Figure 4-5b shows the same array when the infrared pulse is present but the exposure time is set to zero.

The array has been shown to be gateable, but the results are comprimised by two factors. First, the spatial extent of the point image is degraded probably completely due to crosstalk in the infrared. Secondly, the rejection ratio was found to be only 20%.

Figure 4-6 shows the results of imaging a wire onto the array while illuminating the wire by a Zenon flash lamp. Figure 4-6a shows the lack of signal when the strobe pulse is outside the exposure time of the array. Figure 4-6b shows the video for a 5 microsecond integration time and a 3 microsecond illumination pulse. The skewed video in this photograph was apparently due to transfer inefficiency during readout. However, any attempt to remedy this by voltage adjustment reduced the signal.

PARAMETERS:

LENS: 50 MM COSMICAR

SOURCE: FAIRCHILD FPE 104 IR DIODE

SOURCE PULSE WIDTH: 500 μSEC

FLOATING GATE AMPLIFIER (FGA)

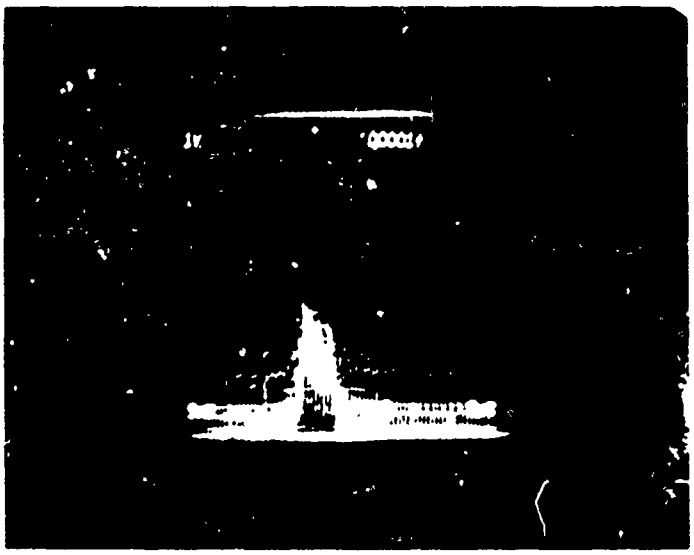

(a)

INTEGRATION TIME = 500 NSEC

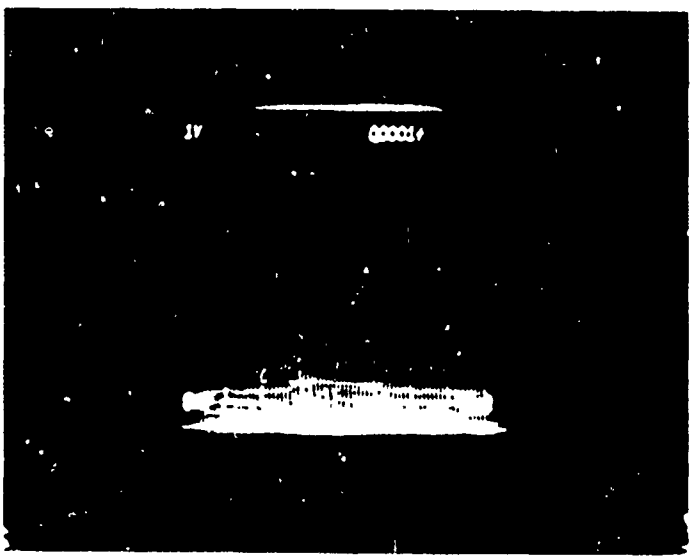

(b)

INTEGRATION TIME = ZERO

FIGURE 4-5 GATING WITH INFRARED DIODE (500 NSEC)

PARAMETERS:

LIGHT SOURCE:	STROBOTAC 1531-A (3 μSEC)
WIRE DIAMETER:	5 MILS, BARE
LENS:	COSMICAR 50MM AT F/1.4
DISTANCE:	15 INCHES

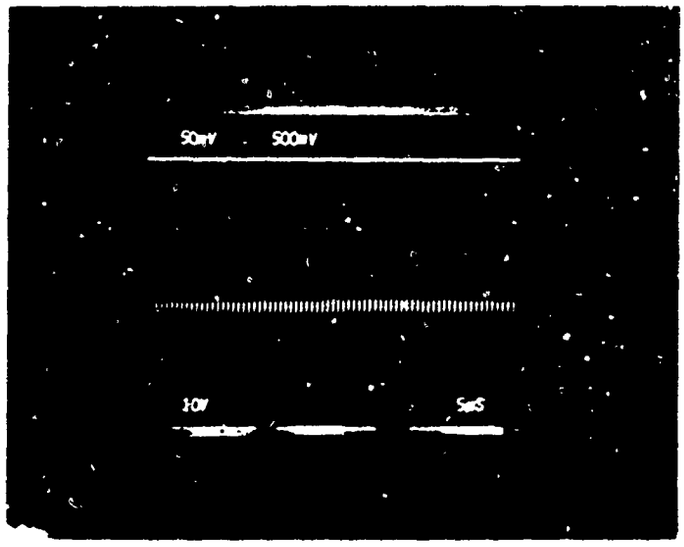

(a)

FULL DRAIN

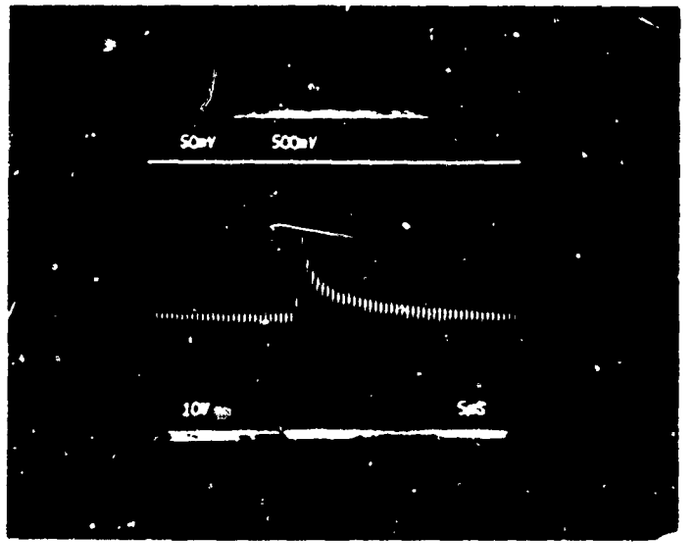

(b)

INTEGRATION TIME = 5 μSEC

FIGURE 4-6 GATING WITH XENON FLASH LAMP

4.1.5 Summary of Gating Results

The results of the previous section show that the ILID 1728 arrays can be used in the gating mode of operation. Wire detection has been achieved for gating pulse widths as short as 500 nanoseconds. However, the performance is marginal with respect to the requirements of the WODS task at short exposure times.

The feasibility experiment has been completed and analyzed.

The gating performance is limited by several factors which include:

- Propagation delay of gating pulse along the exposure control electrode.
- Attenuation of gating pulse along electrode.
- Increasing crosstalk as a direct function of wavelength.
- Transfer inefficiency as a function of wavelength.

The first effect tends to limit the permissible switching time, while the others tend to reduce the signal obtained in the video output. Therefore, it has become apparent during the experiment that the particular array architecture is not fully suitable for gating operation. For exposure times below 1 microsecond, recommendations for further development will be discussed in Section V.

On the other hand, the ILID 1728 arrays were found to perform well in the normal integration mode. The array No. 5C W1 #17 was of the highest sensitivity and was chosen for the WODS scanner whose performance is described in the next section.

4.2 SCANNER PERFORMANCE

The array number 5C W1 #17 had the highest sensitivity as well as best visual display appearance and so was utilized with the WODS scanner in the normal integration mode. The WODS scanner was tested by imaging various types of targets including pictoral, TV test targets, and wires. The results clearly show that the ILID 1728 performs well in the normal integration mode and provides high resolution detection capable of locating wires smaller than the pixel size. The next sections discuss the performance achieved with the WODS scanner.

4.2.1 General Image Quality

Figure 4.7a shows the image quality obtained with the WODS scanner for an actual size photo located at 100 inches (8.3 feet). The figure photograph was obtained by polaroid recording from the faceplate of the CONRAC high resolution TV monitor (1029 TV lines). No attempt was made here to capture all grey scales that the CCD is capable of recording. Furthermore, only about 1/3 of the available CCD line scan output is displayed on the CRT.

The photograph demonstrates the clarity of detail obtainable with the WODS scanner, the linearity of the mirror scan system, and the noise free characteristics of the sweep circuits. The active scan was written onto the scan converter so that it could be displayed continuously for up to 1/2 hour.

Figure 4-7b shows a magnified portion of the top photograph obtained by use of the zoom control of the Hughes scan converter. Careful inspection of this photograph shows the individual pixels arranged in an interlaced fashion as discussed in Section 3.3. In a conventional imaging system, the full output of the array would not

(a)

(b)

IMAGE QUALITY: 75mm Lens Resolution Element = .17 MRAD
(a) Normal Scan (1/3 of Array Output)
(b) Full Zoom Showing Individual Pixels

FIGURE 4-7 WODS IMAGE QUALITY-PICTORIAL

be magnified to such extent. However, in the present application it is precisely the individual pixels which are of interest.

A standard TV test target is shown as photographed from the TV monitor in Figure 4-8a. In the zoom mode, Figure 4-8b, the image is seen to be composed of individual pixels showing the ODD-EVEN effect explained above.

It should be noted that the small bar groupings are beyond the resolution of the CCD array/optics combination at this distance as expected from simple geometrical considerations.

4.2.2 Wire Object Detection

A number of tests were performed in order to show the capability of the WODS scanner to detect unresolved wires in the optical field-of-view. Table 4-3 lists the parameters for this test. Normal AC lamps were used to provide illumination. These lamps included both standard tungsten (2854°K) and photoflood-lamps (6000°K). No difference was found in detection ability due to color temperature. The optics used was a 75MM Cosmicar in order to guarantee that the MTF of the lens does not degrade the image quality.

The scale of the experiment was chosen to simulate wire objects of interest consistent with geometry of field conditions of 300 meters distance. Wires as small as 3MM at 300 meters are a threat. For these objects the angular subtense is .01 MRAD. Therefore, we choose wire sizes of 1,3, and 5 mils at target ranges of 100 inches to simulate realistic wire sizes. Secondly, wires were sprayed with thinned enamel to provide reflectivities of 45%, 15% and 8%. One group of wires were left bare to explore the glint/diffuse return from metal.

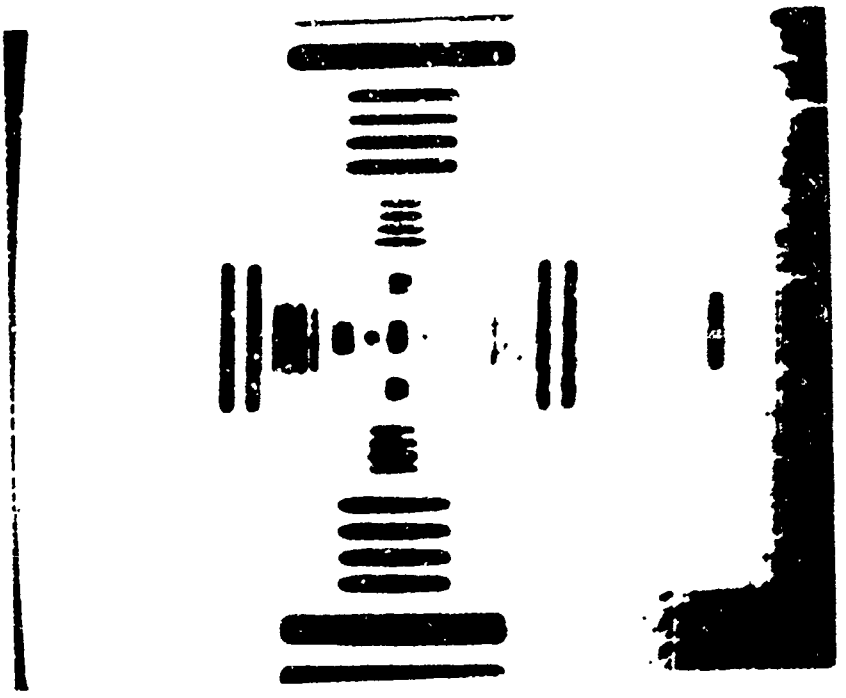

(a)

(b)

(a) Normal Scan
(b) Full Zoom

FIGURE 4-8 WODS IMAGE QUALITY - TV TEST TARGET

TABLE 4-3 SINGLE SITE ACTIVATION DEMONSTRATION

- Source: Photoflood Lamps 2854° and 3200°
  As available
- Optics: COSMICAR 75 mm Lens
  f/1.4, Resolution = 0.17 MRAD
- Scale: Wires used: 1 mil , 3 mil , 5 mil
  Bare and Diffuse
  Distance: 100 inches

WIRE SIZE INCHES	ANGULAR SUBTENSE MRAD	PIXEL FRACTION	EQUIVALENT DIA AT 300M
.001	.01	.058	3MM
.003	.03	.173	9MM
.005	.05	.289	15MM

Reflectivities : 45%
15%
8%

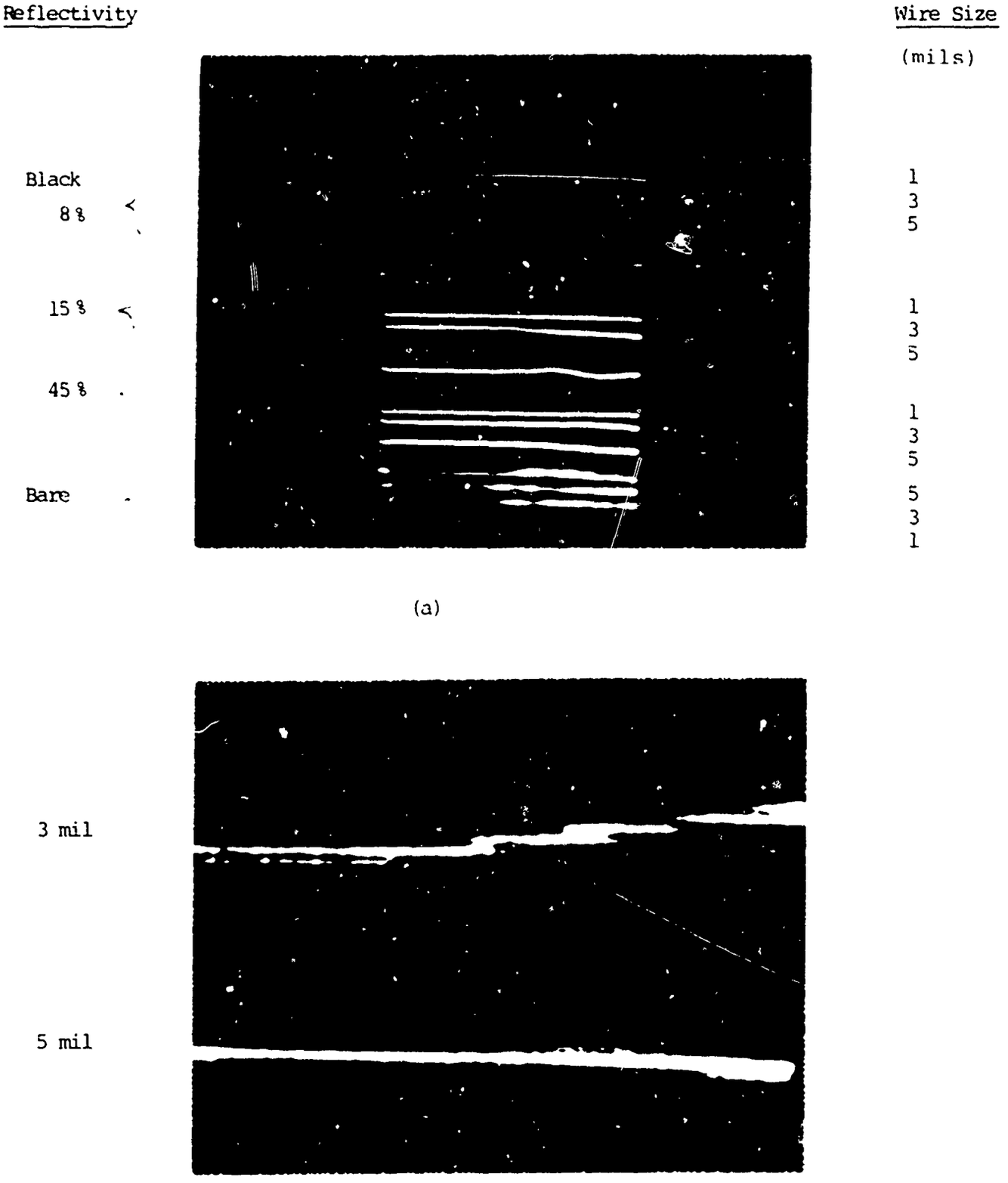

SINGLE SITE ACTIVATION

(a) Full Scan
(b) Zoom: Black Wires Only

FIGURE 4-9 WODS WIRE DETECTION

Figure 4-9 shows polaroid photographs obtained from the high resolution TV monitor. The top photograph shows the four groups of different reflectivity. The WODS scanner detects the wires for all reflectivities used. The bottom photograph shows a magnified portion of the 8% reflectivity wires. Wire recording is seen to consist of essentially individual pixels breaking up the curved wire into line segments. The photograph clearly shows single site activation. The 3 MIL and 5 MIL wires subtend pixel fractions of only 5.8% and 17.3%, respectively, so that the energy is contained within the pixel. Some optical spreading has been noted due to optical blurring, and perhaps crosstalk of the CCD but this is not significant.

Note that the top wire in this photograph is gently curving upwards. The image of the wire consists of a string of straight line segments (single site) with portions where the wire breaks up into two separate lines in the vertical direction. This is because the energy falling at or near the intersection of two pixels is split and falls into both pixel locations because there is no dead space in this type of array. This photograph is a dramatic confirmation of single site activation.

4.2.3 Single Site Activation

Figure 4-10 shows photographs of the video measured on an oscilliscope. The top photograph, Figure 4-10a includes a vertical scan of the 8% reflectivity wires shown in Figure 4-9b.

Figure 4-10a has two wire detections in the video. On the left is a single wire detected primarily within one pixel. On the right is the return from a brighter wire that appears to be split between two adjacent pixels.

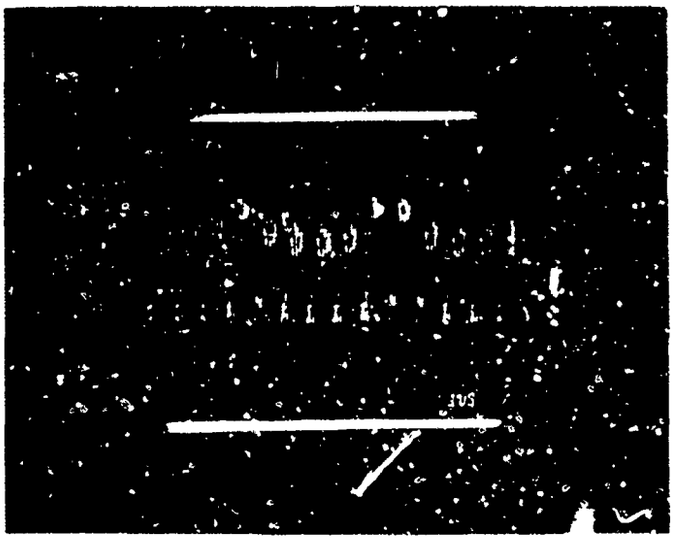

(a)

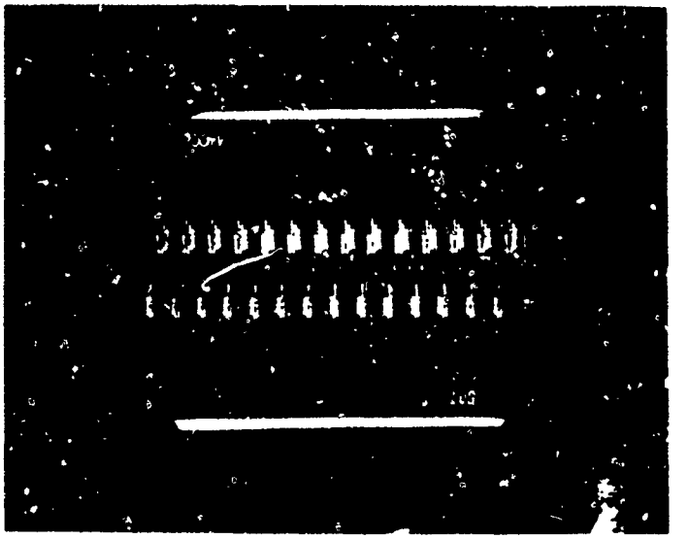

(b)

SINGLE SITE ACTIVATION; CCD ILID 1728
(a) Single Site (b) Background Only

FIGURE 4-10 SINGLE SITE ACTIVATION ILID 1728 ARRAY

Oscilliscope photo 4-10b is the background only when wires are removed from the field-of-view. The differential signal level is on the order of 0.2 volts and is sufficiently high to implement various processing techniques such as transversal filter or threshold circuitry.

4.3 SUMMARY OF WODS PERFORMANCE

The WODS Scanner has successfully demonstrated wire detection over a range of wire reflectivities and sizes. The complete camera has been delivered to USAECOM, Fort Monmouth as part of this contract. The versatility of this camera can be used to implement a study to further define and characterize wire target signatures and optical effects which may be encountered in realistic field situations.

5.0 CONCLUSIONS AND RECOMMENDATIONS

The studies required to define a wire object detection system utilizing a CCD array have resulted in clarifying several factors related to the definition and configuration:

- The analytic studies have defined and characterized the single site detection problem in terms of requirements for the optical parameters including probability of detection, probability of false alarm, and, number of scans required to detect a wire. It has been shown that in order to detect a wire with an overall reliability of, 0.99, single site probability of detection of 0.998 and false alarm of .02 is required.

- A transversal filter approach has been outlined that offers advantages in defining the single site detection and suppressing effects of sensor noise and scene background.

- The best scanning technique for the WODS application appears to be separate transmitter and receiver optics, boresighted, and scanned across the 15 degree FOV in the horizontal direction by either a mirror (in object space) or by the use of a rotary scan of the entire optics. In order to use laser energy in an optimum way, the transmitter laser beam should be fan shaped (10 Deg x 0.1 MRAD) and the receiver FOV should exactly match the transmitted beam.

- Based upon a parametric study, the optimum laser wavelength is found to be in the spectral band of 0.8 to 0.9μm. In practical cases, the choice would narrow down to a GaAl solid state laser (at λ= .90 μm) if "on-chip" CCD gating is

available. Otherwise the laser would need be a GaAlAs solid state device tuned to the spectral region of 0.8 to 0.85 μm in order to be compatible with the spectral sensitivity of available image intensifiers.

- Gating techniques have been reviewed. Electro-optical techniques such as the Kerr cell or Pockel cell have been found to be limited by insertion loss as well as poor gating times for large fields-of-view. On the other hand, gating with image intensifiers is within the state-of-the-art at the present time and is suitable for direct coupling to linear CCD arrays to provide electrical output. In the long term an "on-chip" gating CCD structure would appear to offer advantages over other techniques in terms of responsivity, spectral region of operation, small size, and low power requirements.

The WODS camera has been designed and fabricated under this contract. This camera has provided the basis for experimental study of both the normal and gated operation of the ILID 1728 CCD Array. The conclusions derived from the experiment are the following:

a. The utility of linear CCD arrays for the detection of wire objects smaller than a pixel has been confirmed by experiment. Wire detection has been demonstrated for wires that subtended only 5% of the pixel. The conclusion is that the CCD array does allow single site detection of wire objects.

b. The gating results for the linear array used to perform the gating experiment (CCDILID 1728) were poor for gating times below several microseconds due to both propagation delay along the polysilicon electrode and finite transfer time effects

from the photosites. Gating was not achievable below 0.5 microsecond for any array tested with this structure. The conclusion is then that present CCD structures cannot achieve the gating performance required for the WODS task.

Our final recommendations for continuation of the Wire Object Detection Program is based upon the key technology issue of gating the CCD array. Since the CCD array is required to achieve single site activation, it is natural to inquire whether gating can be achieved "on chip" as well.

Detailed investigations of linear CCD structures should be undertaken with the goal of defining an array suitable for the WODS task. Key parameters are low noise equivalent signal (less than 20 electrons, RMS), large number of pixels (1745), low crosstalk, and high responsivity in the spectral range of 0.8 to 0.9 μm, with capability of gating with pulse durations of 100 Nsec, or less.

APPENDIX A

WIRE DETECTION SYSTEM ANALYSIS

The detection and timely warning of the presence of wire-like obstacles in the flight path of aircraft would overcome one of the principal barrier problems to low altitude day/night operation of aircraft.[1] Specifically, wires that exceed 1/8" diameter should be detected at ranges which permit the aircraft sufficient time to maneuver appropriately. The required minimum detection range depends on the type of aircraft; 300 meters might be considered the lower limit of range while a range of one kilometer would be more desirable. It is further required that a system be capable of operating by day or night and in adverse weather conditions or atmospheres with high particulate concentrations.

Clearly, a "passive" system, i.e., one that depends on ambient illumination alone, would be advantageous in a military environment, but a passive system cannot achieve the above requirements. However, an "active" system employing a pulsed laser illuminator and a range gated image intensifier CCD can provide "seeing" of wire-like objects in adverse weather or aerosol atmospheres.

The field-of-view of such an active system should be at least 15° in azimuth by 10° in elevation and a resolution on the order of 0.2 milliradian is desirable. It will be shown in the detailed discussions of this proposal that a system utilizing linear imaging Charge Coupled Device (CCD) as a pickup device with a gated image intensifier can satisfy the WODS requirements.

A.1 ATMOSPHERIC CONSIDERATIONS

For normal atmospheric conditions, the atmospheric absorption is relatively small over the ranges and operating wavelengths being considered, namely, 300 to 500 meters and λ = .85 um respectively. Most of the attenuation is caused by scattering from particulate matter in the atmosphere. Except for such cases as dense black smoke, the scattered energy is not absorbed but redistributed without being absorbed.

(1) Kleider, A., "An Experimental Evaluation of Gated Low Light Level TV (GL^3TV) for Wire Obstacle Detection", Report No. ECOM-4321, May, 1975.

The scattering processes[2] are:

a) Rayleigh scattering which applies when the radiation wavelength is much larger than the particle size. The scattering coefficient varies as $1/\lambda^4$.

b) Mie scattering applies when the particle size is comparable to the radiation wavelength. The Mie scattering area coefficient (ratio of the area of incident wavefront that is affected by the particle to the cross-sectional area of the particle itself) varies with particle size from 0 to 4 and asymptotically approaches the value 2 for large particles. A range of particle size and wavelength exists for which the scattering coefficient is wavelength dependent.

c) Non-selective scattering exists when the particle size is very much larger than the radiation wavelength. In this case the scattering is not wavelength dependent and the area scattering coefficient has the value 2 which is the same as the asymptotic value obtained for Mie scattering as the particle size gets large.

The loss mechanism that predominates for most atmospheres is Mie scattering since the particulate size normally found in atmospheric aerosols falls in that range. Scattering calculations[3] made for dielectric spheres with refractive index n = 1.25 (n = 1.33 for water) show that for particles with a diameter of 0.02 λ the normalized intensity backscattered (180°) equals that scattered forward (0°). However, the absolute magnitude of this scattering is small. At particle sizes of 1 λ, the forward scatter increases 10 orders of magnitude while the backscatter increases about 7 orders of magnitude. Thus, in conditions of heavy haze or fog, backscattering becomes a significant factor in limiting visibility. The limitation in visibility is not because insufficient illumination reached the target but rather because the high background illumination caused by backscattering serves to lower the target contrast.[4]

(2) Handbook of Military Infrared Technology, ONR, 1965, p 204.

(3) M. Born, E. Wolf, Principles of Optics, The Macmillan Co., NY, 1964, p 654.

(4) Middleton, W.E.K., Vision Through the Atmosphere, University of Toronto Press, 1952, p 68.

A.2 RANGE GATED DETECTION

Range gating is a technique for virtually eliminating the backscattered contribution to background signal. The region closest to the camera and illuminator is the most troublesome since the illuminator's initial intensity is the highest in this region and the backscattered radiation is least attenuated. Reference to Figure 1 serves to illustrate the problem for a continuous (CW) source of illumination and high ambient illumination as well.

The illumination source and detector or camera are shown to be near each other with the illuminator divergence θ, equal to the detector field-of-view (FOV). A lambertion target of area A_t and relectivity r_t is located at range R_o, and a diffuse background with reflectivity r_b, is located at range, R_b. The illuminator power is P_o watts, while the ambient illumination is P_a watts/meter^2 - um.

Let us examine the various signals received by the detector. They will be compared on the basis of energy since any detector or camera is an integrator with integration time τ. The detector will integrate all of the scattered energy within its field-of-view out to a range $R = c\tau$ where c is the speed of light. However, in the case of Figure 1, a background scene located at R_b curtails this spatial integration provided $c\tau \geq R_b$. The various signals seen by the detector are described in paragraphs 2.2.1 through 2.2.5.

.2.1 Energy Returned from Target for CW Illumination

The illumination power density at the target ,

$$P_{ot} = \frac{P_o}{\frac{\pi}{4} R_o^2 \theta^2} e^{-\alpha R_o} \qquad (1)$$

where

P_{ot} = incident power density at target in watts-meter^{-2}

P_o = illuminator power in watts

R_o = distance to target or range in meters

θ = illuminator divergence = camera FOV in radians

α = atmospheric attenuation coefficient in meters^{-1}

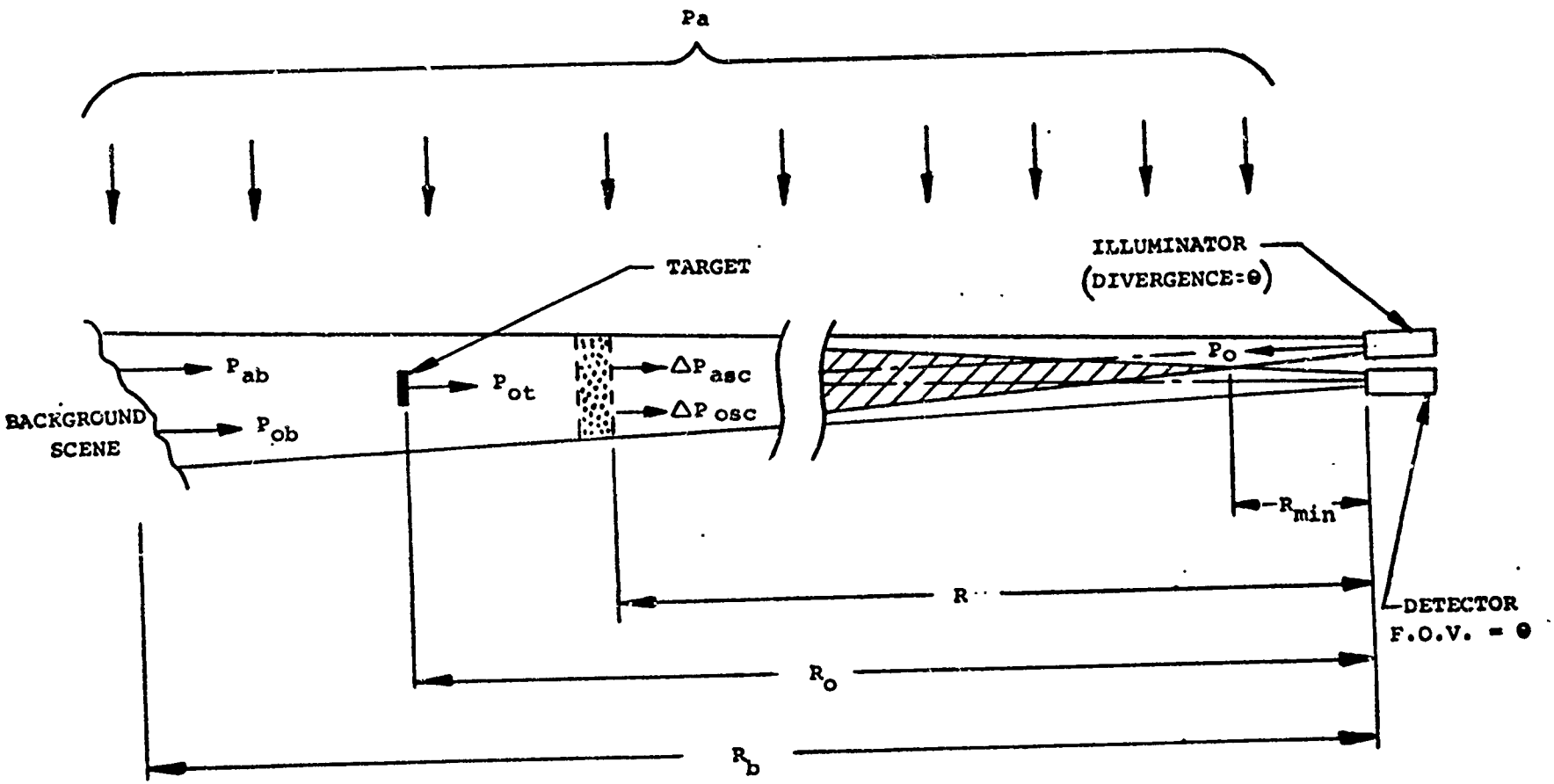

FIGURE A-1 DETECTOR WITH C.W. ILLUMINATION

If the target is assumed lambertian, the power scattered by the target is,

$$P_o = \frac{P_{ot} A_t r_t}{\pi} \tag{2}$$

where

P_{ot} = power leaving target in watts-steradian^{-1}

r_t = diffuse reflectivity of target (dimensionless)

A_t = area of target in meters^2

The energy from the target that reaches the detector is,

$$E_t = P_{ot} \cdot \frac{\pi d^2}{4} \cdot \frac{1}{R_o^2} \cdot T_f T_l \tau_e^{-\alpha R_o} \tag{3}$$

where

E_t = energy from target on detector in joules

d = diameter of lens in meters

T_l = transmission of lens

T_f = transmission of bandpass filter

τ = integration time in seconds

A bandpass filter peaked at the emission wavelength of the illuminator would be a necessity for daylight operation.

Combining equations (1), (2) and (3) results in the detected energy from the target as,

$$E_t = \frac{P_o A_t r_t d^2 T_f T_l \tau}{\pi \theta^2} \cdot \frac{e^{-2\alpha R_o}}{R_o^4} \tag{4}$$

A.2.2 Backscattered Illuminator Energy

Consider an incremental thickness of atmosphere ΔR at a distance R from the illuminator and detector as shown in Figure 1. The increment of power scattered by this volume in a direction toward the detector is,

$$\Delta P_{osc} = K_b \frac{\alpha P_o e^{-\alpha R}}{4\pi} \Delta R \qquad (5)$$

where

ΔP_{osc} = incremental backscattered power in watts-steradians^{-1}

α = atmospheric scattering coefficient in meters^{-1}

ΔR = incremental range in meters

K_b = a coefficient relating the intensity of light scattered in a given direction, (in this case), backwards, by atmospheric particles to the intensity from isotropic scatters; K_b varies with particle size and wavelength; 0.24 is a good average value for wavelengths in the range 0.4 to 1 μm.[5]

In this case 4π steradians is the solid angle into which the energy is scattered.

The incremental energy received by the detector due to backscattering is,

$$\Delta E_{osc} = \Delta P_{osc} \frac{\pi d^2}{4} T_f T_l \tau \frac{e^{-\alpha R}}{R^2} \qquad (6)$$

while the total received backscattered illuminator energy in joules is,

$$E_{osc} = \frac{K_b \alpha P_o d^2 T_f T_l \tau}{16} \int_{R_{MIN}}^{R_B} \frac{e^{-2\alpha R}}{R^2} dR \qquad (7)$$

(5) Deirmendjian, D., "Scattering and Polarization Properties of Water Clouds and Hazes in the Visible and Infrared", Applied Optics, Vol 3, No. 2, February 1964, p 187, Figure 4.

where

E_{osc} = energy at detector due to backscattered illumination in joules

R_{min} = range from detector to closest illuminated particles within detectors field-of-view in meters.

Equation (7) is amenable to solution since it falls into the family of "Exponential Integrals" which are tabulated.[6] The solution takes the form,

$$E_{osc} = \frac{K_b \alpha P_o d^2 T_f T_l \tau}{16} \left[\frac{E_2 (2\alpha R_{min})}{R_{min}} - \frac{E_2 (2\alpha R_{max})}{R_{max}} \right] \quad (8)$$

where

$E_2 (2\alpha R_{min})$ = exponential integral evaluated at $2\alpha R_{min}$ (value is maximum)

$E_2 (2\alpha R_{max})$ = exponential integral evaluated at $2\alpha R_{max}$ (value is minimum)

Equation (8) shows the near in backscattering to be considerably larger than that further away from the detector.

(6) Handbook of Mathematical Functions, U.S. Department of Commerce, N.B.S. Applied Mathematics Series, 55, 1964

A.2.3 Ambient Illumination Energy Scattered to Detector

Consider ambient illumination as the sun at zenith. Further, consider the incremental atmospheric section shown in Figure 1 which is shown expanded in Figure 2 to illustrate the geometry for ambient scattering calculations. A thin horizontal slab of atmosphere with scattering coefficient taken through this disc will have an area $\Delta R \times W$. Hence, the ambient power impinging on this surface is $P_a W \Delta R$.

The thickness of this slab is $Rd\phi$ so that the power scattered by this slab is $P_a (W \Delta R) R d\phi$. W is given by $2\sqrt{R^2\phi^2_m - R^2\phi^2}$ which can be deduced from Figure 2. Thus, the power radiated by the slab is,

$$dP_a = 2\alpha P_a R^2 \Delta R \sqrt{\phi_m^2 - \phi^2}\, d\phi \qquad (9)$$

where

P_a = ambient illumination at operating wavelength in watts-meter^{-2} - μm^{-1}

ϕ = integration variable related to FOV by $\theta = 2\phi_m$ in radians

It is assumed that the power passing through the total height of the disc is not appreciabley altered by the scattering process, then the power scattered by this disc toward the detector is given by,

$$\Delta P_{asc} = \frac{2K_q \alpha P_a R^2 \Delta R}{4\pi} \left[2 \int_{\phi=0}^{\phi_m} \sqrt{\phi_m^2 - \phi^2}\, d\phi \right] \qquad (10)$$

where

ΔP_{asc} = incremental power scattered toward detector in watts-steradian^{-1} - μm^{-1}

K_q = quadrature scattering ratio dependent on atmospheric particle size and wavelength; typically 0.016[7]

(7) Deirmendjian, D., op. cit.

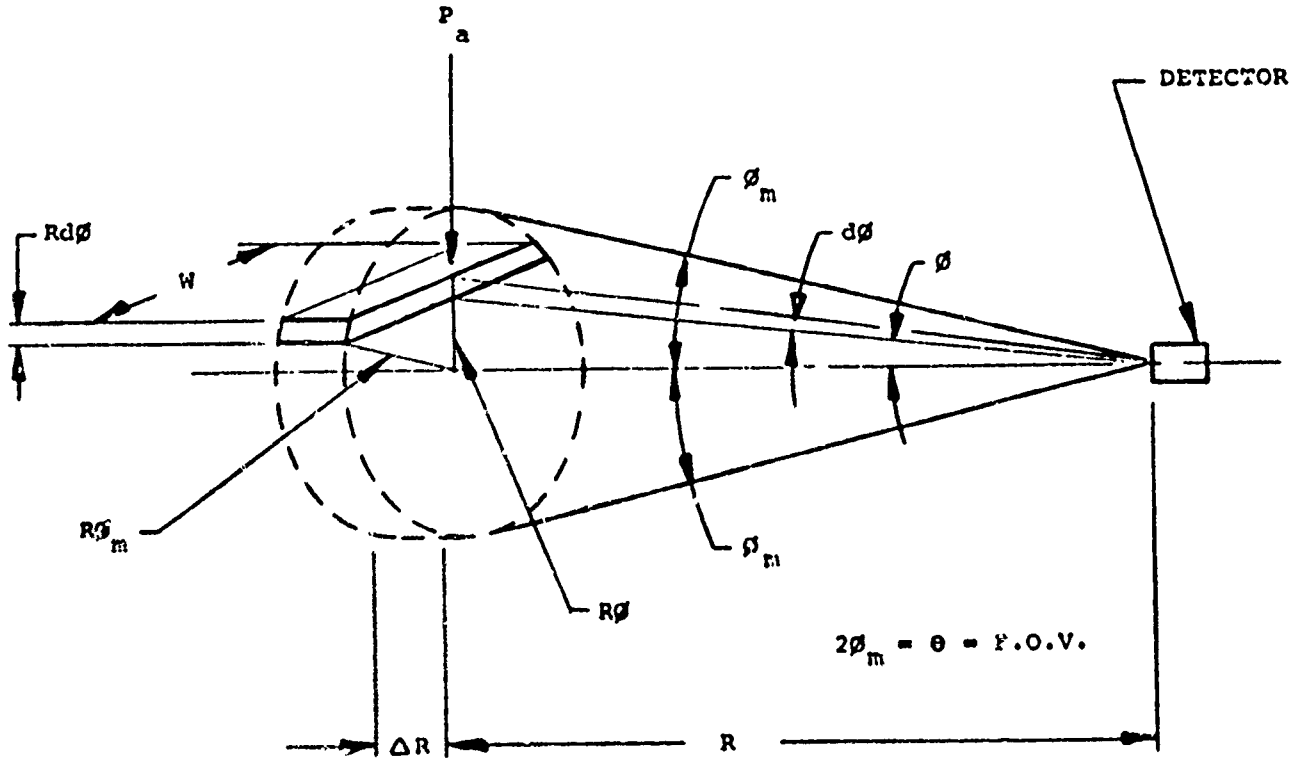

FIGURE A-2 GEOMETRY FOR CALCULATION OF AMBIENT SCATTER

Integrating equation (10) and substituting $\phi_m = \theta/2$ one obtains the following for a given wavelength,

$$\Delta P_{asc} = \frac{K_q \ \alpha \ P_a \ \theta^2}{16} \qquad R^2 \ \Delta R \qquad (11)$$

The energy seen by the detector in joules is,

$$E_{asc} = \int_{R=0}^{R_b} \Delta P_{asc} \cdot \frac{\pi d^2}{4} \cdot \frac{e^{-\alpha R}}{R^2} \cdot T_f T_l \ \tau \ \Delta\lambda \qquad (12)$$

where

$\Delta\lambda$ = filter bandwidth in μ meters

Combining equations (11) and (12) leads to,

$$E_{asc} = \frac{\pi \ K_q \ P_a \cdot \theta^2 \ d^2 T_f \ T_l \ \tau\Delta\lambda}{64} \int_0^{R_b} \alpha e^{-\alpha R} \, dR \qquad (13)$$

Integration yields the detected ambient scattered energy as,

$$E_{asc} = \frac{\pi \ K_q \ P_a \ \theta^2 \ d^2 \ T_f \ T_l \ \tau\Delta\lambda}{64} \qquad \left[1 - e^{-\alpha R_b}\right] \qquad (14)$$

In can be seen that the ambient scattered energy received by the detector is strongly dependent on the field-of-view, integration time and bandwidth; also, it reaches a maximum as R_b approaches infinity.

A.2.4 Ambient Background Energy Received by Detector

Assume the background to be lambertian and inclined at β to the line of sight. Under these conditions, the ambient background power radiated toward the detector in the spectral range of the filter is,

$$P_{ab} = \frac{P_a \, r_b \, \text{Cos}\, \beta}{\pi} \cdot \frac{\pi R_b^{\,2} \theta^2}{4} \Delta\lambda \qquad (15)$$

where

β = angle between normal to background scene and detector axis in degrees

r_b = reflectance of background

P_{ab} = ambient background power reflected toward detector in watts-steradian^{-1}

The energy seen by the detector is

$$E_{ab} = P_{ab} \, T_f \, T_l \, \tau \, \frac{\pi d^2}{4} \cdot \frac{1}{R_b^{\,2}} \, e^{-\alpha R_b} \qquad (16)$$

Combining equations (15) and (16) and assuming $\beta = 45°$, we get

$$E_{ab} = \frac{\pi \, P_a \, r_b \, d^2 \, \theta^2 \, T_f \, T_l \, \tau \Delta\lambda}{16\sqrt{2}} \, e^{-\alpha R_b} \qquad (17)$$

This energy is seen to be dependent on the field-of-view, the integration time and the bandwidth of the filter.

A.2.5 Illuminator Energy Reflected by Background

Making the same assumptions as in the previous paragraph, the illuminator power reflected toward the detector is,

$$P_{ob} = \frac{P_o \, r_b \, \text{Cos}\, \beta}{\pi} \, e^{-\alpha R_b} \qquad (18)$$

where

P_{ob} is the illuminator power diffusely reflected toward the detector for a background inclined at angle β in watts-steradian^{-1}.

The energy seen by the detector is,

$$E_{ob} = P_{ob} \frac{\pi d^2}{4} T_f T_\ell \tau \frac{e^{-\alpha R_b}}{R_b^2} \tag{19}$$

Combining equations (18) and (19) and assuming $\beta = 45°$ we obtain

$$E_{ob} = \frac{P_o r_b d^2 T_f T_\ell \tau}{4\sqrt{2}} \frac{e^{-2\sigma R_b}}{R_b^2} \tag{20}$$

The parameters influencing this return signal are clearly evident.

A.2.6 Range Gating

Figure 3 shows typical timing of various signals for range gated systems. The illuminator is pulsed for a short duration Δt, as would be the case for a pulsed laser. During the time required for the illuminator pulse to reach the target and return, the camera is gated off. At the instant the pulse returns the camera is turned on for a time $\Delta\tau$ long enough to capture all of the energy in the pulse. Note in the timing diagram of Figure 3, how the illuminator scattering return is almost eliminated because only a thin slab of the atmosphere is scattering during the integration time $\Delta\tau$. The return of illuminator energy diffusely reflected from the background scene is completely eliminated. Ambient scattering and reflection are reduced by virtue of the fact that the integration time is reduced to the short interval $\Delta\tau$.

The paragraphs that follow estimate the gated signals at the detector.

A.2.6.1 Energy Returned From Target (Laser Illuminator)

If the illuminator is a pulsed laser with energy output E_o in joules and pulse width Δt in seconds its power output P_o in watts is $E_o/\Delta t$. Examination of equation (4) shows that the integration time τ need be equal to or somewhat longer than Δt. Substituting for P_o and making $\tau = \Delta t$ in equation (4) alters it to,

$$E_t = \frac{E_o A_t r_t d^2 T_f T_\ell}{\pi \theta^2} \cdot \frac{e^{-2\sigma R_o}}{R_o^4} \tag{4a}$$

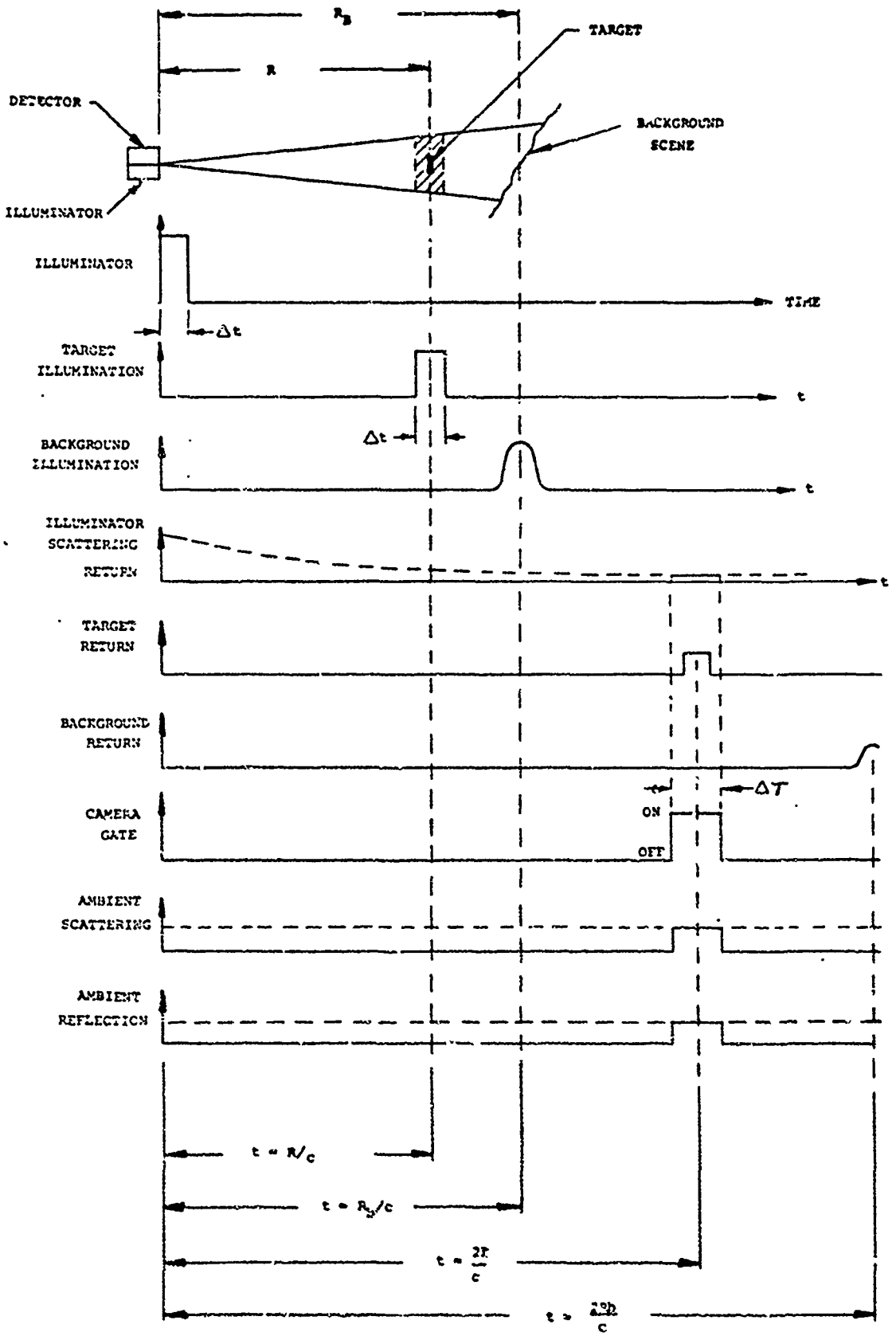

FIGURE A-3 RANGE GATE TIMING

A.2.6.2 Backscattered Illuminator Energy (Range Gated)

In this case the slab of atmosphere contributing to the detected signal is only $\Delta R = C\Delta\tau$ where C = velocity of light and $\Delta\tau$ = camera integration time even though the light pulse Δt might be shorter than the camera integration time $\Delta\tau$. Thus the effective spatial integration limits used in equations (7) and (8) are

$$R_{min} = R_o - \frac{C\Delta\tau}{2}$$

and

$$R_{max} = R_o + \frac{C\Delta\tau}{2}$$

Substituting these limits and replacing P_o and τ in equation (8) results in:

$$E_{osc} = \frac{K_b \sigma E_o d^2 T_f T_\ell}{16} \cdot \frac{\Delta\tau}{\Delta t} \left[\frac{E_2 \left[2\sigma\left(R_o - \frac{C\Delta\tau}{2}\right)\right]}{\left(R_o - \frac{C\Delta\tau}{2}\right)} - \frac{E_2 \left[2\left(R_o + \frac{C\Delta\tau}{2}\right)\right]}{\left(R_o + \frac{C\Delta\tau}{2}\right)} \right] \quad (8a)$$

The magnitude of this return energy is extremely small since $\left(R_o - \frac{C\Delta\tau}{2}\right) \cong \left(R_o + \frac{C\Delta\tau}{2}\right)$ and the values of the two exponential integrals will be close to each other, hence their difference will be small.

A.2.6.3 Scattered Ambient Illumination (Gated Camera)

The only change to equation (14) in this case is the substitution of $\Delta\tau = \tau$. Equation (14) becomes,

$$E_{asc} = \frac{\pi K_q P_a \theta^2 d^2 T_f T_\ell \Delta\lambda}{64} \Delta\tau \left[1 - e^{-\alpha R_b}\right] \quad (14a)$$

A.2.6.4 Ambient Reflected Background (Gated Camera)

Again, the only substitution to be made in equation (13) is $\Delta\tau = \tau$; the ambient energy diffusely reflected to the camera is,

$$E_{ab} = \frac{\pi P_a r_b d^2 \theta^2 T_f T_\ell \Delta}{16\sqrt{2}} \Delta\tau \quad e^{-\alpha R_b} \quad (13a)$$

A 2.6.5 Background Reflected Laser Energy (Gated Camera)

As shown in Figure 3, the laser energy diffusely reflected from the background arrives at the camera outside the integration time span of the camera ($\Delta\tau$). This is true provided the background is sufficiently separated from the target to permit the camera gate to discriminate against the return signal. In other words R_b should be somewhat greater than $R_o + C\Delta\tau$.

A.3 ILLUMINATOR DIVERGENCE, FIELD OF VIEW AND RESOLUTION CONSIDERATIONS

The field of view of the camera and the divergence of the illuminator strongly influence the ratio of the signal returned from the target to that signal caused by scattering and/or reflection of ambient illumination. Backscattering and reflection of illuminator energy from the background are also affected by divergence and FOV. These signals would seriously limit system performance except that range gating virtually eliminates background reflected illumination energy and illuminator backscatter.

It would be convenient now to express the various signals of consequence in terms of the camera IFOV and illuminator divergence; the signals will be those seen by a single element of an array. Assuming that the CCD Pixel diameter is larger than the point spread function of the optics and image intensifier. Reference to Figure 4 shows that the area A_t of the target seen by an element is:

$$A_t = DR_o\Delta\theta_H \tag{21}$$

where:

A_t = target area within IFOV in meters^2

D = diameter of wire in meters

$\Delta\theta_H$ = horizontal (azimuthal) subtense of single photosite of CCD in radians referenced to the input of the image intensifier

Furthermore, the area of illumination in previous equations has been calculated in the form $\pi R^2\theta^2/4$; this expression should be replaced by $R^2\theta_H\theta_V$. Similarly, the camera FOV, $\pi R^2\theta^2/4$ is replaced by the photo-element IFOV which is $R^2\Delta\theta_H\Delta\theta_V$. Manipulation of equations (4a), (14a) and (17a) result in the following:

a) Energy from target.
By inserting equation (21) and $\pi\theta^2 = 4\theta_H\theta_V$ into equation (4a) we obtain,

$$E_t = \frac{E_o r_t d^2 T_f T_\ell D\Delta\theta_H}{4\theta_H\theta_V}\left[\frac{e^{-2dR_o}}{R_o^3}\right] \qquad (4\ )$$

b) Ambient scattered energy.
By substituting $\pi\theta^2 = 4\Delta\theta_H\Delta\theta_V$ in equation (14a) we obtain:

$$E_a = \frac{P_a d\ T_f T_\ell \Delta\theta_H\Delta\theta_V\ \Delta\lambda\ \Delta\tau}{4}\left[\frac{Kq}{4}\left(1 - e^{-\alpha R_b}\right)\right] \qquad (14b)$$

c) Ambient reflected energy.
Again using $\pi\theta^2 = 4\Delta\theta_H\Delta\theta_V$ one can express equation (17a) as,

$$E_{ab} = \frac{P_a d\ T_f T_\ell \Delta\theta_H\Delta\theta_V\ \Delta\lambda\Delta\tau}{4}\left[\frac{r_b}{\sqrt{2}}\ e^{-\alpha R_b}\right] \qquad (17b)$$

It would be useful to compare the ambient scattered energy to the ambient energy reflected from the background if present. The ratio of scattered to reflected ambient energies is therefore,

$$\frac{Easc}{Eab} = \frac{\frac{Kq}{4}\left(1 - e^{-\alpha R_b}\right)}{\frac{r_b}{\sqrt{2}}\left(e^{-\alpha R_b}\right)} \qquad (22)$$

If a visibility is considered (8) the attenuation coefficient α at a wavelength of 0.85 um is 0.18 kilometers^{-1}, while the scattering ratio at 90°, Kq, is 0.016. Assuming the background to be at 315 meters, equation (22) becomes

$$\frac{Easc}{Eab} = \frac{\frac{0.016}{4}(1-0.945)}{0.707\, r_b\,(0.945)} = \frac{0.004\,(0.055)}{0.668\, r_b} = \frac{0.00033}{r_b}$$

Note that for the visibility conditions assumed, even with a low background reflectance, say $r_b = 0.1$, the detected scattered ambient energy is only 0.0003 times the reflected ambient.

The ratio of the target return to the ambient reflected energy must be examined. If one assumes that $R_b \cong Ro$ then this ratio is,

$$\frac{E_t}{Eab} = \frac{2\, E_o D r_t}{P_a \Delta\lambda \Delta\tau \theta_H \theta_V \Delta\theta_V r_b} \left[\frac{e^{-\alpha R_o}}{R_o^3}\right] \qquad (23)$$

Examination of this expression shows that the target return energy relative to reflected ambient is increased as the vertical resolution of the camera becomes better, i.e., smaller. Furthermore, if a linear CCD array is used as a pickup device, more target return is effected by allowing θ_H to approach $\Delta\theta_H$. In other words the target is illuminated with a fan shaped beam having $\Delta\theta_H$ horizontal divergence and θ_V vertical divergence.

No advantage is gained on an overall power basis since the total FOV has to be scanned and eventually covered with many more pulses. However, advantages on an individual pulse basis are effected through increased signal to noise ratio and reduced peak pulse power required of the laser which will be a gallium aluminum arsenide injection type laser.

(8) Dermendjian, D., op. cit., Table I.

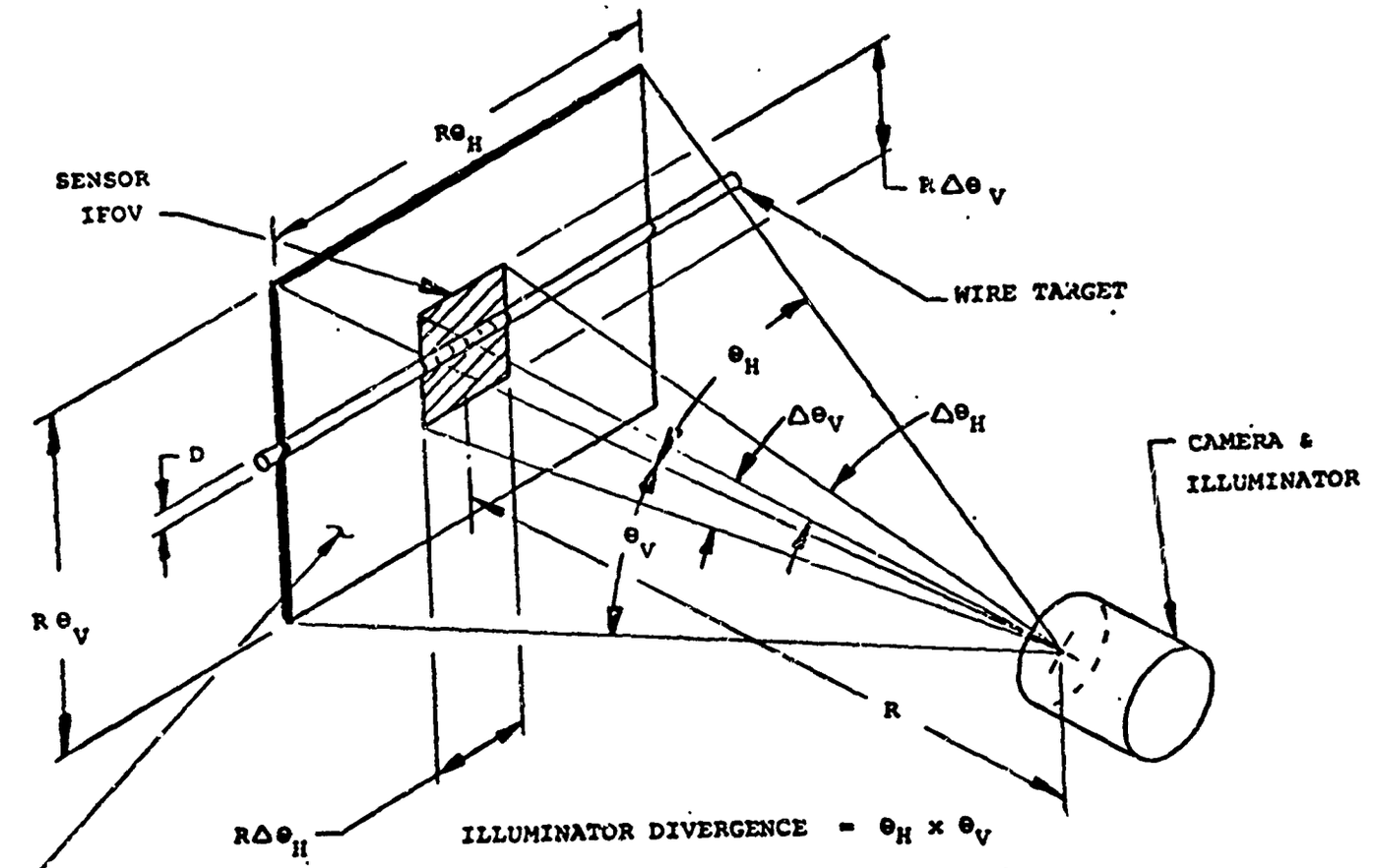

FIGURE 4 ILLUMINATOR DIVERGENCE & CAMERA F.O.V.

APPENDIX B

WIDE OPTACLE DETECTION SYSTEM
TECHNICAL MEMO 6113-650-1
A.J. KLEEMANN 14 Jan. 1977

EXPERIMENT TEST PLAN
EXHIBIT B

ABSTRACT

This technical memo constitutes the final test plan required by Task 650 of the WODS contract. The report is organized into four sections.

In Section I the experimental goals are summarized. The details of FPA array selection is set forth in Section II. In Section III the feasibility demonstration for both single site activation and gating is outlined. Lastly, block diagrams are contained in Section IV.

OUTLINE

I. Experiment Goals.

II. Array Selection

- a. Measurement conditions
- b. Test descriptions
  - 1) pre-selection
  - 2) special testing.

III. Experiment Description

- a. Single site activation
- b. Gating demonstration

IV. Simplified Block Diagram

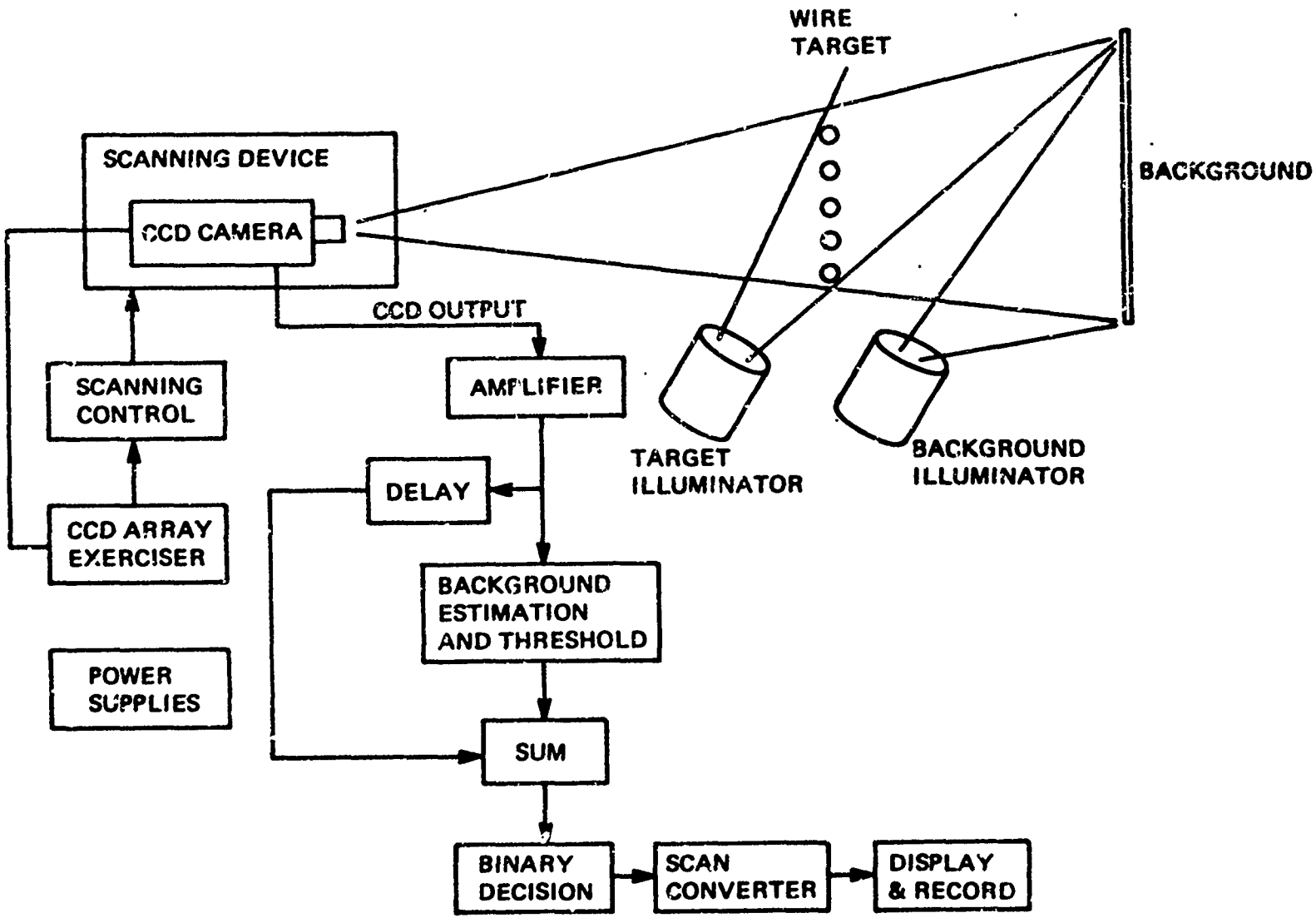

FIGURE B-1

SIMPLIFIED BLOCK DIAGRAM OF SINGLE SITE ACTIVATION EXPERIMENT

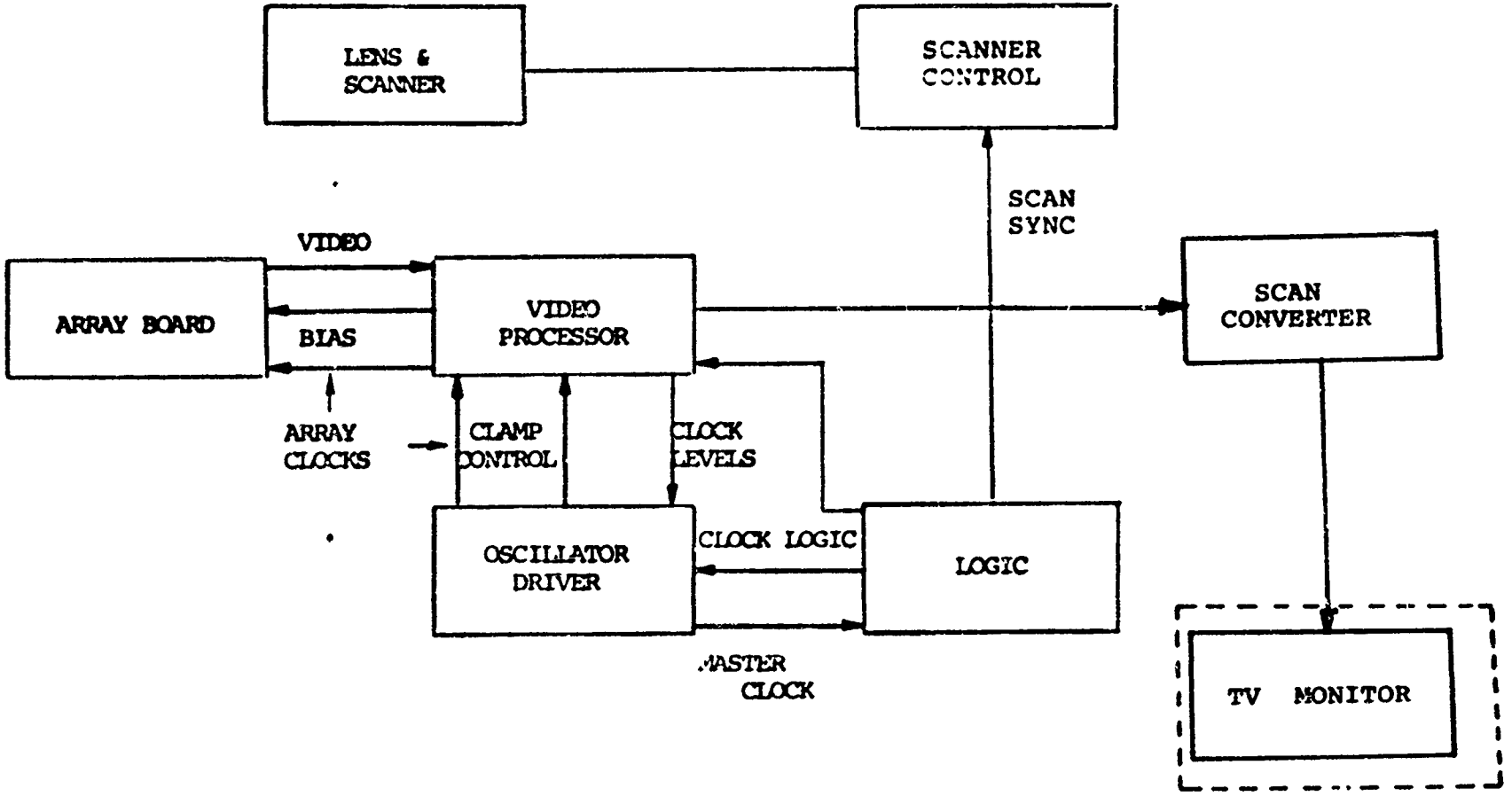

B-2 CAMERA BLOCK DIAGRAM

I. EXPERIMENT GOALS.

This experimental program constitutes a feasibility demonstration, and acceptance test of a gatable CCD scanner system. The CCD ILID 1728 Y array chosen for this application will be tested in both a gated and normal mode of operation.

The experimental approach will be to test the capability of the array within the framework of the WODS task. The relevant WODS requirements are as follows:

SINGLE SITE ACTIVATION

Signal-to-noise Ratio 4.5

Scan volume: 15 deg/sec, horizontal

Clock rate: 1.728 mHz

Integration time: 1 MSEC

Refresh rate: 0.5 Hz maximum

Linear Array: 1728 pixels vertical.

GATING

Gate-on time: 100-300 nsec goal to several microseconds, max.

Signal-to-noise ratio: 4.5

II. ARRAY SELECTION.

The twenty one ILID 1728 Y arrays that Fairchild Imaging Systems have made available to this contract will be measured for characteristics relevant to the wire obstacle detection task. The best array will be incorporated into the camera and scanner breadboard device which will be tested and delivered to ECOM. Since the requirements of the WODS task, especially related to the gating capability, are unique, it is necessary to select the arrays according to suitable criteria. The following measurements will be made to determine the best available array.

a. Measurement conditions.

1) Measurements will be performed at room temperature (25 C)

2) When DC illumination is used, it will be provided by a photoflood tungsten lamp operating at 2854 K color temperature.

3) Nominal clock frequency of 1.728 mHz will be used. This provides a normal integration time of 1 msec for the SSA mode. The arrays will be exercised via the logic, drivers, and controls defined in schematic drawing 6113-250 SDI (12 Jan. 1977)* Measurements will be displayed on a oscilloscope and recorded.

4) Complete setup records and data will be made available to ECOM upon request.

5) Any deviations from the above condition will be specified.

b. Test descriptions.

The arrays which are available will be screened for proper electrical and optical performance for both the SSA and gating portions of the experiment. It is our goal to find an array which will satisfy both aspects of the experiment. However, it is possible that two separate arrays may be employed if it is found necessary or advantageous. The following tests will be performed.

1) With fixed uniform DC illumination on the array the electrical factors to be tested are the following:

Signal voltage level, uniformity and blemish, exposure control response, Dark current.

These broad area response characteristics will be compared. Several attractive arrays will then be tested in more detail.

2) Special testing. (WODS application)

With the array in place in the exerciser and illuminated by a uniform source as before, further testing will characterize the gating capability of the array.

TEST 1. Signal output versus integration time (for SSA mode)

TEST 2. Signal output versus exposure control voltage (VEC)

The exposure control function is determined by the value of VEC. The range of values are +12V full drain (0% of signal)

- 5.0V full storage (100% signal)

12 < V > -5 exposure control region

The measurement will be made at discrete integration times on the signal transfer curve established in the previous measurement (Test 1).

* or revision as appropriate

TEST 3 Signal output versus exposure time.

The exposure time is variable from about 100 nsec to over 200 usec. The range is controlled by digitally counting 1024 coarse steps of 300 nsec. Fine control is accomplished by a ten turn pot further dividing one 300 nsec interval. The waveforms for this case is shown in Figure 1.

The objective of this test is to determine the minimum gating time for each array.

TEST 4 Voltage output versus propagation time.

Study to date indicates that the gating capability of this array is limited by the propagation time along the polysilicon electrode. Estimates are that the propagation time is in the range of 0.5 usec to 8 usec. This effect can be characterized by inverting the polarity of VEC (i.e. pulsing the voltage from normally store level to drain level). In this case the video will show attenuation of signal after some delay which is directly related to the propagation time.

This measurement will be made with VEC pulses of various durations (consistent with Test 3).

TEST 5 Verification of gating capability.

Test 1 through Test 4 will exercise the array with a DC illumination source. This test is intended to verify gated operation with an actual high speed light pulse.

The array will be operated as in Test 3 with integration time set for minimum value for the specific array. The light pulse will be provided by a RED light emitting diode (pulse duration less than 20 nsec). The light will uniformly illuminate the CCD array.

The temporal phasing between the LED pulse and the ILID integration window can be continuously adjusted by a coarse (digital switch) plus a fine (10 turn pot) control. Therefore, the LED pulse can be "scanned across" the integration window. In this way the gating capability can be verified and secondly, the "off time" signal rejection can be explored.

A fast rise time PIN photodiode (rise time less than 10 nsec) will be used to verify the timing of the pulse.

III EXPERIMENT DESCRIPTION

The complete camera system will be assembled incorporating the previously tested array and control logic, with the galvanometer scanner, and scan converter. The system will be debugged. Testing of the system performance against wire targets will proceed in two parts. Part I will test the performance for single site activation using DC illumination. Part II will test the performance with pulsed light sources.

a. Single site activation

A test fixture will be made that will hold a matrix of wires used at the object plane. The wires will be bare metal (SiAl alloy) ranging in size from one mill to five mill diameter. If time is available, various procedures will be used to provide different surface properties for the wire, thereby allowing signature analysis. The fixture will allow angle and position adjustment. Initially, the background will be simply a black area with no illumination in order to simplify the setup.

Laboratory AC and DC lamps will be provided to illuminate the background and target plane independently.

The camera will be mated with a 135mm lens commercially available. Tests will be performed to determine the optimum F/number for operation with unresolved point sources. Once found the F/number will be fixed for all parts of the experiment.

The instantaneous field-of-view of the CCD element when used with the given lens is

$$\text{IFOV} = \frac{d}{F} \text{ (Radians)}$$

d CCD C-C PITCH (13 um)

F Focal length (135 mm)

For our experiment the resolution in both dimensions is slightly less than 0.1 MRAD as required in the SOW. We will choose the distance from the wire plane to the lens so that the largest wire (5 mill) just fills the CCD element. Therefore, the distance will be on the order of 50 inches. The 3 mill and the 1 mill wire will image to 0.6 and 0.2 of the CCD element respectively.

The following tests will be performed in the scanning mode.

SINGLE SITE ACTIVATION

In this test the "scene" including the wires will be scanned at refresh rates of 0.5Hz.

The video output will be stored on the target of a memory tube of a Hughes 639 scan converter. Intermittent video will be displayed on a TV monitor operating at either 512 TVL (standard) or 1029 TVL (high resolution). The entire FOV of 15 x 10 degrees will be scanned by the mirror galvanometer. However, only about 2-3 degree horizontal will be displayed at any one time as consistent with the display resolution. Video recordings will be made for each part of the experiment.

Oscilliscope photographs will be made. Signal voltages and peak-to-peak noise will be measured and recorded.

Absolute light levels at the target and background planes will be measured with a Prichard spotmeter or other calibrated instrument as required.

The factors to be varied during this portion of the experiment are the following:

a. Angle of wire to camera and light source

b. Light level for background and target wire

c. Distance of wire plane from camera.

Variation of these factors over a range of values will allow us to predict the utility of this type of scanner over a wide range of conditions relevant to the WODS task.

Verification of single site activation will be accomplished by oscilliscope measurements of the contents of illuminated (and adjacent) CCD elements.

GATING DEMONSTRATION

The DC lamp used to illuminate the wire plane in the above test will be replaced by a pulsed light source. Provisions have been made to use a light emitting diode or a Xenon flash lamp.

The array will be operated in the gated mode with gating times as determined during the selection procedure.

Data collection, calibration and recording will proceed as outlined above.

Summary of data will be presented in the final report.

IV SIMPLIFIED BLOCK DIAGRAM

a. DSA

b. Gating

c. List of components

FAIRCHILD IMAGING SYSTEMS
A Division of Fairchild Camera and Instrument Corporation

LIST OF EQUIPMENT

ITEM	
1	Symmar S 5.6/135mm Lens
2	Practica 2.5/135mm Lens
3	General Radio Type 1531-A Strobotec Zenor flash lamp Flash duration 0.8 usec 1×10^6 candlepower with external trigger
4	Hughes 639 scan converter 525 TVL and 1029 TVL readout
5	Photoflood lamp 500w
6	DC power supply for above
7	Fixture for test wire
8	General scanning Type G300PD Galvanometer Type CCX 102 driver
9	Control logic CCD/Gate (Schematic drawing 6113-250SD1, or revision)
10	UDT pin-5 photodiode (TO-5)
11	Red LED
12	Conrac monitor
13	Textronix oscilloscope
14	Various laboratory power supplies